

Coulomb Drag and Jahn-Teller Effect in Two-Dimensional Electron Systems in Strong Magnetic Fields

Von der Fakultät für Mathematik und Physik der Universität Stuttgart
zur Erlangung der Würde eines Doktors der
Naturwissenschaften (Dr. rer. nat.) genehmigte Abhandlung

Vorgelegt von

Sergej Brener

aus Moskau

Hauptberichter:

Prof. Dr. W. Metzner

Mitberichter:

Prof. Dr. A. Muramatsu

Tag der mündlichen Prüfung:

11. Mai 2006

Max-Planck Institut für Festkörperforschung

2006

Contents

Deutsche Zusammenfassung	5
1 Overview	9
2 Theory of Coulomb Magneto-Drag	11
2.1 Introduction	11
2.2 History of the problem. Experiment.	12
2.3 History of the problem. Theory.	17
2.3.1 Early works.	17
2.3.2 Boltzmann equation approach.	20
2.3.3 Diagrammatic approach.	22
2.3.4 Magneto-drag. Early diagrammatic approach.	29
2.3.5 Negative magneto-drag. First explanation attempt. . .	30
2.3.6 Diagrammatic calculation of magneto-drag in the SCBA.	33
2.4 Semiclassical theory of electron drag in strong magnetic fields	41
2.4.1 Drag between parallel links.	46
2.4.2 Drag between non-parallel links.	70
2.4.3 Connection to two-dimensional drag.	80
2.5 Conclusion	81
3 Possible Jahn-Teller effect in Si-inverse layers	83
3.1 Introduction	83
3.2 Hamiltonian of electron gas on Si interface	85
3.3 SU(4) Symmetric Case	88

3.4	Jahn-Teller effect	92
3.5	Phase diagram	96
3.6	Anisotropic energy of skyrmion	98
3.7	Conclusion	102
3.8	Appendix A	102
3.9	Appendix B	103
3.10	Appendix C	103
4	Summary	107

Deutsche Zusammenfassung

Seit Jahrzehnten zogen zwei-dimensionale elektronische Systeme das Interesse vieler Physiker und Technologen an. Der Grund dafür ist nicht nur - wie man sich naiv vorstellen könnte - die technologische Anwendung in Rechnerprozessoren. Die scheinbar einfache physikalische Konfiguration zwei-dimensionaler Elektronensysteme führt zu unerwartet vielen experimentell beobachtbaren Effekten und theoretischen Modellen, die eine eigene Bedeutung für die Entwicklung von Physik, Technologie, Computerrechnungen usw. haben.

Seit der Entdeckung des Quanten-Hall-Effekts [1] galt zwei-dimensionalen elektronischen Systemen in starken Magnetfeldern (sogenannte Quanten-Hall-Systeme) ein besonders starkes Interesse. Die physikalischen Effekte, die in solchen Systemen zu beobachten sind, sind ein Resultat der Zusammenarbeit von Landau-Quantisierung der elektronischen Bewegung, Elektron-Elektron-Wechselwirkung, Bandstruktur des Materials (normalerweise Si oder GaAs), Unordnungseffekte usw. Unter den interessanten Aspekten zwei-dimensionaler elektronischer Systeme kann man folgende Themen nennen: Quanten-Hall-Effekt, Coulomb-Drag, skyrmionische Phasen, Energietal-Aufspaltung (valley splitting) in Si-Inversionsschichten, Auswirkung der Mikrowellenstrahlung auf die Transporteigenschaften der Quanten-Hall-Systeme und viele andere.

In der vorgelegten Dissertation beschäftige ich mich mit zwei mit Quanten-Hall-Systemen verbundenen Effekten: dem Coulomb-Drag im Kapitel 2 und dem Jahn-Teller-Effekt in Si-Inversionsschichten im Kapitel 3.

Kapitel 2 ist ein Resultat der durch die Werke [2, 3] motivierten Untersuchung des sogenannten anomalen Magneto-Drag, der in den obengenannten Referenzen experimentell entdeckt wurde. Der Drag (auch Coulomb-Drag genannt) ist ein physikalischer Effekt, der in elektronischen Doppelschichtsystemen beobachtet wird. Durch eine Schicht wird Strom geführt, der in der zweiten Schicht eine elektrische Spannung verursacht. Falls das System sich in einem senkrechten Magnetfeld befindet, wird der Drag als Magneto-Drag bezeichnet. Der anomale Magneto-Drag besteht darin, dass unter gewissen Umständen der Magneto-Drag sein Vorzeichen wechselt und negativ wird. In diesem Kapitel stelle ich detaillierte Resultate für ein Modellproblem, das eng mit dem anomalen Magneto-Drag verbunden ist, dar. Nach einer kurzen Einführung gebe ich im zweiten Teil eine kurze Übersicht der Experimente, die in den letzten 15 Jahren durchgeführt wurden. Besondere Aufmerksamkeit ist denjenigen Experimenten gewidmet, die sich auf das Dissertationsthema beziehen. Der dritte Teil enthält eine detaillierte Zusammenfassung der heutigen theoretischen Ansätze zum Dragproblem. Insbesondere wird erläutert, warum diese Ansätze nicht genügen, um die überraschenden Eigenschaften des Magneto-Drag zu beschreiben. Der vierte Teil ist der Hauptteil des Kapitels. Hier führe ich zunächst das Modell ein, mit dem ich mich in diesem Teil beschäftigen werde. Dann zeige ich verschiedene Wege, mit denen das Modell behandelt werden kann, vergleiche die Resultate, bespreche ihre Relevanz und Zuverlässigkeit. Schliesslich zeige ich die Verbindungen zwischen dem betrachteten Modell und dem Originalproblem und bringe überzeugende Argumente um zu zeigen, dass diese Verbindungen stark genug sind, um viele (wenngleich nicht alle) interessante Eigenschaften des zwei-dimensionalen Magneto-Drags zu erklären.

Kapitel 3 ist ein Versuch, den Jahn-Teller-Effekt in Si-Inversionsschichten vorherzusagen. Dieser ist ein Resultat der Zusammenwirkung von Energietal-Aufspaltung, Elektron-Phonon- und Elektron-Elektron-Wechselwirkungen in diesen Systemen. Das Kapitel ist wie folgt aufgebaut. Im Teil 3.2 wird der Hamilton-Operator des Systems eingeführt, der in einen $SU(4)$ -symmetrischen

und einen nicht $SU(4)$ -symmetrischen Teil aufgespaltet wird. Im Teil 3.3 wird der $SU(4)$ -symmetrische Fall untersucht. In den Teilen 3.4, 3.5 führe ich die anisotropen Terme des Hamilton-Operators ein und untersuche deren Einfluss auf den Grundzustand des Systems für verschiedene ganzzahlige Füllfaktoren. Im Teil 3.5 wird das Phasendiagramm für den interessanteren Fall $\nu = 2$ gegeben. Dabei werden drei Phasen vorhergesagt, nämlich eine ferromagnetische, eine Spin-Singlet und eine antiferromagnetische Phase. Im Teil 3.6 wird der Effekt der nicht-symmetrischen Terme im Hamilton-Operator auf die Energie eines Skyrmions untersucht.

Kapitel 4 enthält schließlich eine kurze Zusammenfassung aller Resultate.

Chapter 1

Overview

Over decades two-dimensional electron systems have drawn the attention of an extremely large number of physicists and technologists. The reason for this interest is not only - as one might naively suppose - due to the technological applications in computer processors. This seemingly simple physical configuration gives rise to an unexpectedly rich variety of experimentally observable effects and theoretical models which are themselves important for the development of physics, technology, computing etc.

Since the discovery of the quantum Hall effect [1] a particular attention has been paid to two-dimensional electron systems subjected to a strong magnetic field (the so-called quantum Hall systems). The physical effects observed in such systems are the result of an interplay between the Landau quantization of the electron motion, the electron-electron Coulomb interaction, the band structure of the material (usually Si or GaAs), disorder effects etc. Among the interesting aspects of the two-dimensional electron physics one can mention the fractional quantum Hall effect, Coulomb drag, skyrmion phases, valley splitting in Si inverse layers, bilayer quantum Hall systems, effects of the microwave radiation on transport properties of the quantum Hall systems and many others.

In this thesis I deal with two effects which are related to the Quantum Hall systems. In the main part of the work, **Chapter 2**, I study the Coulomb

magneto-drag, particularly concentrating on the question of the so-called anomalous drag recently observed experimentally [2, 3]. The observed sign reversal of the drag signal poses an intriguing task for theoretical investigations.

Chapter 3 is an attempt to predict possible a Jahn-Teller effect in Si inverse layers. There I consider the interplay between the valley splitting, the electron-phonon and electron-electron interactions in these systems and their effect on the ground state and low-lying skyrmionic excitations.

In **Chapter 4** a short summary of the results is given.

Chapter 2

Theory of Coulomb Magneto-Drag

2.1 Introduction

In this chapter I will present extended results for a model problem closely related to the well-known and still not closed problem of the two-dimensional magneto-drag. In the next section I'll give a brief review of history of the experiments during the last 15 years. Special attention will be drawn to the results closely related to the theme of this work. In the third section I'll give a detailed overview of the present theoretical approaches to the drag problem. An important part of that section will be devoted to explaining of why do these approaches fail to explain the striking features of the magneto-drag. The fourth section is the main part of the work. There I'll start with presenting the model, I'll deal with in that section. Then I'll show different approaches to that model, compare the results, discuss their relevance and reliability. Finally, I'll show links between the considered model and the initial problem and will bring convincing arguments to show that these links are strong enough to explain many (though not all) interesting features of the two-dimensional drag.

2.2 History of the problem. Experiment.

Electron-electron interactions are responsible for a multitude of fascinating effects in condensed matter. They play an important role in such different phenomena as high-temperature superconductivity, fractional quantum Hall effect, Wigner crystallization or Coulomb gaps in disordered media. The effects of this interaction on transport properties, however, are difficult to measure. In the beginning of the 90-ties, a new technique has been proved to be effective in measuring the scattering rates due to the Coulomb interaction directly. [4].

This technique is based on an earlier proposal by Pogrebinskiĭ [5, 6]. The prediction was that for two conducting systems separated by an insulator (a semiconductor-insulator-semiconductor layer structure in particular) there will be a drag of carriers in one film due to the direct Coulomb interaction of the carriers in the other film. This effects resembles conventional friction that is why Coulomb drag is often referred to as frictional drag. Unlike the one-layer case, where Coulomb forces alone can not lead to finite conductance due to momentum conservation, in the double layer setup current in one layer leads to a finite mean force acting on the carriers in the other layer, which in turn leads to a finite current there. If the second layer is an open circuit the interaction with the electrons from the first layer leads to redistributing of charge density and to building a voltage in the second layer which opposes the frictional force and exactly cancels it. This voltage is referred to as *drag voltage*.

The standard experimental setup can be seen in Fig. 2.1. A constant low-frequency current (typically 25 Hz) is imposed on one of the layers (drive layer), and the drift of those electrons creates a frictional drag on the electrons in the adjacent layer (drag layer). Although for theoretical investigations it is more convenient to consider both layers as closed circuits, in practice the drag layer is an open one which allows to measure the drag voltage induced there. Typical experimental parameters for drag experiments are: the well thickness δ ranges from 10 to 30 nm, the layer separation d lies typically between 20 and

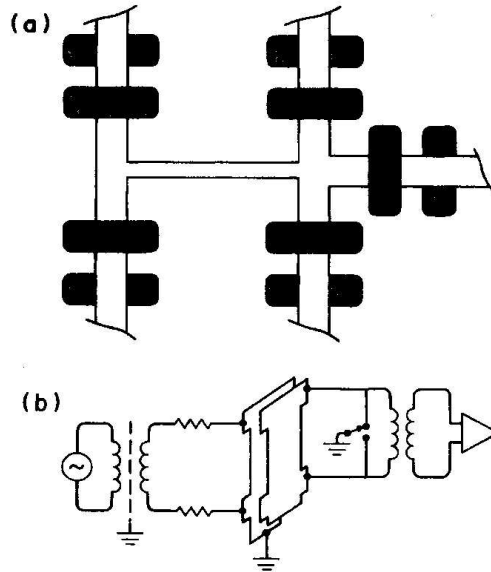


Figure 2.1: (a) Sample geometry, including the mesa and the front and back gates in gray. The central bar is $20 \mu\text{m}$ wide. Each mesa arm is terminated with an indium diffusion contact roughly 1.5 mm from this central region. (b) Schematic of the measurement configuration [4].

120 nm . This ensures that no tunneling occurs between the layers and that the only way the electrons from different layers may interact is the direct (screened) Coulomb force (or, under certain circumstances, quasi particle-mediated interaction may occur, such as phonon or plasmon interaction).

The measured value is the so-called *drag resistance* which is defined as

$$\rho_D = -\frac{V_D}{I}. \quad (2.1)$$

Here V_D is the drag voltage and I is the current driven through the drive layer. The minus sign means that the direction of the drag voltage is normally opposite to that of the current.

The experimental plots can be seen in Figs. 2.2, 2.3. It can be seen that the naive phase space arguments that predict T^2 low-temperature behavior of the drag (only a layer of electrons around the Fermi surface of the order

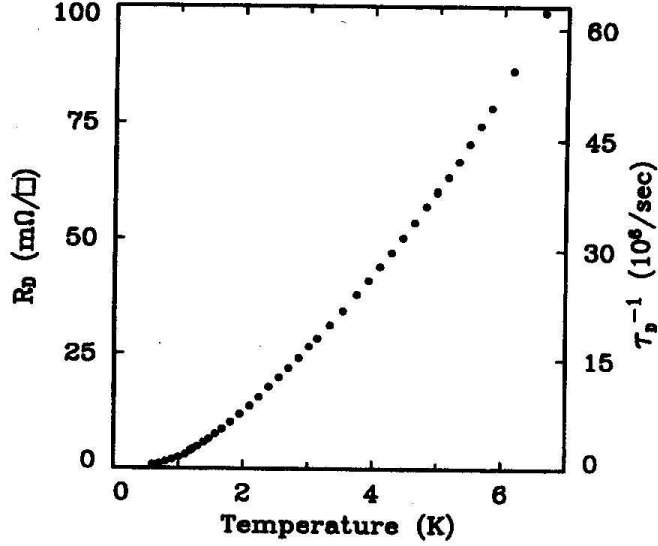


Figure 2.2: Temperature dependence of the observed frictional drag between two 2D electron systems separated by 175-Å barrier. Data are plotted as an equivalent resistance and a momentum-transfer rate [4].

of T in each layer contributes to drag) do not give a complete explanation of the temperature dependence. The roots of this discrepancy will be discussed in the next section. Here I just mention that in the field of the frictional drag in the absence of a magnetic field at the moment there are no open questions (for a review see [7]). Among other papers on drag worth mentioning is the work [8] in which electron-hole drag is studied. As one would expect, the drag signal in this case is negative if defined according to Eq. (2.1).

A boost of interest to the theme of Coulomb drag is due to drag experiments in presence of a finite magnetic field. First such experiments lead back to 1992 [9]. Many other followed [10, 11, 12].

In 1998 though a new, completely unexpected phenomenon has been found by X. Feng et al. [2], see Fig. 2.4. The new aspect in this work is the study of magneto-drag with different electron densities in the layers. The unusual and somewhat counterintuitive observation is the negative drag, i.e. electrons are accelerated in the direction opposite to the net transferred mo-

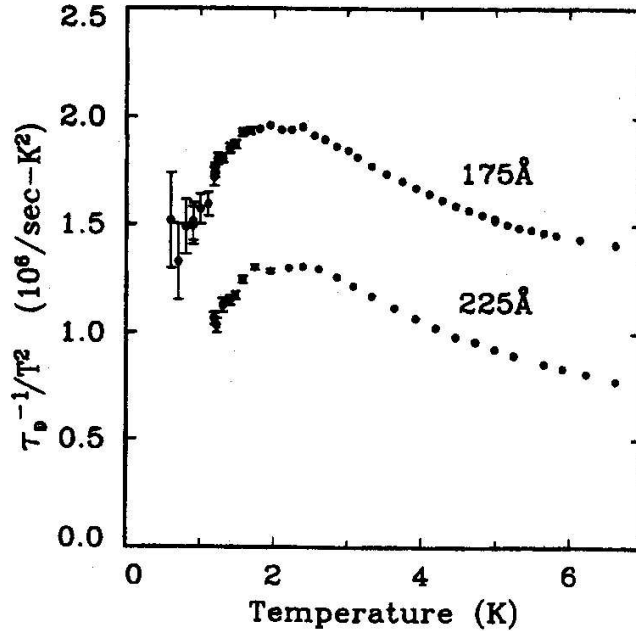


Figure 2.3: Temperature dependence of the interwell momentum transfer rate divided by T^2 for both the 175- and 225-Å barrier samples [4].

mentum. A closer look at the data of this paper (see Fig. 2.5), and at further papers [3, 13] (Figs. 2.6, 2.7) allows us to see that the negative drag occurs when in one of the layers the top Landau level is more than half filled, while in the other one it is less than half filled.

An analysis of the experimental data shows that the negative drag is observed only under quite specific conditions. First, the mobility of the samples should be quite high (more than $2 \times 10^6 \text{ cm}^2\text{V}^{-1}\text{s}^{-1}$), second, the magnetic field should be neither too low, nor too high (the effect was observed for filling factors ν between 6 and ≈ 70), and finally the temperature should be quite low (for a cleaner sample the negative drag could be observed only for temperatures under 1.8 K, while for a dirtier one the allowed temperature range extends and at some particular magnetic field even reaches 18 K). Another important feature revealed recently [13] is the activated low-temperature behavior of the drag signal with the activation energy periodically depending

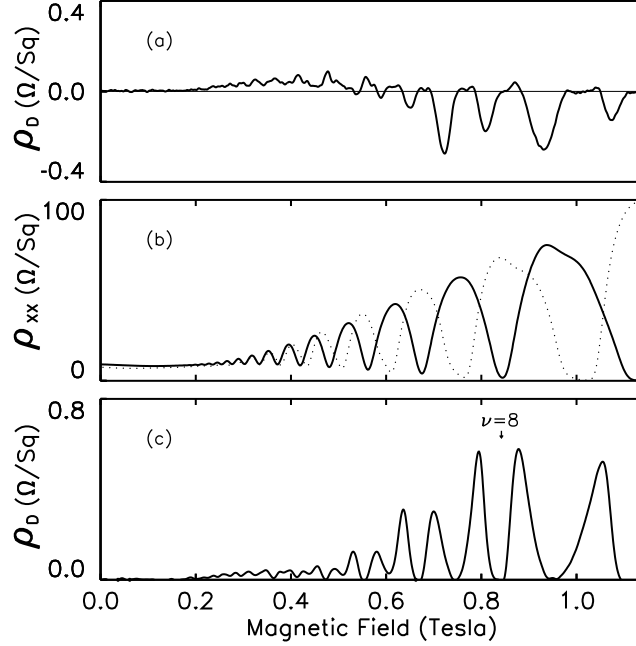


Figure 2.4: Drag versus magnetic field for matched (c) and unmatched (a) layer densities at 1.15K. The longitudinal magneto-resistance (b) for the drive layer in both cases ($1.66 \times 10^{11}/cm^2$) (solid line), the dotted line is the drag layer with a mismatched density ($1.49 \times 10^{11}/cm^2$). A clear difference in filling factors is evident for negative drag (a) [2].

on the magnetic field (see Fig. 2.7). The activation energy reaches its maximum when the Fermi level lies between two Landau levels and drops to zero when the Fermi level hits the center of either of the two spin-split Landau levels. All the above indicates the important role of disorder.

For high-mobility samples the disorder potential mainly comes from the inhomogeneity of the distribution of donors. They are localized in a layer ~ 50 nm away from each electron layer. Such setup, supposing uncorrelated distribution of donors, results in a smooth random potential in the electron layer with the correlation length equal to the distance between the donor and electron layers. This property of the random potential is crucial for the rest of the work.

The above-mentioned works of Feng *et al.* and Lok *et al.* attracted my

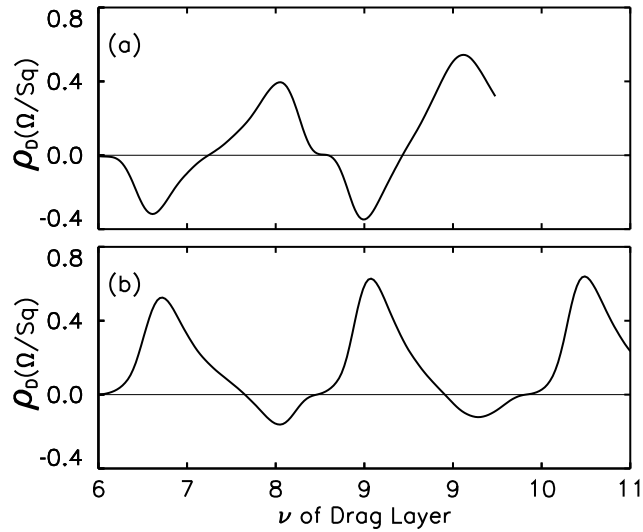


Figure 2.5: Drag versus drag layer filling factor(density). The drive layer density is fixed at $1.66 \times 10^{11}/cm^2$, with magnetic fields for (a)/(b) of 0.92/0.81 Tesla, and drive layer ν of 7.39/8.47. Nearly periodic behavior is observed [2].

supervisor's interest to this question so that he proposed me this problem as a topic for my doctor thesis. The observed effect being simultaneously simple and elusive for theoretical understanding for quite a long time (see next section) presented a challenge for us.

2.3 History of the problem. Theory.

2.3.1 Early works.

As mentioned above, the drag effect was first predicted theoretically [5, 6] long before it became possible for the experimentalists to produce double-layer systems with the necessary properties to observe the effect. These early works did not in fact present any calculations of what we call drag resistance, but rather gave just the idea that there might be a momentum transfer between two parallel systems separated by an insulator, only due to Coulomb interaction, without matter transfer.

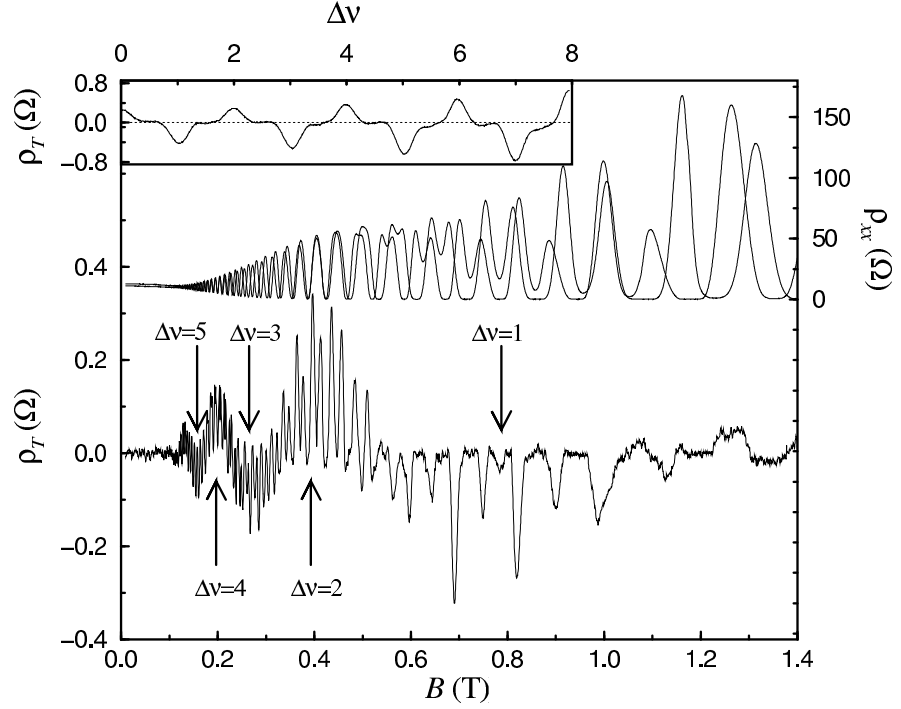


Figure 2.6: Drag resistivity ρ_T (bottom) and conventional longitudinal resistivity ρ_{xx} (top) for two 2DEGs at mismatched densities ($n_1=2.27$ and $n_2=2.08 \cdot 10^{11} \text{ cm}^{-2}$) as a function of magnetic field at $T=0.25$ (K). Two sets of oscillations can be distinguished in ρ_T : i) a quick one resulting from the overlap of the Landau levels in the 2DEGs and ii) a slow one which causes (*positive*) maxima in ρ_T whenever the filling factor difference between the 2DEGs is *even*, and (*negative*) minima whenever this difference is *odd*. The inset shows ρ_T at fixed magnetic field of 0.641 (T) versus filling factor difference [3].

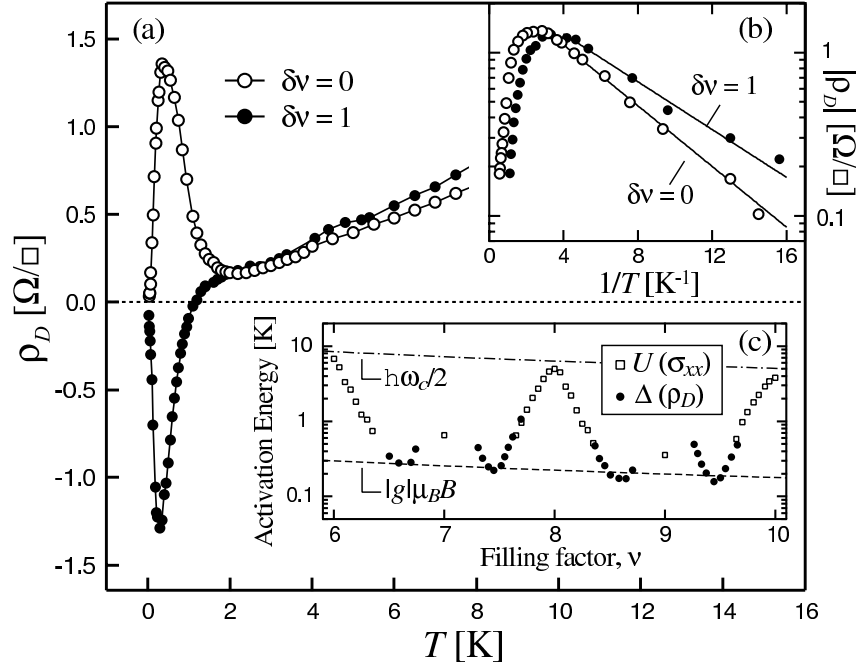


Figure 2.7: (a) ρ_D for matched and mismatched densities with $(\nu_F, \nu_B) = (9.5, 9.5)$ and $(8.5, 9.5)$. (b) Arrhenius plot of $|\rho_D|$ at low T , demonstrating the activated behavior. (c) measured activation energies, $\Delta(U)$, of $\rho_D(\sigma_{xx})$ for matched densities vs. ν . Data of U are shown for the front layer only, in regions where $\sigma_{xx} \propto \exp(-U/T)$. The bare Zeeman energy in GaAs with $|g| = 0.4$ is shown as a reference [13].

In the work [5] the author mainly concentrated on solving electrodynamic equations in a semiconductor-insulator-semiconductor heterostructure, taking into account the drag effect. The main result of that paper is the current-voltage characteristic of an SIS structure under drag conditions.

The work [6] is devoted to calculating of the energy transfer between the neighboring layers in a heterostructure due to Coulomb inter-layer scattering.

Thus, both of these pioneering works have only indirect connection to the theme of my work, but they should definitely be mentioned, as it is in these works that the idea of Coulomb inter-layer scattering was first mentioned.

2.3.2 Boltzmann equation approach.

First theoretical works in which approaching the drag problem has been set as the main goal were published in 1993. First A.-P. Jauho and H. Smith published a work where they used a Boltzmann equation approach to calculate the drag [14] and then L. Zheng and A.H. MacDonald used memory function formalism for the same goal [15]. Here I will review the former work not only because of its priority but also as the method elaborated there will be important for me later (see section 2.4.1).

The starting point is the standard linearized Boltzmann equation

$$\dot{\mathbf{k}}_2 \frac{\partial f_2^0}{\partial \mathbf{k}_2} = \left[\frac{\partial f_2}{\partial t} \right]_{\text{coll}}, \quad (2.2)$$

where

$$\dot{\mathbf{k}}_2 = -eE_2, \quad (2.3)$$

E_2 being the electric field induced in the drag layer, and

$$\begin{aligned} \left[\frac{\partial f_2}{\partial t} \right]_{\text{coll}} = & - \int \frac{d\mathbf{k}_1 d\mathbf{k}'_2}{(2\pi)^4} w(1, 2; 1', 2') (\psi_1 + \psi_2 - \psi_{1'} - \psi_{2'}) \\ & \times f_1^0 f_2^0 (1 - f_{1'}^0) (1 - f_{2'}^0) \delta(\epsilon_1 + \epsilon_2 - \epsilon_{1'} - \epsilon_{2'}) \end{aligned} \quad (2.4)$$

is the linearized collision integral. $w(1, 2; 1', 2')$ determines the probability of scattering of two electrons from states 1,2 to 1',2', f is the distribution function, f^0 is the equilibrium distribution function. Indices 1 and 2 refer to the initial states in the drive and drag layers respectively, 1' and 2' to the final states. Spin indices are omitted here; $\mathbf{k}_{1'} = \mathbf{k}_2 + \mathbf{k}_1 - \mathbf{k}_{2'}$ due to momentum conservation. The deviation function ψ is defined by

$$f - f^0 = f^0(1 - f^0)\psi. \quad (2.5)$$

The current flowing in the layer 1 is assumed to be limited by impurity scattering, corresponding to

$$\psi_1 = -\frac{1}{T} \tau_1 e v_{1x} E_1, \quad (2.6)$$

where E_1 is the electric field in the drive layer, directed along the x axis, and τ_1 is the momentum relaxation time.

The authors set $\psi_2 = 0$ "since no current is flowing in the drag layer". Here I will follow their line of reasoning and discuss the validity of this statement later. Collecting all the above, multiplying the Boltzmann equation by k_{2x} , integrating over \mathbf{k}_2 , and using the antisymmetry of the integrand on the RHS with respect to interchange of 2 and 2' they get

$$eE_2 n_2 = -\frac{eE_1 \tau_1}{8mT} \int \frac{d\mathbf{q} d\omega}{(2\pi)^2} [\Im \chi(q, \omega)]^2 w(1, 2; 1', 2') \frac{q^2}{\sinh^2(\omega/2T)}, \quad (2.7)$$

with n_i being the electron density in the i th layer. Energy transfer ω is introduced by formal substitution

$$\delta(\epsilon_1 + \epsilon_2 - \epsilon_{1'} - \epsilon_{2'}) = \int d\omega \delta(\epsilon_1 - \epsilon_{1'} + \omega) \delta(\epsilon_2 - \epsilon_{2'} - \omega), \quad (2.8)$$

$\mathbf{q} = \mathbf{k}_{2'} - \mathbf{k}_2 = -\mathbf{k}_{1'} + \mathbf{k}_1$, and the susceptibility χ is defined as

$$\chi(\mathbf{q}, \omega) = - \int \frac{d\mathbf{k}_2}{(2\pi)^2} \frac{f_2^0 - f_{2'}^0}{\epsilon_2 - \epsilon_{2'} + \omega + i0}. \quad (2.9)$$

Further evaluation of this expression will be discussed in the next section. Here, to round off the reviewing of this work I want to discuss why ψ_2 may be set to zero. In fact, the kinetic equation used in [14] is incomplete. This can be seen extremely clearly for the closed circuit set-up, i.e. no electric field, but finite current. Then nothing prevents the current in the drag layer to grow infinitely. To resolve this problem one must add the collision term for the electrons in the drag layer. Having done this it is possible to leave out the ψ_2 -terms in the inter-layer collision integral i.e. consider it as a functional of the equilibrium distribution function for the electrons in the drag layer. That is justified as the correction to this distribution function must be proportional both to the non-equilibrium part of the distribution function in the drive layer (i.e. to the electric field E_1) and to the inter-layer interaction squared (as the scattering probability $w(q)$ is proportional to it). That means that keeping ψ_2 in the inter-layer collision term would result in a term containing the 4th power of the interaction, which is small compared to the intra-layer

collision integral. Taking some specific (for example τ -approximation) form of the intra-layer collision term and using the zero-current condition

$$\int dk_2 \frac{\partial \epsilon_2}{\partial k_2} f_2^0 (1 - f_2^0) \psi_2 = 0, \quad (2.10)$$

one can in principle find ψ_2 which is *not* equal to zero. (In fact the Boltzmann equation with the intra-layer collision term gives ψ_2 as a function of E_2 , the latter is then found from the condition for the current to be 0.) But to determine E_2 it is not needed: it is enough to multiply the Boltzmann equation by k_2 and integrate over k_2 — that is exactly what is done in the paper — then the intra-layer collision term disappears due to the fact that there is no current in the drag layer. This explains why using a physically wrong form of the Boltzmann equation the authors still got a physically consistent and correct result for the drag. I will refer to this arguments later, in the main part of the work.

In the work [15] the authors derive the same equation (2.7) using the memory function formalism. Reviewing this work lies beyond the scope of the present thesis.

2.3.3 Diagrammatic approach.

An important step in the theoretical understanding of drag was made in 1995 by Kamenev and Oreg [16]. They formalized all what was done before them and got some new results, and, what is more important, showed how this problem can be handled generally and how, in principle, new results can be obtained. The authors used the general linear response theory method, i.e. the Kubo formula in its diagrammatic representation. The calculations were done in the lowest non-vanishing order in the inter-layer interaction, all intra-layer effects (electron-electron interaction, impurities etc.) can, in principle, be included up to arbitrary order of perturbation theory in their method.

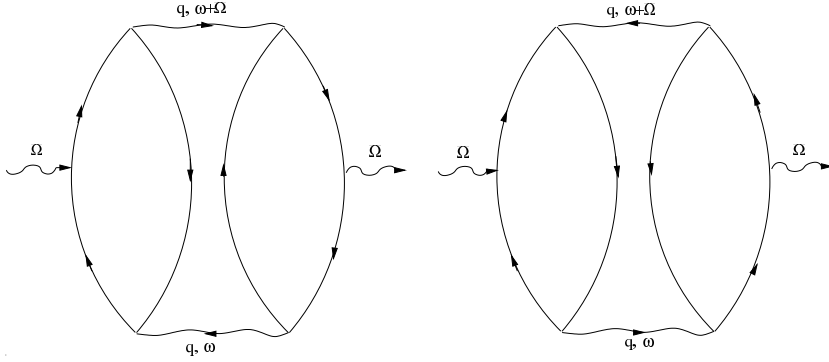


Figure 2.8: Two diagrams contributing to the transconductance to the second order in the inter-layer interaction.

The starting point is the general linear response expression of the conductivity via a current-current correlation function.

$$\sigma_D^{ij}(\vec{Q}, \Omega) = \frac{1}{\Omega S} \int_0^\infty dt e^{i\Omega t} \left\langle \left[J_1^{i\dagger}(\vec{Q}, t), J_2^j(\vec{Q}, 0) \right] \right\rangle. \quad (2.11)$$

Here $i, j = \hat{x}, \hat{y}$; \vec{Q}, Ω are the wave vector and the frequency of the external field, respectively; S is the area of the sample; and J_l^i is the i th component of the current operator in the l th layer. Diagrams corresponding to Eq. (2.11) include two separate electron loops with a vector (current) vertex on each one of them, coupled only by the inter-layer interaction lines. The first non-vanishing order in the limit $\vec{Q} \rightarrow 0$ in the inter-layer interaction is the second order. In this order there are two diagrams, shown in Fig. 2.8.

Analytically, this two diagrams may be written in a symmetric form:

$$\sigma_D^{ij} = \frac{T}{2i\Omega_m S} \sum_{\vec{q}, \omega_n} \Gamma_1^i(\vec{q}, \omega_n + \Omega_m, \omega_n) \Gamma_2^j(\vec{q}, \omega_n, \omega_n + \Omega_m) U(\vec{q}, \omega_n + \Omega_m) U(\vec{q}, \omega_n), \quad (2.12)$$

where T is the temperature, $U(\vec{q}, \omega)$ is the inter-layer screened Coulomb interaction and the vector $\vec{\Gamma}_{1(2)}(\vec{q}, \omega_1, \omega_2)$ is the three-legged object given by the two diagrams depicted in Fig. 2.9 (the factor $1/2$ in Eq. (2.12) is included to prevent double counting). In Eq. (2.12) the usual Matsubara technique with $\Omega_m = 2\pi imT$ is employed. After summing over the boson frequencies

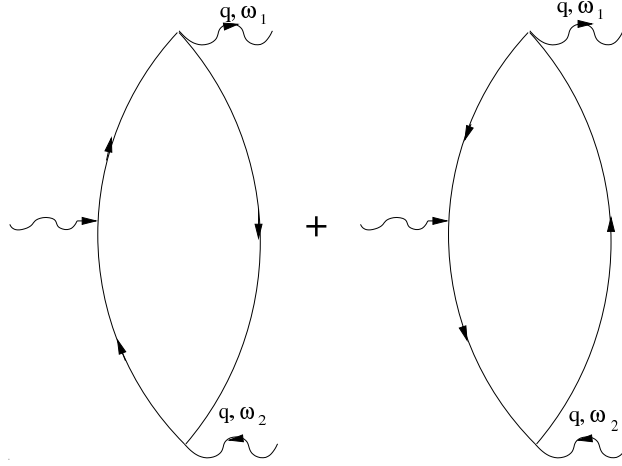


Figure 2.9: Diagrams defining the three-legged vertex, $\Gamma(\vec{q}, \omega_1, \omega_2) = \Gamma(-\vec{q}, -\omega_1, -\omega_2)$

ω_n , one should perform an analytical continuation to real values of Ω , and finally the limit $\Omega \rightarrow 0$ should be taken. The sum over ω_n is done by a contour integration in the complex ω plane along the contour shown in Fig. 2.10.

After the sum over ω_n is taken we can finally perform the analytical continuation $\Omega_m \rightarrow \Omega$ and take the limit $\Omega \rightarrow 0$. The result is:

$$\sigma_D^{ij} = \frac{1}{16\pi TS} \sum_{\vec{q}} \int_{-\infty}^{\infty} \frac{d\omega}{\sinh^2 \frac{\omega}{2T}} \Gamma_1^{i+-}(\vec{q}, \omega, \omega) \Gamma_2^{j-+}(\vec{q}, \omega, \omega) |U^+(\vec{q}, \omega)|^2. \quad (2.13)$$

The $+$, $-$ indices indicate the way the analytical continuation is performed, see Fig. 2.11 for explanation.

Eq. (2.13) gives the final expression for the transconductivity. The important feature is that the integrand decouples into one part depending only on the interaction potential and two other factors, that are functions of the layers' properties only. The latter factors, i.e. the Γ 's are called the rectification coefficients. They are in fact nonlinear susceptibilities of the two-dimensional electron gases in an external ac field, and give the proportionality coefficient between the square of a time-dependent scalar potential $\phi(\vec{q}, \omega)$ and the dc

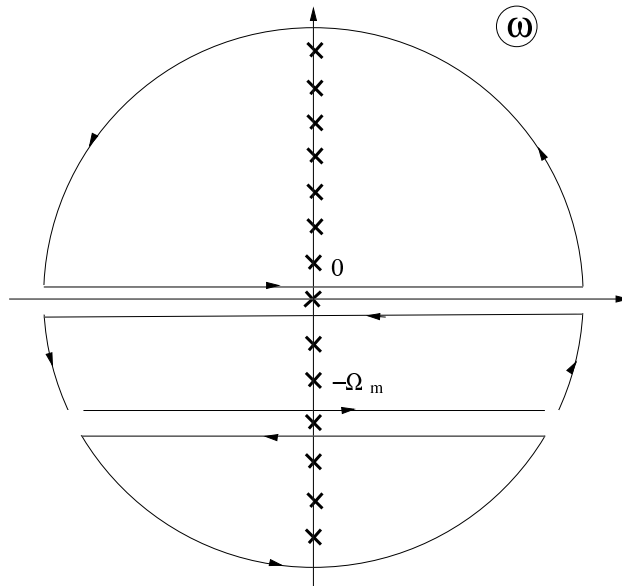


Figure 2.10: The contour of integration in the complex ω plane employed to perform the sum over the Matsubara boson frequencies in Eq. (2.12).

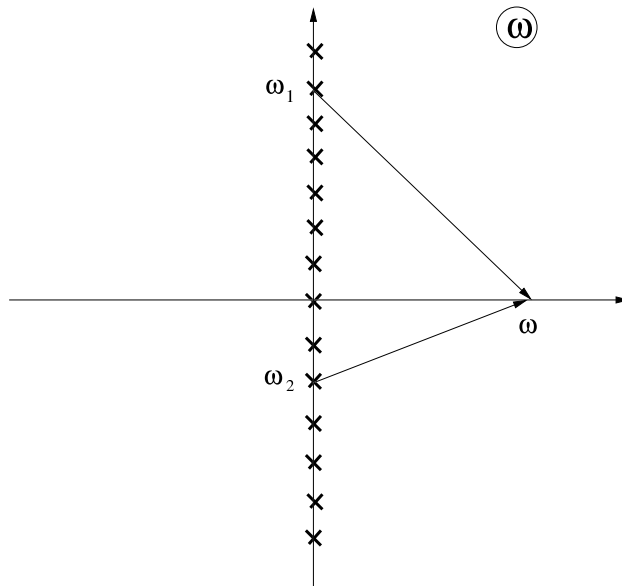


Figure 2.11: The way in which the analytical continuation of $\vec{\Gamma}(\vec{q}, \omega_1, \omega_2) \longrightarrow \vec{\Gamma}^{+-}(\vec{q}, \omega, \omega)$ is performed.

current in a layer:

$$\vec{J} = \vec{\Gamma}^{-+} |\phi(\vec{q}, \omega)|^2. \quad (2.14)$$

The next parts of the paper are devoted to evaluating of the general formula (2.13) in different cases. To this end the authors calculate the nonlinear susceptibility Γ . The case of normal metals without intra-layer interaction is considered. Then

$$\vec{\Gamma}(\vec{q}, \omega_1, \omega_2) = T \sum_{\epsilon_n} \text{Tr} \left\{ \mathcal{G}_{\epsilon_n} \mathcal{G}_{\epsilon_n + \omega_2} \hat{I} \mathcal{G}_{\epsilon_n + \omega_1} + \mathcal{G}_{\epsilon_n} \mathcal{G}_{\epsilon_n - \omega_1} \hat{I} \mathcal{G}_{\epsilon_n - \omega_2} \right\} \quad (2.15)$$

Here \mathcal{G} stands for the one-electron Green function and the trace is taken over exact eigenstates of the disordered system. The sum over fermionic Matsubara frequencies is evaluated similarly to the sum over bosonic frequencies. After the analytical continuation (as shown in Fig. 2.11) the final result for the nonlinear susceptibility reads:

$$\begin{aligned} \vec{\Gamma}^{+-}(\vec{q}, \omega, \omega) &= \frac{1}{4\pi i} \int d\epsilon \left(\tanh \frac{\epsilon + \omega}{2T} - \tanh \frac{\epsilon}{2T} \right) \text{Tr} \left[(\mathcal{G}_{\epsilon}^{-} - \mathcal{G}_{\epsilon}^{+}) \mathcal{G}_{\epsilon + \omega}^{-} \hat{I} \mathcal{G}_{\epsilon + \omega}^{+} \right] \\ &+ \{ \vec{q}, \omega \longrightarrow -\vec{q}, -\omega \}. \end{aligned} \quad (2.16)$$

Here \mathcal{G}^{\pm} stands for the retarded (advanced) single-electron Green function. This result is valid in the absence of a magnetic field, when the trace of three advanced or three retarded Green functions vanishes.

Then the authors evaluate the last formula in special cases of clean and dirty systems and find that in the absence of intra-layer electron-electron correlations the main results of previous works [14, 15] (i.e. expressing the drag signal via the imaginary parts of polarization operators (2.7)) holds, though not generally, rather only up to the first non-vanishing order in $1/\epsilon_F \tau$, where ϵ_F is the Fermi energy and τ is the elastic mean free time.

In order to do it, they take the simplest model, i.e. delta-correlated impurities, and calculate the diagram for Γ (Fig. 2.9) in the diffuson approximation (in the next section, also the weak-localization corrections are considered). The result in the diffusive regime ($\omega \ll 1/\tau$ and $q \ll 1/l$ [$l = v_F \tau$ is the

mean free path]) is:

$$\vec{\Gamma}^{+-}(\vec{q}, \omega, \omega) = e \frac{2D\vec{q}}{\epsilon_F} \left[2S\nu \frac{\omega Dq^2}{(Dq^2)^2 + \omega^2} \right], \quad (2.17)$$

here D is the diffusion coefficient and ν is the density of states at the Fermi level. The expression (2.17) has the form

$$\vec{\Gamma}^{+-}(\vec{q}, \omega, \omega) = \vec{\Gamma}^{-+}(\vec{q}, \omega, \omega) = e \frac{2D\vec{q}}{\epsilon_F} \Im \Pi^+(\vec{q}, \omega), \quad (2.18)$$

with

$$\Pi^+(\vec{q}, \omega) = 2S\nu \frac{Dq^2}{Dq^2 - i\omega} \quad (2.19)$$

being the polarization operator in the diffusive regime.

For the ballistic regime ($q > 1/l$ or $\omega > 1/\tau$) Γ turns out to be

$$\vec{\Gamma}^{+-}(\vec{q}, \omega, \omega) = e \frac{2D\vec{q}}{\epsilon_F} \left[2S\nu \frac{\omega}{v_F q} \theta(v_F q - \omega) \right], \quad (2.20)$$

where $\theta(x)$ is the Heaviside step function. As in the previous case, this expression has the form (2.18) with

$$\Im \Pi^+(\vec{q}, \omega) = 2S\nu \frac{\omega}{v_F q} \theta(v_F q - \omega). \quad (2.21)$$

An important observation, that one could make, is that the above results can be obtained only if one takes into account the non-linearity of the dispersion around the Fermi surface. More precisely, two terms in Eq. (2.16) cancel each other if the calculations are done in a usual way, by linearizing the dispersion near the Fermi surface. From the physical point of view it means that the electron-hole asymmetry is crucial for the Coulomb drag. If we had exact electron-hole symmetry the electron and hole drags would cancel each other completely.

Ultimately the drag conductivity is calculated. Here I'll list the results in different cases. It is distinguished between the results for ballistic, $l \gg d$ and diffusive, $l \ll d$ samples. In the former case, the dominant contribution to the transresistance comes from the ballistic part of the plane ($\omega < v_F q$, $q > 1/l$, see Fig. 2.12) and one can obtain:

$$\rho_D = \frac{\hbar}{e^2} \frac{\pi^2 \zeta(3)}{16} \frac{T^2}{\epsilon_{F_1} \epsilon_{F_2}} \frac{1}{(\kappa_1 d)(\kappa_2 d)} \frac{1}{(k_{F_1} l_1)(k_{F_2} l_2)}, \quad (2.22)$$

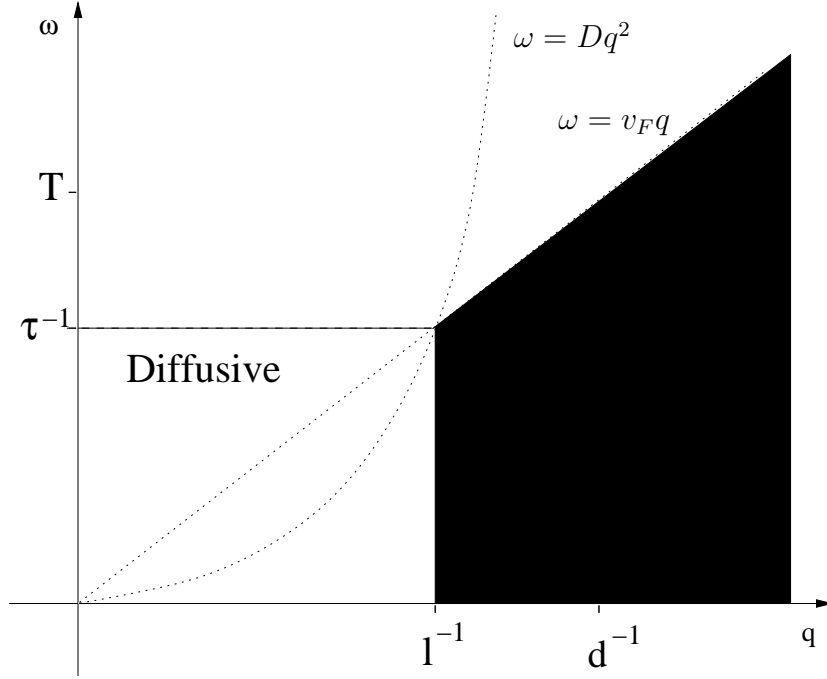


Figure 2.12: Domains in the (q, ω) plane. The dashed area represents (schematically) the regions where $\Im\Pi^+ \neq 0$.

where $\kappa_{1,2}$ are the Thomas-Fermi momenta in the two layers.

On the contrary, for diffusive samples the entire contribution comes from the diffusive part of the (q, ω) -plane ($\omega < 1/\tau$, $q < 1/l$). For $T \ll \min(\tau^{-1}, T_0)$ [where $T_0 \equiv D \min(\kappa_1, \kappa_2)/d$ arises due to divergence of the interaction potential at small momenta] one obtains

$$\rho_d = \frac{\hbar \pi^2}{e^2} \frac{T^2}{12 \epsilon_{F_1} \epsilon_{F_2}} \ln \frac{T_0}{2T} \frac{1}{(\kappa_1 d)(\kappa_2 d)} \frac{1}{(k_{F_1} d)(k_{F_2} d)}. \quad (2.23)$$

For higher temperatures, $T, T_0 \gg \tau^{-1}$, the energy integration is dominated by the region $\omega \approx \tau^{-1}$, the result is

$$\rho_D \approx \frac{\hbar}{e^2} \ln T_0 \tau \frac{1}{(\kappa_1 d)(\kappa_2 d)} \frac{1}{(k_{F_1} l_1)(k_{F_2} l_2)}. \quad (2.24)$$

Actually in this temperature region the plasmon contribution becomes dominant (see for example [17]), but this goes far beyond the scope of the present work.

Table 2.1: Temperature and inter-layer distance dependence of the drag coefficient, ρ_D , for different mobilities.

$T \ll \min(T_0, \tau^{-1})$		$T \gg \min(T_0, \tau^{-1})$
$l \ll d$	$d^{-2}T^2 \ln T$	$d^{-2}T$
$l \gg d$	$d^{-4}T^2$	

To summarize, I give the dependence of the drag resistance on the temperature and the inter-layer distance for different parameter ranges in table 2.1.

To finish off the review of this very important paper, I'll mention that in section IV the authors calculated the corrections to the drag resistance due to weak localization and in section VI the drag above the superconductor transition was considered. In the former case the formula (2.18) was found to be correct in the lowest order in $1/k_F l$, while in the latter case, where the intra-layer electron correlations play an important role, this formula turned out to be wrong. This shows that although the diagrammatic approach does reproduce the old results, they are not general enough and under specific conditions the old approach fails.

2.3.4 Magneto-drag. Early diagrammatic approach.

After the publication of the work discussed in the previous section the next logical step would be to extend the diagrammatic approach to the drag in presence of a strong quantizing magnetic field. This was done by M. C. Bønsager et al. in 1997. This section is devoted to a critical review of their work. The starting point was the same as in the work of Kamenev and Oreg, i.e. the drag was expressed in terms of a convolution of two rectification coefficients. The results of the paper are all based on expressing the rectification coefficient (triangle function) in terms of the imaginary part of the polarization function (see (2.18)). As we will see, unlike the case without magnetic field

that was considered in the previous section, here the authors did not show rigorously that the formula (2.18) is correct, so all their results are based on an *assumption* that it is true.

The starting point of their calculations is the formula (2.13). Then they try to prove the relation (2.18) in presence of magnetic field in the limit $\omega_c\tau \gg 1$ (ω_c being the cyclotron frequency). Doing this the authors make some dubious statements (see Appendix B of their work) which turn out to be not correct, most importantly, the claim that the scalar vertex corrections are negligible for $n \neq n'$ is wrong. The direct calculations in work [18] show this. Also only the delta-correlated disorder case is considered, which is rather far from real experimental conditions.

The results of the work consist in a numerical evaluation of the resulting expression for the drag resistivity

$$\rho_{12}^{xx} = -\frac{\hbar^2}{4e^2 n_1 n_2 k_B T} \frac{1}{S} \sum_q a^2 \int \frac{d\omega}{2\pi} |U(q, \omega)|^2 \frac{\Im \Pi_1(q, \omega) \Im \Pi_2(q, \omega)}{\sinh^2 \hbar\omega/2k_B T}, \quad (2.25)$$

which is obtained by substituting (2.18) into (2.13) and inverting the transconductivity tensor. $U(q, \omega)$ is taken in the random phase approximation, i.e.

$$U(q, \omega) = \frac{V_{12}(q)}{[1 - \Pi(q, \omega)V_{11}(q)]^2 - [\Pi(q, \omega)V_{12}(q)]^2}, \quad (2.26)$$

V_{11} and V_{12} being the non-screened intra- and inter-layer Coulomb electron-electron interactions. The layers were assumed identical i.e. $\Pi_1 = \Pi_2 \equiv \Pi$.

Further evaluation (particularly the expression for $\Pi(q, \omega)$) in the work is also based on the erroneous omitting of the scalar vertex correction for $n \neq n'$ and thus does not merit a special discussion.

2.3.5 Negative magneto-drag. First explanation attempt.

The results of the experimental works [2, 3] remained for quite a while completely understood. Indeed, from the generally accepted formula (2.25) it

is absolutely impossible to get negative drag due to analytical properties of the imaginary part of the polarization function. So the obvious decision is to go one step back, to the expression (2.13) and try to make a more careful analysis. The first attempt to do this was made by F. von Oppen et al. in 2001 [19]. In this work an evaluation of the triangle function Γ was made. Unfortunately there was a mistake in the calculations for the experimentally relevant ballistic limit, that led to a completely wrong result: negative drag occurred for matched densities and not for mismatched as one observes experimentally.

Still I think it is worth presenting this work here for several reasons, the most important of which is a very simple semiclassical derivation of the non-linear susceptibility that gives a simple and clear physical picture of it, and also, in principle, can give a negative value for the drag resistivity. This derivation is based on the assumption that the current is related to the electric field locally in time and space and that the conductivity depends only on the local density of charge carriers:

$$\mathbf{J}(\vec{r}, t) = -\hat{\sigma}[n(\vec{r}, t)]\nabla\phi(\vec{r}, t). \quad (2.27)$$

In addition to the current, the perturbation $\phi(\mathbf{q}, \omega)$ also induces a density perturbation $\delta n(\mathbf{q}, \omega) = -\Pi(\mathbf{q}, \omega)e\phi(\mathbf{q}, \omega)$ due to the polarizability $\Pi(\mathbf{q}, \omega)$. Up to quadratic order in the applied potential,

$$\mathbf{J}(\vec{r}, t) = -\left[\hat{\sigma}(n_0) + \frac{d\hat{\sigma}}{dn}\delta n(\vec{r}, t)\right]\nabla\phi(\vec{r}, t). \quad (2.28)$$

Taking the time and space average of the second term yields a dc contribution to the current given by

$$\mathbf{J}_{dc} = -\sum_{\mathbf{q}, \omega} \left(\frac{d\hat{\sigma}}{dn}\right) [\Pi(\mathbf{q}, \omega)e\phi(\mathbf{q}, \omega)i\mathbf{q}\phi(-\mathbf{q}, -\omega)], \quad (2.29)$$

or, equivalently, the rectification coefficient is given by

$$\Gamma(\mathbf{q}, \omega) = \frac{d\hat{\sigma}}{d(en)} \cdot \mathbf{q}\Im\Pi(\mathbf{q}, \omega). \quad (2.30)$$

At zero magnetic field this expression reproduces (2.18) and thus leaves no possibility for drag sign change. On the contrary, in presence of a magnetic field, in the quantum Hall and SdH regimes the derivative of the longitudinal component of the conductance changes sign as a function of the electron density. This opens the possibility for a sign change in the drag resistivity as a function of density. Substituting (2.30) into (2.13) and inverting the transconductivity tensor one gets up to an overall positive pre-factor for the drag resistivity tensor:

$$\hat{\rho}_D \sim \hat{\rho}^p \frac{d\hat{\sigma}^p}{d(en)} \frac{d\hat{\sigma}^a}{d(en)} \hat{\rho}^a, \quad (2.31)$$

where $\hat{\rho}^{p(a)}$ and $\hat{\sigma}^{p(a)}$ are the resistivity and conductivity tensors of the passive (active) layer. This expression easily reproduces some standard results. In the absence of a magnetic field, the tensor structure is trivial. Observing that the conductivity increases (decreases) with increasing electron density for electron (hole) layers, we recover that coupled layers with the same type of charge carriers exhibit positive drag, while coupled electron-hole layers have a negative drag resistivity. If the system is strictly electron-hole symmetric, the derivative of the conductivity with respect to density vanishes and, consequently, there is no drag.

In the presence of strong magnetic fields new effects appears. To see this we can multiply out the products in (2.31), keeping in mind that already for quite small magnetic fields $\rho_{xy} \gg \rho_{xx}$. Up to an overall positive pre-factor:

$$\rho_{xx}^D \sim \rho_{xy}^p \left\{ \frac{d\hat{\sigma}_{yy}^p}{d(en)} \frac{d\hat{\sigma}_{yy}^a}{d(en)} + \frac{d\hat{\sigma}_{yx}^p}{d(en)} \frac{d\hat{\sigma}_{xy}^a}{d(en)} \right\} \rho_{yx}^a. \quad (2.32)$$

Generally, the derivative of the longitudinal conductivity σ_{xx} changes sign as the magnetic field or Fermi energy is varied in the SdH and integer quantum Hall regimes, being positive for less than half filled of the topmost Landau level and negative for more than half filled one. By contrast, the Hall conductivity generally increases monotonically with n , and its derivative is therefore positive.

The obvious problem with this result is that for equal densities in the two layers the drag is negative as $\rho_{xy} = -\rho_{yx}$ in contradiction with the experimental results [2, 3]. This is due to the fact that the above treatment can be justified only in the diffusive limit $\omega\tau, Dq^2\tau \ll 1$ which is experimentally irrelevant.

In order to calculate the rectification coefficient in the ballistic limit the authors use the diagrammatic approach, starting from the expression (2.16) from the work [16]. Here a mistake was made, as we will see later, this equation is inapplicable in the presence of a magnetic field, as important terms involving traces of three Green's functions of the same type are omitted. Thus further reviewing of this work may be only of calculational interest and will therefore not be done.

2.3.6 Diagrammatic calculation of magneto-drag in the SCBA.

The work [19] gave the wrong result in the experimentally relevant ballistic limit. But the idea of the work was mainly correct. This line was drawn to its logical end in the work [18] which I will review in this section.

In this work the authors calculated the magneto-drag diagrammatically in the self-consistent Born approximation i.e. for short-range disorder, which is rather not the experimentally relevant case. Still, it is quite important to look at one of the limiting cases (high Landau levels, intermediate magnetic fields), and as this was done in the considered work and as the results are similar to the experimentally observed data I can not leave this work out of consideration.

The starting point is once again the expression (2.12) which is evaluated in the standard way by going from the summation over Matsubara frequencies to contour integration (see sec. 2.3.3, particularly Fig. 2.10). The triangle function $\Gamma(\mathbf{q}, \omega)$ is then obtained by analytic continuation like in sec. 2.3.3,

see Fig. 2.11. and is given by $\mathbf{\Gamma} = \mathbf{\Gamma}^{(a)} + \mathbf{\Gamma}^{(b)}$ with the two contributions:

$$\begin{aligned} \mathbf{\Gamma}^{(a)}(\mathbf{q}, \omega) = & \int \frac{d\epsilon}{4\pi i} \tanh \frac{\epsilon + \omega - \mu}{2T} \text{Tr} \{ \mathbf{v} \mathcal{G}^+(\epsilon + \omega) e^{i\mathbf{q}\mathbf{r}} \mathcal{G}^+(\epsilon) e^{-i\mathbf{q}\mathbf{r}} \mathcal{G}^+(\epsilon + \omega) \\ & - \mathbf{v} \mathcal{G}^-(\epsilon + \omega) e^{-i\mathbf{q}\mathbf{r}} \mathcal{G}^-(\epsilon) e^{i\mathbf{q}\mathbf{r}} \mathcal{G}^-(\epsilon + \omega) \} + (\omega, \mathbf{q} \rightarrow -\omega, -\mathbf{q}), \end{aligned} \quad (2.33)$$

$$\begin{aligned} \mathbf{\Gamma}^{(b)}(\mathbf{q}, \omega) = & \int \frac{d\epsilon}{4\pi i} \left(\tanh \frac{\epsilon + \omega - \mu}{2T} - \tanh \frac{\epsilon + -\mu}{2T} \right) \\ & \times \text{Tr} \{ \mathbf{v} \mathcal{G}^-(\epsilon + \omega) e^{i\mathbf{q}\mathbf{r}} [\mathcal{G}^-(\epsilon) - \mathcal{G}^+(\epsilon)] e^{-i\mathbf{q}\mathbf{r}} \mathcal{G}^+(\epsilon + \omega) \} + (\omega, \mathbf{q} \rightarrow -\omega, -\mathbf{q}). \end{aligned} \quad (2.34)$$

Here \mathcal{G}^\pm denotes the advanced (retarded) Green function for a given realization of the random potential. Note that for zero magnetic field only $\mathbf{\Gamma}^{(b)}$ survives [16]. By contrast, in strong magnetic fields both $\mathbf{\Gamma}^{(a)}$ and $\mathbf{\Gamma}^{(b)}$ should be retained. In the work [19] $\mathbf{\Gamma}^{(a)}$ was left out which led to wrong results in the ballistic limit.

For small ω , the expressions for $\mathbf{\Gamma}(\mathbf{q}, \omega)$ simplify to

$$\mathbf{\Gamma}^{(a)}(\mathbf{q}, \omega) = \frac{\omega}{2\pi i} \text{Tr} \{ \mathbf{v} \mathcal{G}^+(\epsilon_F) e^{i\mathbf{q}\mathbf{r}} \mathcal{G}^+(\epsilon_F) e^{-i\mathbf{q}\mathbf{r}} \mathcal{G}^+(\epsilon_F) - (\mathcal{G}^+ \rightarrow \mathcal{G}^-) \}, \quad (2.35)$$

$$\mathbf{\Gamma}^{(b)}(\mathbf{q}, \omega) = \frac{\omega}{\pi i} \text{Tr} \{ \mathbf{v} \mathcal{G}^-(\epsilon_F) e^{i\mathbf{q}\mathbf{r}} [\mathcal{G}^-(\epsilon_F) - \mathcal{G}^+(\epsilon_F)] e^{-i\mathbf{q}\mathbf{r}} \mathcal{G}^+(\epsilon_F) \}. \quad (2.36)$$

For well-separated Landau levels this approximation holds as long as ω is small compared to the Landau level width Δ . We also mention that $\mathbf{\Gamma}^{(a)}(\mathbf{q}, \omega)$ gives only a longitudinal contribution (parallel to \mathbf{q}) to $\mathbf{\Gamma}(\mathbf{q}, \omega)$.

Then the averaging over impurities is done using the SCBA [20]. White-noise disorder is assumed:

$$\langle U(r)U(r') \rangle = \frac{1}{2\pi\nu\tau} \delta(r - r'). \quad (2.37)$$

The SCBA (it neglects the crossing impurity diagrams) gives the leading contribution in the high Landau levels. Although the authors realize that this approximation is, strictly speaking, not justified for the experimental samples, where the disorder potential is correlated on the scale of the distance between the two-dimensional sample and the donor layer, they still expect their results to reflect reality adequately.

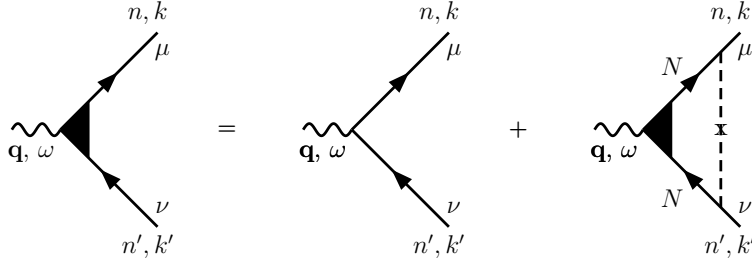


Figure 2.13: Diagrammatic representation of the equation for the vertex corrections $\gamma_{nk,n'k'}^{\mu\nu}(\epsilon + \omega, \epsilon, \mathbf{q})$ of the scalar vertices in the SCBA [18].

The impurity averaged Green function (denoted by $G^\pm(\epsilon)$) in the SCBA is given by the expression

$$G_n^\pm(\epsilon) = \frac{1}{\epsilon - E_n - \Sigma^\pm(\epsilon)}, \quad (2.38)$$

with the Landau energies $E_n = \hbar\omega_c(n + 1/2)$. For energies ϵ within a Landau level, the self-energy is given by

$$\Sigma_n^\pm(\epsilon) = \frac{1}{2}\{\epsilon - E_n \pm i[\Delta^2 - (\epsilon - E_n)^2]^{1/2}\}. \quad (2.39)$$

The broadening of the Landau level Δ can be expressed in terms of the zero-field scattering time τ as

$$\Delta^2 = \frac{2\omega_c}{\pi\tau}. \quad (2.40)$$

For white-noise disorder there is no correction of the vector vertex in $\mathbf{\Gamma}$, while the corrections of the scalar vertices include impurity ladders (see Fig. 2.13).

$$\gamma_{nk,n'k'}^{\mu\nu}(\epsilon + \omega, \epsilon, \mathbf{q}) = \gamma^{\mu\nu}(\mathbf{q}, \omega) \langle nk | e^{i\mathbf{q}\mathbf{r}} | n'k' \rangle. \quad (2.41)$$

Here, the indices $\mu, \nu = \pm$ indicate the type of Green functions involved in the vertex; ϵ is set to ϵ_F . For $\Delta \ll \hbar\omega_c$ the vertex corrections at $\omega = 0$ are

$$\gamma^{++}(\mathbf{q}, \omega = 0) = \frac{1}{1 - J_0^2(qR_c)[\Delta/2\Sigma^-]^2}, \quad (2.42)$$

$$\gamma^{+-}(\mathbf{q}, \omega = 0) = \frac{1}{1 - J_0^2(qR_c)}, \quad (2.43)$$

where $J_n(z)$ denotes the Bessel functions.

The bare vertex is given by

$$\begin{aligned} \langle nk|e^{i\mathbf{q}\mathbf{r}}|n'k'\rangle &= \delta_{q_y, k-k'} \frac{2^{n-n'} n!}{n!} \exp \left[-\frac{1}{4} q^2 l_H^2 - \frac{i}{2} q_x (k+k') l_H^2 \right] \\ &\times [(q_y + i q_x) l_H]^{n-n'} L_{n-n'}^{n-n'}(q^2 l_H^2 / 2), \end{aligned} \quad (2.44)$$

where $l_H = (\hbar c / eH)^{1/2}$ is the magnetic length and L_m^n is the associated Laguerre polynomial and $n \geq n'$. The expression for the matrix element for $n < n'$ can be obtained from Eq. (2.44) by complex conjugation with the replacement $q \rightarrow -q$, $nk \leftrightarrow n'k'$. For high Landau levels, which are considered in [18], $n, n' \gg 1$, $|n - n'|$ and $q \ll k_F$, Eq. (2.44) can be simplified to

$$\langle nk|e^{i\mathbf{q}\mathbf{r}}|n'k'\rangle = \delta_{q_y, k-k'} i^{n-n'} e^{-i\phi_q(n-n')} e^{-iq_x(k+k')l_H^2/2} J_{n-n'}(qR_c^{(m)}), \quad (2.45)$$

where ϕ_q is the polar angle of \mathbf{q} , $R_c^{(n)} = l_H \sqrt{2n+1}$ is the cyclotron radius of the n th Landau level, and $m = (n + n')/2$.

Now I sum up the evaluation of the triangle vertex $\Gamma(\mathbf{q}, \omega)$. Let us first look at the leading order. As already mentioned $\Delta/\omega_c \ll 1$ and the valence Landau level $N \gg 1$. The relevant diagrams are shown on Fig. 2.14. In the lowest order in Δ/ω_c two of the three Green functions should be evaluated on the N th Landau level. The third one (adjacent to the vector vertex) should be taken on the $(N \pm 1)$ th Landau level as the matrix elements of the velocity are non-zero only for Landau levels differing by one:

$$\langle nk|v_x|n'k'\rangle = \delta_{kk'} \frac{i}{ml\sqrt{2}} (\sqrt{n}\delta_{n,n'+1} - \sqrt{n+1}\delta_{n,n'-1}), \quad (2.46)$$

$$\langle nk|v_y|n'k'\rangle = \delta_{kk'} \frac{1}{ml\sqrt{2}} (\sqrt{n}\delta_{n,n'+1} + \sqrt{n+1}\delta_{n,n'-1}). \quad (2.47)$$

For $\omega, T \ll \Delta$ one gets, using the simplified expressions (2.35), (2.36),

$$\Gamma^{(a)}(\mathbf{q}, \omega) = -2\hat{\mathbf{q}} \frac{\omega R_c}{\pi^2 l_H^2} J_0(qR_c) J_1(qR_c) \frac{1}{2i} [G_N^+ \gamma^{++}]^2 - [G_N^- \gamma^{--}]^2, \quad (2.48)$$

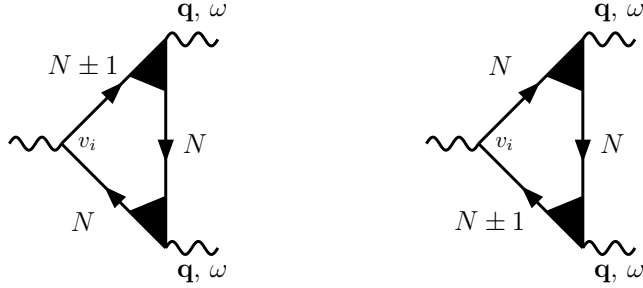


Figure 2.14: The diagrams, contributing to the triangle vertex in the SCBA to the leading order, in the limit of well-separated Landau levels and large N [18].

$$\begin{aligned} \mathbf{\Gamma}^{(b)}(\mathbf{q}, \omega) &= 2\hat{\mathbf{q}} \frac{\omega R_c}{\pi^2 l_H^2} J_0(qR_c) J_1(qR_c) \\ &\quad \times \frac{1}{2i} [G_N^+ \gamma^{++} \gamma^{+-} - G_N^- \gamma^{+-} \gamma^{--}] \cdot [G_N^+ + G_N^-]. \end{aligned} \quad (2.49)$$

Here $\hat{\mathbf{q}} \equiv \mathbf{q}/q$, $\gamma^{\mu\nu} \equiv \gamma^{\mu\nu}(\mathbf{q}, 0)$. The sum of the two contributions gives

$$\mathbf{\Gamma}(\mathbf{q}, \omega) = \hat{\mathbf{q}} \frac{4\omega R_c}{\pi^2 l_H^2} J_0(qR_c) J_1(qR_c) \Re[G_N^+(\gamma^{++} - \gamma^{+-})] \Im[G_N^+] \gamma^{++}. \quad (2.50)$$

For arbitrary T , $\omega < \omega_c$, this contribution takes the form

$$\begin{aligned} \mathbf{\Gamma}(\mathbf{q}, \omega) &= \hat{\mathbf{q}} \frac{8R_c}{\pi^2 l_H^2 \Delta^2} \frac{J_1(qR_c)}{J_0(qR_c)} \int_{-\infty}^{\infty} d\epsilon \left[\tanh \frac{\epsilon + \omega - \mu}{2T} - \tanh \frac{\epsilon - \mu}{2T} \right] \\ &\quad \times \Re[\gamma^{-+}(\mathbf{q}, \omega) - \gamma^{++}(\mathbf{q}, \omega)] \Im \gamma^{++}(\mathbf{q}, \omega). \end{aligned} \quad (2.51)$$

The q -integration in (2.12) is cut off at $q \sim 1/d$ (d is the interlayer distance). Thus, depending on the relation between R_c and d , one can distinguish between ballistic ($d \ll R_c$) and diffusive ($d \gg R_c$) regimes. In the typical experimental setups $R_c > d$ (for the magnetic fields for which the results of [18] are applicable), so the authors mainly concentrate on the ballistic regime in which both the ballistic ($qR_c \gg 1$) and diffusive ($qR_c \ll 1$) momenta are relevant.

For diffusive momenta γ^{+-} has a singular behavior, so γ^{++}, γ^{--} can be neglected compared to γ^{+-} . So only $\mathbf{\Gamma}^{(b)}$ contributes to (2.50). The result

is the equation (2.30) (multiplied by 2, as spin has been taken into account) with the SCBA conductivity [20]

$$\sigma_{xx} = \frac{e^2}{\pi^2} N \left[1 - \frac{(\mu - E_N)^2}{\Delta^2} \right], \quad (2.52)$$

and the polarization function in the diffusive limit given by Eq. (2.19), which is valid also in presence of the magnetic field if the diffusion constant $D(\epsilon) = R_c^2/2\tau(\epsilon)$ is taken to be energy dependent with the elastic scattering time in the SCBA being

$$\tau(\epsilon) = \frac{1}{\sqrt{\Delta^2 - (\epsilon - E_n)^2}}. \quad (2.53)$$

For ballistic momenta ($qR_c \gg 1$) $\gamma^{++}(\mathbf{q}, \omega) \approx \gamma^{+-}(\mathbf{q}, \omega) \approx 1$. Thus, in the leading order Eq. (2.50) yields zero. I emphasize that only the sum of the two contributions (2.48) and (2.49) vanishes, and not each of them separately. As in the work [19] the contribution (2.48) was missed, the result in that work in the ballistic limit is wrong. To calculate Γ in the ballistic limit it is therefore necessary to look at the next order contributions. There are three kinds of such contributions: (i) contributions of the order of $1/qR_c$, (ii) contributions of the order of Δ/ω_c , and (iii) contributions of the order of q/k_F . Here I present only the results.

(i). Keeping the contributions of the order of $1/qR_c$ in (2.42) and (2.43), and plugging them into (2.50) one gets for $\omega, T \ll \Delta$

$$\Gamma^{(1/qR_c)}(\mathbf{q}, \omega) = -\hat{\mathbf{q}} \frac{64\omega R_c (\mu - E_N) [\Delta^2 - (\mu - E_N)^2]^{3/2}}{\pi^2 l^2 \Delta^6} J_1(qR_c) J_0^3(qR_c). \quad (2.54)$$

For arbitrary $\omega, T < \omega_c$ one can also find the considered contribution by using Eq. (2.51). Here and for the two other contributions I present only the result for low temperatures.

(ii). Contributions of the order of Δ/ω_c come from two sources. First one can evaluate the diagrams in Fig. 2.14 more accurately, keeping the self-energy parts of the Green function of the Landau levels $N \pm 1$, and second one can consider the diagrams in Fig. 2.15. The result is

$$\Gamma^{(\Delta/\omega_c)} = -\hat{\mathbf{q}} \times \hat{\mathbf{z}} \frac{16\omega R_c (\mu - E_N) [\Delta^2 - (\mu - E_N)^2]}{\pi^2 l^2 \omega_c \Delta^4} J_1(qR_c) J_0(qR_c). \quad (2.55)$$

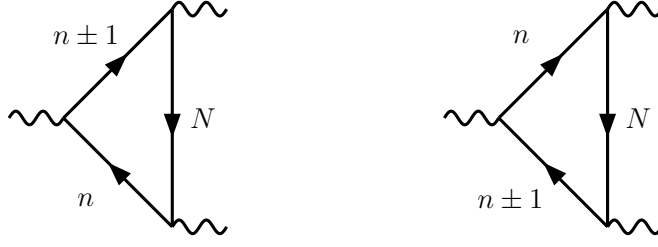


Figure 2.15: Diagrams contributing to the corrections of the order Δ/ω_c in the triangle vertex [18].

(iii). The contribution of the order of q/k_F arises from a more accurate treatment of the matrix elements involved in the scalar vertices, particularly, the dependence of R_c on the Landau level number. This contribution is the direct consequence of the zero- B electron spectrum curvature. For $T, \omega \ll \Delta$ it reads

$$\mathbf{\Gamma}^{(q/k_F)} = \mathbf{q} \times \hat{\mathbf{z}} \frac{8\omega \Delta^2 - (\mu - E_N)^2}{\pi^2 \Delta^4} J_0^2(qR_c). \quad (2.56)$$

Having computed the triangle vertex one can go on to calculate the drag resistivity. As the Hall conductivity dominates over the longitudinal one, the drag resistivity can be approximated by

$$\rho_{xx}^D \approx \rho_{xy}^{(1)} \sigma_{yy}^D \rho_{yx}^{(2)}, \quad (2.57)$$

or, using Eq. (2.12),

$$\rho_{xx}^D = -\frac{B}{en_1} \frac{B}{en_2} \frac{1}{9\pi} \int_{-\infty}^{\infty} \frac{d\omega}{2T \sinh^2(\omega/2T)} \times \int \frac{d^2\mathbf{q}}{(2\pi^2)} \Gamma_y^{(1)}(\mathbf{q}, \omega, B) \Gamma_y^{(2)}(\mathbf{q}, \omega, -B) |U_{12}(\mathbf{q}, \omega)|^2. \quad (2.58)$$

The overall minus sign is due to the relation $\rho_{xy} = -\rho_{yx}$. It follows that for identical layers, the longitudinal ($\mathbf{\Gamma} \propto \hat{\mathbf{q}}$) component $\mathbf{\Gamma}_{\parallel}$ of the triangle vertex gives rise to *negative* drag, since $\mathbf{\Gamma}_{\parallel}(-B) = \mathbf{\Gamma}_{\parallel}(B)$, while the transverse ($\mathbf{\Gamma} \propto \hat{\mathbf{z}} \times \hat{\mathbf{q}}$) component $\mathbf{\Gamma}_{\perp}$ yields *positive* drag as $\mathbf{\Gamma}_{\perp}(-B) = -\mathbf{\Gamma}_{\perp}(B)$.

In what follows the authors mainly concentrate on the ballistic regime

$$\omega_c/\Delta \ll R_c/d \ll N\Delta/\omega_c. \quad (2.59)$$

It turns out that in this regime the (ii) contribution (2.55) dominates over (2.54) and (2.56); indeed, this is easy to see by comparing the order of magnitude for these contributions. This is valid provided that the Landau level number is sufficiently high: $N > (\omega_c/\Delta)^2$. Without going into details of the calculation, I will just mention the result. For $T \ll \Delta$, the drag resistivity is given by

$$\rho_{xx}^D = \frac{32}{3\pi^2 e^2} \frac{1}{(k_F d)^2 (\kappa R_c)^2} \left(\frac{T^2}{\Delta} \right) \ln \left(\frac{R_c \Delta}{d \omega_c} \right) \times \left(\frac{\mu - E_N}{\Delta} \left[1 - \frac{(\mu - E_N)^2}{\Delta^2} \right] \right)_1 \left(\frac{\mu - E_N}{\Delta} \left[1 - \frac{(\mu - E_N)^2}{\Delta^2} \right] \right)_2. \quad (2.60)$$

The subscripts 1 and 2 mean that the whole parenthesis refers to the 1st(2nd) layer. This yields an *oscillatory* sign of the drag. For identical layers the drag is positive.

The authors also computed the drag resistance for other ranges of parameters. Without going into details of the calculations, I just show the results in form of a schematic plot, see Fig. 2.16.

In the section devoted to the comparison with the experiment the authors optimistically state that their results in the ballistic regime fully explain the experimental data. I find this statement somewhat exaggerated for the following reasons. First, the theory of the discussed paper predicts T^2 low-temperature dependence of ρ^D , while experimentalists claim the behavior is activated with the activation energy periodically depending on the filling factor. Second, for the ballistic regime in their terminology to be present in the first place the condition $N \gg (\omega_c/\Delta)^2$ must be fulfilled. Or in other words $N \gg \omega_c \tau \gg 1$. This condition makes doubtful the presence of the discussed regime, or in any case, restricts it to a quite narrow range of magnetic fields, while experimentally the negative drag is observed in a broad region of magnetic fields and the Landau level numbers for which it is observed range from $N = 4$ to $N \approx 40$. Indeed, taking the experimental parameters from [2]: $\Delta = 1.7\text{K}$ for $H = 0.1\text{T}$, I estimate $\tau \approx 0.5\text{K}^{-1}$. Thus $\omega_c \tau \approx 10 \cdot H[\text{T}]$. N for the electron density $n_0 = 2 \cdot 10^{11}\text{cm}^{-3}$ is equal to $4/H[\text{T}]$. Substituting the

above values into the condition $N \gg \omega_c \tau$, one obtains $H \ll 0.6T$ or $N \gg 7$. Then, the definition of the ballistic regime (2.59) reads

$$4 \cdot H[T]^{1/2} \ll \frac{70}{d[\text{nm}]B[T]} \ll \frac{1}{H[T]^{3/2}}.$$

Both these conditions restrict the magnetic field from above and for, say, $d = 35\text{nm}$ one gets $H \ll 0.25\text{T}$ from the second inequality and for $d = 100\text{nm}$ — $H \ll 0.3\text{T}$ from the first one. The condition $\omega_c \tau \gg 1$ yields $H \gg 0.1\text{T}$.

Thus it seems very desirable to elaborate a theory which is valid for high magnetic fields (low Landau levels) and accounts for the long-range disorder and localization which is totally omitted in the approach elaborated by Gornyi *et al.* in [18].

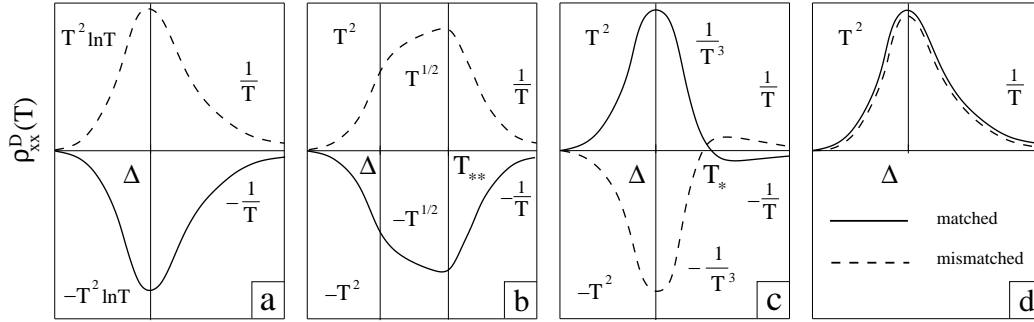


Figure 2.16: Schematic temperature dependence of the low-temperature drag in different regimes: (a) diffusive, $R_c/d \ll 1$; (b) weakly ballistic, $1 \ll R_c/d \ll \omega_c/\Delta$, $T_{**} \equiv \omega_c(d/R_c)$; (c) ballistic, $\omega_c/\Delta \ll R_c/d \ll N\Delta/\omega_c$, $T_* \equiv \Delta \ln^{1/2}(R_c\Delta/d\omega_c)$; (d) ultraballistic, $N\Delta/\omega_c \ll R_c/d$ [18].

2.4 Semiclassical theory of electron drag in strong magnetic fields

To accomplish the task defined at the end of the previous section it is necessary to work with long range disorder. Let us first consider the relevant length and energy scales in the double-layer system. The distance between

the layers varies from 30 to 120 nm. The disorder is due to remote donors, which leads to a smooth disorder potential with a correlation length ξ of order 50-100 nm. The Landau level broadening, which is related to the amplitude of the disorder potential, has been estimated from low-field Shubnikov-de-Haas oscillations to lie in the range 0.5-2 K [2, 3]. The magnetic fields at which drag minima at odd integer filling and/or negative drag at mismatched densities are observed vary over a relatively wide range from 0.1 T to 1 T for the cleanest samples, and up to 5 T for samples with a slightly reduced mobility. This corresponds to magnetic lengths l_H between 15 and 80 nm. Hence, ξ and l_H are generally of the same order of magnitude, which makes a quantitative theoretical analysis rather difficult.

Since the anomalous drag phenomena are observed over a wide range of fields, one may hope that qualitative insight can be gained also by analyzing limiting cases. For $\xi \ll l_H$ a treatment of disorder within the self-consistent Born approximation is possible [21]. This route has been taken by Gornyi et al. in the work [18] discussed above. Localization is not captured by the Born approximation, and consequently the resistivities obey power-laws rather than activated behavior for $T \rightarrow 0$. For stronger magnetic fields, on the other hand, localization will become important, and a semiclassical approximation is a better starting point, which is the route I take in what follows. Applying a criterion derived by Fogler et al. [22] I estimate that (classical) localization may set in already at 0.1 T. (According to Eq. (1.7) of [22] localization occurs for $B > \frac{\sqrt{mc^2 E_F}}{e\xi} \left(\frac{W}{E_F}\right)^{2/3}$, m being the effective mass and W the amplitude of the potential; substituting typical experimental values $\xi = 60\text{nm}$, $W = 1.7\text{K}$, $n = 2 \cdot 10^{11}\text{cm}^{-2}$ [2, 3, 13] one gets the above mentioned value.) The localization is classical in the sense that the electrons' classical trajectories are closed. From the quantum mechanical point of view it means that the electron's wave function is localized in space. More precisely, an electron is moving along the contours of equal energy of the random potential or, in a more general case, along the contours of equal energy of the averaged random potential defined as [22]:

$$U_0(x, y) = \oint \frac{d\phi}{2\pi} U(x + R_c \cos \phi, y + R_c \sin \phi). \quad (2.61)$$

These contours form closed loops, corresponding to localized states, except at a single energy ϵ_0 in the center of each Landau level, for which there is a percolating contour through the whole system (Fig. 2.17) [23, 24, 25, 26, 27]. If the Landau level broadening induced by the disorder potential and also $k_B T$ is much smaller than $\hbar\omega_c$, as is the case in the anomalous drag regime, all Landau levels except one are either fully occupied in the bulk of the whole sample or completely empty. At zero temperature and for $\epsilon_F < \epsilon_0$ the sample then consists of islands where the highest (partially) occupied Landau level is locally full, while it is locally empty in the rest of the sample; for $\epsilon_F > \epsilon_0$ the empty regions form islands. In reality, the percolating contour at the center of the Landau level is broadened to a percolation region for two reasons. First, electrons near the percolating contour can hop across saddle points from one closed loop to another, by using for a moment some of their cyclotron energy [22]. Second, electrons near the center of the Landau level can screen the disorder potential, such that the percolating equipotential line at ϵ_0 broadens to form equipotential terraces [28, 29]. Hence, there is a region around the percolating path, where states are extended.

The percolating region forms a two-dimensional random network consisting of links and crossing points [30]. For simplicity we assume that the links are straight lines (Fig. 2.18). The region near the link (except near the end points) can be parameterized by a Cartesian coordinate system with a variable y following the equipotential lines parallel to the link and x for the transverse direction. The disorder potential varies essentially only in transverse direction, and can thus be represented by a function $U(x)$. In the Landau gauge $\mathbf{A} = (0, Hx)$ the Hamiltonian for electrons on the link is then translation invariant in y -direction and the Landau states

$$\psi_{nk}(x, y) = C_n e^{-(x+l^2k)^2/(2l_H^2)} H_n[(x+l^2k)/l_H] e^{iky} \quad (2.62)$$

are accurate solutions of the stationary Schrödinger equation. Here H_n is the n -th Hermite polynomial and C_n a normalization constant. The correspond-

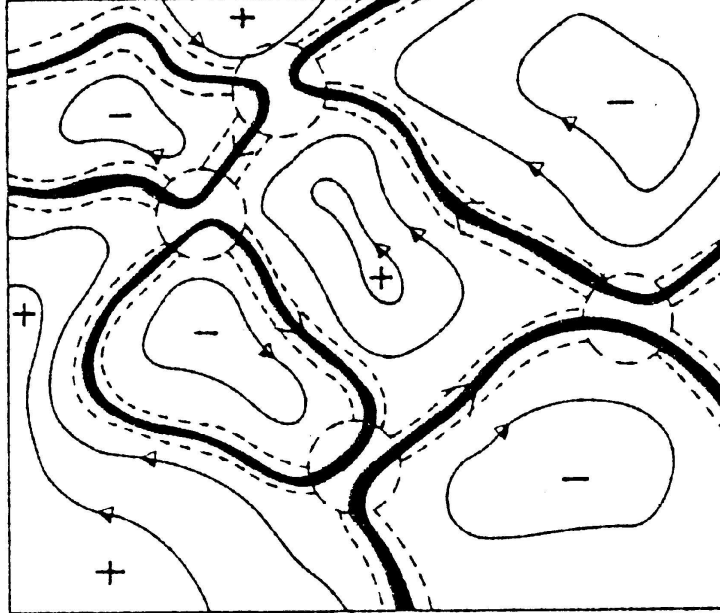


Figure 2.17: Schematic pattern of the contours of equal energy [24].

ing energy is simply

$$\epsilon_{nk} = (n + 1/2) \omega_c + U(l_H^2 k) . \quad (2.63)$$

In the following we drop the Landau level index n , because only the highest occupied level is relevant. The quantum number k is the momentum associated with the translation invariance in y -direction. It is proportional to a transverse shift $x_0 = l_H^2 k$ of the wave function. The potential U lifts the degeneracy of the Landau levels and makes energies depend on the momentum along the link. The group velocity

$$v_k = \frac{d\epsilon_k}{dk} = l_H^2 U'(x_0) \quad (2.64)$$

corresponds to the classical drift velocity of an electron in crossed electric and magnetic fields. In our simplified straight link approximation $U'(x_0)$ does not depend on y . In general it will depend slowly on the longitudinal coordinate, but near percolating paths away from crossing points it has a fixed sign, and hence the group velocity has a fixed direction, that is the motion on the links is chiral.

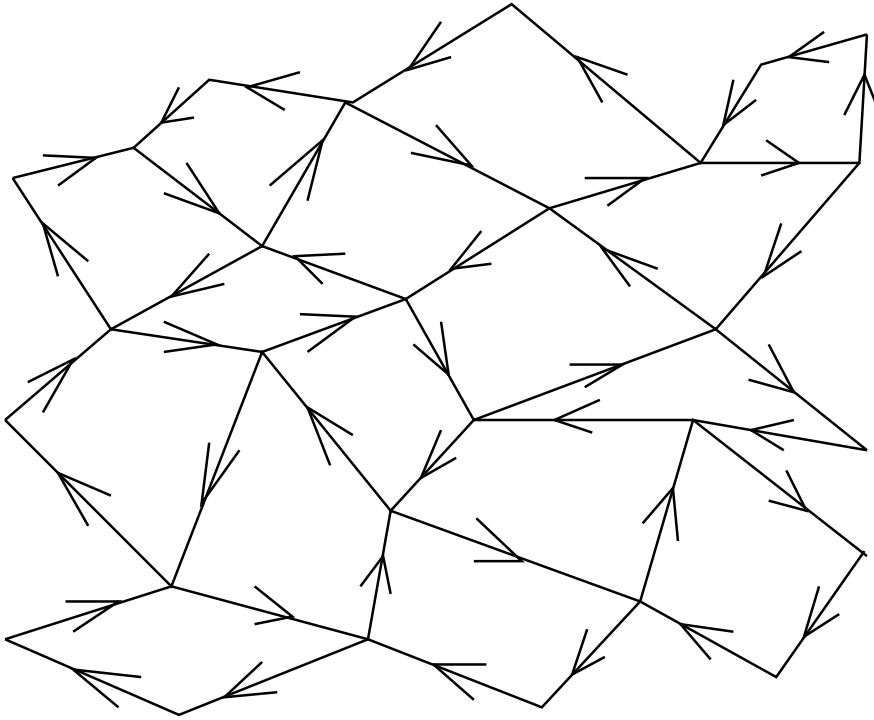


Figure 2.18: Schematic pattern of the percolating region network.

The drag between two parallel layers is dominated by electrons in the percolating region, corresponding to states near the center of the Landau level, since electrons in deeper localized states are not easily dragged along. In the network picture, macroscopic drag arises as a sum of contributions from interlayer scattering processes between electrons in different links. If no current is imposed in the drive layer, both layers are in thermal equilibrium and the currents on the various links cancel each other on average. Now assume that a small finite current is switched on in the drive layer such that the electrons move predominantly in the direction of the positive y -axis (the electric current moving in the opposite direction). This means that the current on links oriented in the positive y -direction is typically larger than the current on links oriented in the negative y -direction. Interlayer scattering processes lead to momentum transfers between electrons in the drive and drag layer. The preferred direction of momentum transfers is such

that the scattering processes tend to reduce the current in the drive layer, that is the interlayer interaction leads to friction.

Now the crucial point is that electrons moving in the disorder potential are not necessarily accelerated by gaining momentum in the direction of their motion, or slowed down by losing momentum (as for free electrons). The fastest electrons are those near the center of the Landau level: they have the highest group velocity on the links of the percolation network and they get most easily across the saddle points. Electrons in states below the Landau level center are thus accelerated by gaining some extra momentum in the direction of their motion, but electrons with an energy above ϵ_0 are pushed to still higher energy by adding momentum and are thus slowed down.

2.4.1 Drag between parallel links.

To make the above speculations more quantitative I consider drag between two parallel quasi one-dimensional links. Instead of the layers for the 2D case I take strips with infinite length which have a potential profile with its value depending only on the transverse coordinate x . The eigenstates of the electrons subjected to a magnetic field and the potential are similar to the eigenstates without the potential if the gauge is taken to be $(0, Hx, 0)$ (the y -axis is directed along the strip, H is the magnetic field). The difference is that the eigenfunctions have contributions from the adjacent Landau levels that results in a finite velocity of the electron proportional to the x -derivative of the potential (2.64). The wave-functions in the zeroth order in the potential are given by (2.62); the corresponding energies in first order of the potential are given by (2.63). From now on the magnetic length l_H will be set to unity, unless the contrary is explicitly mentioned.

This shows us that there is an effective dispersion law for the electron. The electron has got a finite mass if the second derivative of U with respect to x is non-zero. In the following calculations I neglect the intra-layer electron-electron scattering and consider only the interlayer interaction. The

corresponding Hamiltonian is of the form

$$\hat{H} = \sum_{n,p,\alpha=1,2} \left[\left(n + \frac{1}{2} \right) \omega_H + U_\alpha(p) \right] c_{\alpha,n,p}^\dagger c_{\alpha,n,p} + \int d^3\mathbf{r}_1 d^3\mathbf{r}_2 \hat{\psi}_1^\dagger(\mathbf{r}_1) \hat{\psi}_2^\dagger(\mathbf{r}_2) V(\mathbf{r}_1 - \mathbf{r}_2) \hat{\psi}_2(\mathbf{r}_2) \hat{\psi}_1(\mathbf{r}_1). \quad (2.65)$$

Here c, c^\dagger are the annihilation and creation operators of the electron in Landau basis, α labels the layers and

$$\hat{\psi}_\alpha(\mathbf{r}) = \sum_{n,p} c_{\alpha,n,p} \Psi_{n,p}(x, y) \delta(z + jd/2) \quad (2.66)$$

with d being the inter-layer distance and $j = 3 - 2\alpha$. Finally $V(\mathbf{r})$ is the Coulomb potential. Substituting (2.66) into (2.65) we obtain

$$\begin{aligned} \hat{H} = & \sum_{n,p,\alpha=1,2} \left[\left(n + \frac{1}{2} \right) \omega_H + U_\alpha(p) \right] c_{\alpha,n,p}^\dagger c_{\alpha,n,p} \\ & + \sum_{\substack{n_1 \dots n_4 \\ p_1 \dots p_4}} \left(c_{1,n_4,p_4}^\dagger c_{2,n_3,p_3}^\dagger c_{2,n_2,p_2} c_{1,n_1,p_1} \right. \\ & \left. \times \int d^2\mathbf{r}_1 d^2\mathbf{r}_2 \Psi_{n_4,p_4}^*(\mathbf{r}_1) \Psi_{n_3,p_3}^*(\mathbf{r}_2) \frac{e^2}{\sqrt{|\mathbf{r}_1 - \mathbf{r}_2|^2 + d^2}} \Psi_{n_2,p_2}(\mathbf{r}_2) \Psi_{n_1,p_1}(\mathbf{r}_1) \right). \end{aligned} \quad (2.67)$$

I model the distribution function in the drive layer in the following way (arguments in favor of this assumption will be given later):

$$n_1(\epsilon_1(n, p)) = n_1^0(\epsilon_1(n, p - \tilde{p})). \quad (2.68)$$

Here ϵ_i is the energy of the electron in i -th layer. It is given by (2.63); n_i is the distribution function and n_i^0 is the Fermi distribution function in the i -th layer

$$n_i^0(\epsilon) = \frac{1}{1 + \exp\left(\frac{\epsilon - \mu_i}{T}\right)},$$

μ_i being the chemical potential in the i -th layer and T the temperature. This assumption corresponds to the shifted Fermi sea for free electrons for velocity \tilde{p}/m . It can also be regarded as a p -dependence of the chemical potential:

$$\mu_1(p) = \mu_1 + \tilde{p} \frac{\partial \epsilon_1}{\partial p}. \quad (2.69)$$

This distribution leads to a non-zero total current in the layer as there are more electrons with positive velocity than those with negative, i.e. more "right-movers" than "left-movers". Expanding $n_1(\epsilon_1(n, p))$ in \tilde{p} we get

$$n_1(\epsilon_1(n, p)) \approx n_1^0(\epsilon_1(n, p)) + \frac{\tilde{p}}{T} \frac{\partial \epsilon_1}{\partial p} n_1^0(\epsilon_1(n, p)) (1 - n_1^0(\epsilon_1(n, p))). \quad (2.70)$$

\tilde{p} can be found knowing the current j_1 in the drive layer: $\tilde{p} = \frac{\pi j_1}{e v_{F1}}$

As the electrons in the two layers interact, the electrons in the drag layer will tend to rearrange, so that the drag current occurs also there. To describe the process quantitatively I use the kinetic equation approach with the collision integral determined in the two-particle approximation using Fermi's golden rule. I restrict myself to the case $T \ll \omega_H$ so that I don't need to take scattering processes that change the Landau level into account. Moreover, provided that condition is fulfilled, I only need to consider the upper Landau levels in both layers as no scattering processes are possible in any other levels due to Pauli principle. I refer to the Landau levels in drive and drag layer as n and n' respectively.

At this point I follow the line of calculations from the work [14] adapted to my model. A detailed review of this work can be found in the section 2.3.2 of the present work. The Boltzmann equation for my model reads:

$$\dot{p}_2 \cdot \frac{\partial n_2^0}{\partial p_2} = \left[\frac{\partial n_2}{\partial t} \right]_{\text{coll}}, \quad (2.71)$$

with $\dot{p}_2 = -eE_2$, where E_2 is the electric field leading to the drag voltage. The interlayer collision term is given by

$$\begin{aligned} \left[\frac{\partial n_2(p_2)}{\partial t} \right]_{\text{coll}}^{12} &= \frac{2\pi}{L} \int \frac{dp_1}{2\pi} \int \frac{dp_4}{2\pi} \int \frac{dp_3}{2\pi} \frac{2\pi}{\hbar} \left| \langle p_1, p_2 | \hat{V} | p_4, p_3 \rangle \right|^2 \\ &\quad \left[n_1(p_1) (1 - n_1(p_4)) n_2(p_2) (1 - n_2(p_3)) \right. \\ &\quad \left. - n_1(p_4) (1 - n_1(p_1)) n_2(p_3) (1 - n_2(p_2)) \right] \\ &\quad \times \delta(\epsilon_1(p_1) + \epsilon_2(p_2) - \epsilon_1(p_4) - \epsilon_2(p_3)). \quad (2.72) \end{aligned}$$

Here \hat{V} is the Coulomb potential operator, $\langle p_1, p_2 |$ and $| p_4, p_3 \rangle$ are the initial and final states, L is the length of the sample, and for brevity I write $n_i(p)$ instead of $n_i(\epsilon_i(p))$. For the drag layer in Eq. (2.72) I will take the distribution to be equilibrium¹:

$$n_2(p) = n_2^0(p).$$

The expression in the square brackets comes from the creation and annihilation operators and represents the difference between incoming and outgoing flows in the phase space, the delta-function ensures the energy conservation. The matrix element is given by

$$\begin{aligned} \langle p_1, p_2 | \hat{V} | p_4, p_3 \rangle = \\ \int d^2 \mathbf{r}_1 d^2 \mathbf{r}_2 \Psi_{n, p_4}^*(\mathbf{r}_1) \Psi_{n', p_3}^*(\mathbf{r}_2) \frac{e^2}{\sqrt{|\mathbf{r}_1 - \mathbf{r}_2|^2 + d^2}} \Psi_{n', p_2}(\mathbf{r}_2) \Psi_{n, p_1}(\mathbf{r}_1). \end{aligned} \quad (2.73)$$

Using (2.62) and the well-known Fourier-transform of the Coulomb potential it can be rewritten in the form:

$$\begin{aligned} \langle p_1, p_2 | \hat{V} | p_4, p_3 \rangle = \\ 2\pi e^2 \int dq_x \frac{e^{-qd}}{\sqrt{q_x^2 + q_y^2}} e^{-\frac{q_x^2 + q_y^2}{2}} L_n \left(\frac{q_x^2 + q_y^2}{2} \right) L_{n'} \left(\frac{q_x^2 + q_y^2}{2} \right) \\ \exp \left(i q_x \frac{(p_1 + p_4) - (p_2 + p_3)}{2} \right) \delta(p_1 - p_4 - p_3 + p_2). \end{aligned} \quad (2.74)$$

Here $q_y = p_1 - p_4 = p_3 - p_2$ is the momentum transfer between the layers. The delta-function shows that the momentum is conserved. L_n is the Laguerre polynomial. Substituting (2.74) into (2.72) one has to keep in mind that squaring the delta functions yields an additional factor of $L/2\pi$.

Now I multiply both sides of the Boltzmann equation by $\partial \epsilon_2 / \partial p_2$ and integrate over p_2 . The left hand side yields $-e \int \frac{dp_2}{2\pi} n_2^{0'}(\epsilon_{p_2}) v_{p_2}^2 E_2$ which tends to $\frac{e}{2\pi} v_{F2} E_2$ at low temperatures. Using the antisymmetry of the integrand of Eq. (2.72) under exchange of p_2 and p_3 , and collecting all the above I can rewrite the result for the drag resistance $\rho_D = E_2 / j_1$:

¹See section 2.3.2 for a detailed discussion

$$\begin{aligned} \rho_D = & \frac{2\pi^2}{e^2 v_{F1} v_{F2} T} \int \frac{dp_1 dp_2 dq_y}{(2\pi)^3} q_y^2 |V(p_1, p_2, q_y)|^2 \frac{\partial^2 \epsilon_1}{\partial p_1^2} \frac{\partial^2 \epsilon_2}{\partial p_2^2} \\ & \times \frac{1}{\cosh \frac{\epsilon_1(p_1) - \mu_1}{2T}} \frac{1}{\cosh \frac{\epsilon_1(p_1 - q_y) - \mu_1}{2T}} \frac{1}{\cosh \frac{\epsilon_2(p_2) - \mu_2}{2T}} \frac{1}{\cosh \frac{\epsilon_2(p_2 + q_y) - \mu_2}{2T}} \\ & \times \delta(\epsilon_1(p_1) + \epsilon_2(p_2) - \epsilon_1(p_1 - q_y) - \epsilon_2(p_2 + q_y)), \quad (2.75) \end{aligned}$$

with

$$\begin{aligned} V(p_1, p_2, q_y) = & 2\pi e^2 \int dq_x \frac{e^{-\sqrt{q_x^2 + q_y^2} d}}{\sqrt{q_x^2 + q_y^2}} e^{-\frac{q_x^2 + q_y^2}{2}} L_n \left(\frac{q_x^2 + q_y^2}{2} \right) L_{n'} \left(\frac{q_x^2 + q_y^2}{2} \right) \\ & \times \exp [iq_x(p_1 - p_2 - q_y)]. \quad (2.76) \end{aligned}$$

To obtain (2.75) I first had to recast the filling factor part of (2.72) using (2.70), the expression for the Fermi distribution, and the energy conservation law. Then the p_4 integral was evaluated using the delta function and the variable $q_y = p_3 - p_2$ was introduced instead of p_3 .

The expression (2.75) turns out to be symmetric with respect to interchanging the layers. The formal reason for it is the choice of the non-equilibrium distribution (2.68). Indeed, the two second derivatives in (2.75) are from different origin — the one from the drag layer comes from the velocity change in the scattering process and is directly connected to the curvature of the dispersion, while the one in the drive layer results from expanding the distribution function (2.68). For any type of the non-equilibrium distribution in the drive layer we get the derivative of the chemical potential over p_1 instead of $\partial^2 \epsilon_1 / \partial p_1^2$; but for the specific form I chose this derivative becomes the second derivative of the energy (compare with (2.69)). Consequently, the symmetry between the layers occurs only for the used form of the non-equilibrium distribution. This is a strong argument in favor of Eq. (2.68).

In the following I describe two different methods of calculating the drag. They differ from each other in the way the electrons' dispersion is parameterized.

First method

I expand the electron energy around the Fermi energy up to second order in $p - p_{i_F}$, where p_{i_F} is the momentum corresponding to the Fermi edge in the i -th layer. This is justified whenever the relevant electron states (i.e. those states that give the essential contribution to the integral in (2.75)) are close enough to the Fermi energy. What this precisely means will be clarified later, now we just mention that this condition might fail in the vicinity of the point where the second derivative of ϵ_i with respect to p vanishes. The expansion yields:

$$\epsilon_i(p) - \mu_i = \alpha_i(p - p_{i_F}) + \frac{\beta_i}{2}(p - p_{i_F})^2. \quad (2.77)$$

From now on, for the sake of brevity, I will write p_i instead of $p_i - p_{i_F}$. It is also important to mention that the first term in (2.77) must be much larger than the second, in order for the expansion to be valid.

The next step is the introduction of the energy transfer ω . This is done by including an additional integration:

$$\delta(\epsilon_1(p_1) + \epsilon_2(p_2) - \epsilon_1(p_1 - q_y) - \epsilon_2(p_2 + q_y)) = \int d\omega \delta(\omega - \epsilon_1(p_1) + \epsilon_1(p_1 - q_y)) \delta(\omega + \epsilon_2(p_2) - \epsilon_2(p_2 + q_y)), \quad (2.78)$$

or, after substituting (2.77),

$$\delta(\epsilon_1(p_1) + \epsilon_2(p_2) - \epsilon_1(p_1 - q_y) - \epsilon_2(p_2 + q_y)) = \int d\omega \delta(\omega - \alpha_1 q_y - \beta_1 p_1 q_y + \frac{\beta_1}{2} q_y^2) \delta(\omega - \alpha_2 q_y - \beta_2 p_2 q_y - \frac{\beta_2}{2} q_y^2). \quad (2.79)$$

This allows us to evaluate the $p_{1,2}$ -integrals in (2.75):

$$\begin{aligned} \rho_D &= \frac{\pi}{e^2 v_{F1} v_{F2} T} \operatorname{sgn}(\beta_1 \beta_2) \int \frac{dq d\omega}{(2\pi)^2} |V(p_1 + p_{1_F}, p_2 + p_{2_F}, q)|^2 \\ &\times \frac{1}{\cosh \left[\frac{1}{4\beta_1 T} \left(\left(\frac{\omega}{q} + \frac{\beta_1 q}{2} \right)^2 - \alpha_1^2 \right) \right]} \frac{1}{\cosh \left[\frac{1}{4\beta_1 T} \left(\left(\frac{\omega}{q} - \frac{\beta_1 q}{2} \right)^2 - \alpha_1^2 \right) \right]} \\ &\times \frac{1}{\cosh \left[\frac{1}{4\beta_2 T} \left(\left(\frac{\omega}{q} + \frac{\beta_2 q}{2} \right)^2 - \alpha_2^2 \right) \right]} \frac{1}{\cosh \left[\frac{1}{4\beta_2 T} \left(\left(\frac{\omega}{q} - \frac{\beta_2 q}{2} \right)^2 - \alpha_2^2 \right) \right]}. \quad (2.80) \end{aligned}$$

Here the momenta $p_{1,2}$ in the argument of V are determined by the delta functions in (2.79).

A significant simplification which allows an analytical analysis arises in the case $d \gg R_c$, where $R_c = \sqrt{2 \max(n, n')} l_H$ is the cyclotron radius of the electron in the layer with higher Landau level². In this limit the expression for $V(p_1, p_2, q)$ reduces to

$$V(p_1, p_2, q) = 2\pi e^2 \int dq_x \frac{e^{-\sqrt{q_x^2 + q^2} d}}{\sqrt{q_x^2 + q^2}} \exp [iq_x(p_1 + p_{1_F} - p_2 - p_{2_F} - q)] = 4\pi e^2 K_0(qD), \quad (2.81)$$

where $K_0(x)$ is the McDonald function and

$$D = \sqrt{d^2 + (p_1 + p_{1_F} - p_2 - p_{2_F} - q)^2}.$$

Now I suppose that $p_{1,2}, q \ll d$ (this will also be checked later), so that D becomes independent on q and ω and is just the distance between the two scattering electrons. This leaves the ω -dependence only in the four cosh-factors in the integrand of (2.80) and thus we are left with the integral

$$\int d\omega \frac{1}{\cosh \left[\frac{1}{4\beta_1 T} \left(\left(\frac{\omega}{q} + \frac{\beta_1 q}{2} \right)^2 - \alpha_1^2 \right) \right]} \frac{1}{\cosh \left[\frac{1}{4\beta_1 T} \left(\left(\frac{\omega}{q} - \frac{\beta_1 q}{2} \right)^2 - \alpha_1^2 \right) \right]} \times \frac{1}{\cosh \left[\frac{1}{4\beta_2 T} \left(\left(\frac{\omega}{q} + \frac{\beta_2 q}{2} \right)^2 - \alpha_2^2 \right) \right]} \frac{1}{\cosh \left[\frac{1}{4\beta_2 T} \left(\left(\frac{\omega}{q} - \frac{\beta_2 q}{2} \right)^2 - \alpha_2^2 \right) \right]}, \quad (2.82)$$

which will be very important in the next parts of the work. When evaluating this integral we have to consider only $q \lesssim \frac{1}{D}$ due to the McDonald function.

It can easily be checked that, if the above mentioned conditions hold, the integrand in the expression (2.80) is invariant under transformations of the

²In real samples this condition is hardly ever met for the magnetic fields for which negative drag is observed. However, no principle changes occur in the behavior of the interaction matrix element: it is still logarithmic for small q 's and falls off exponentially for large ones.

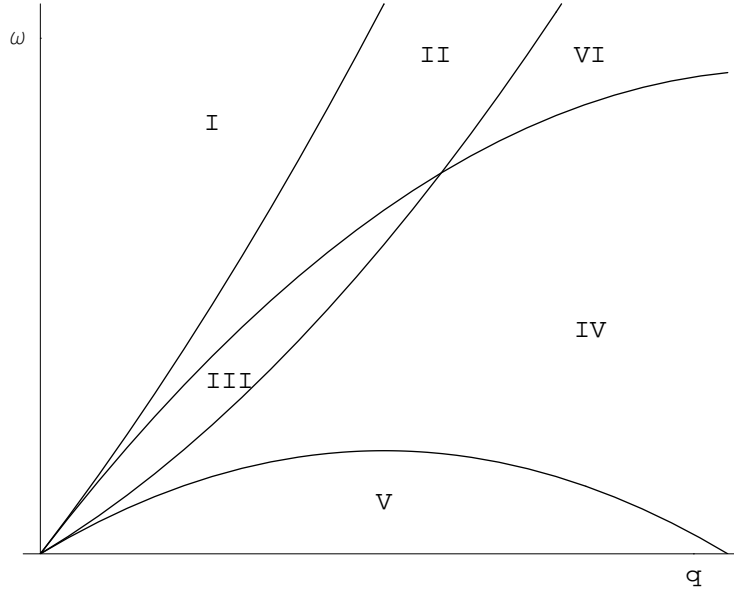


Figure 2.19: The four curves are $\omega = \alpha_{1,2}q \pm \frac{\beta_{1,2}q^2}{2}$. q^* is the q -coordinate of the touching point of III and VI

type $\alpha_i \rightarrow -\alpha_i$, $\beta_i \rightarrow -\beta_i$, $q \rightarrow -q$ and $\omega \rightarrow -\omega$. This allows to consider only positive values of α_i and β_i and to restrict the q, ω -integration to the first quadrant, multiplying the final result by 4. Moreover, the factor $\text{sgn}(\beta_1\beta_2)$ shows that for the same signs of curvatures the drag is positive, while for different signs it is negative.

I first consider small temperatures (we will see what it means later). If the temperature is small enough, one can replace $\cosh^{-1}(A/T)$ by $2 \exp(-|A|/T)$. Then in the integrand of (2.82) I obtain the exponential of the sum of two expressions of the type $|\omega - \alpha q + \beta q^2/2|(\omega + \alpha q + \beta q^2/2) + |\omega - \alpha q - \beta q^2/2|(\omega + \alpha q - \beta q^2/2)$. That leads to the splitting of the integration region in 6 subregions (see Fig. 2.19), so that (2.82) can be rewritten as

$$16 \int d\omega e^{-A/2T},$$

with A given by different expressions in different regions of the (q, ω) -plane (see Fig. 2.19) (we take $\alpha_1 > \alpha_2$):

$$A(q, \omega) = \begin{cases} \frac{\omega^2}{q^2} \frac{\beta_1 + \beta_2}{\beta_1 \beta_2} + \frac{\beta_1 + \beta_2}{4} q^2 - \left(\frac{\alpha_1^2}{\beta_1} + \frac{\alpha_2^2}{\beta_2} \right) & \text{for I;} \\ \omega + \frac{\omega^2}{\beta_2 q^2} + \frac{\beta_2 q^2}{4} - \frac{\alpha_2^2}{\beta_2} & \text{for II;} \\ \frac{\omega^2}{q^2} \frac{\beta_1 - \beta_2}{\beta_1 \beta_2} + \frac{\beta_2 - \beta_1}{4} q^2 - \frac{\alpha_2^2}{\beta_2} + \frac{\alpha_1^2}{\beta_1} & \text{for III;} \\ \omega - \frac{\omega^2}{\beta_1 q^2} - \frac{\beta_1 q^2}{4} + \frac{\alpha_1^2}{\beta_1} & \text{for IV;} \\ -\frac{\omega^2}{q^2} \frac{\beta_1 + \beta_2}{\beta_1 \beta_2} - \frac{\beta_1 + \beta_2}{4} q^2 + \left(\frac{\alpha_1^2}{\beta_1} + \frac{\alpha_2^2}{\beta_2} \right) & \text{for V;} \\ 2\omega & \text{for VI.} \end{cases} \quad (2.83)$$

For a given $q < q^* = 2(\alpha_1 - \alpha_2)/(\beta_1 + \beta_2)$, $A(\omega)$ reaches its minimum (i.e. the integrand in (2.82) reaches its maximum) on one of the banks of III, depending on which of the two β 's is bigger. Indeed, as can be seen from (2.83), $A(\omega)$ is decreasing in V and IV, increasing in I and II, and either decreasing or increasing in III depending on the sign of $\beta_1 - \beta_2$. For an analytical analysis it is enough to consider only the case $\beta_1 > \beta_2$, which means that the minimum of A is reached along the line $\omega = \alpha_2 q + \frac{\beta_2 q^2}{2}$. On this line $A(q)$ is given by:

$$A(q, \omega = \alpha_2 q + \frac{\beta_2 q^2}{2}) = \frac{\alpha_1^2 - \alpha_2^2}{\beta_1} - q^2 \frac{(\beta_1 - \beta_2)^2}{4\beta_1} + \alpha_2 q \frac{\beta_1 - \beta_2}{\beta_1}, \quad (2.84)$$

and the integral in (2.82) is proportional to $\exp(-A(q, \omega = \alpha_2 q + \frac{\beta_2 q^2}{2}))/2T$. As the McDonald function for small arguments is logarithmic, we conclude that the q -integral for small T is determined by $q \sim \frac{T\beta_1}{\alpha_2(\beta_1 - \beta_2)}$. For such q 's the q^2 term in A is negligible for $T \ll \frac{\alpha_2^2}{\beta_1}$.

To calculate the pre-factor I linearize $A(\omega)$ with respect to $\omega - (\alpha_2 q + \frac{\beta_2 q^2}{2})$ and calculate the integral (2.82). Analytical calculation can be done in the limit $|\alpha_1 - \alpha_2| \ll \alpha_1$, $|\beta_1 - \beta_2| \ll \beta_1$, so I restrict myself to such values. I denote $\beta \approx \beta_1 \approx \beta_2$, $\alpha \approx \alpha_1 \approx \alpha_2$, $\Delta\beta = \beta_1 - \beta_2$, $\Delta\alpha = \alpha_1 - \alpha_2$. Now I will show that under the conditions mentioned above, for $T \ll T^* = \alpha q^* = \alpha\Delta\alpha/\beta$ the integral in (2.80) is determined by the region III. Indeed, the

ω -integral of $e^{-A/2T}$ over III is

$$\begin{aligned} & \exp \left[-\frac{1}{T} \left(\frac{\alpha_1^1 - \alpha_2^2}{2\beta_1} + \alpha q \frac{\Delta\beta}{\beta} \right) \right] \\ & \times \int_{\alpha_2 q + \frac{\beta_2 q^2}{2}}^{\alpha_1 q - \frac{\beta_1 q^2}{2}} d\omega \exp \left(-\frac{1}{2T} \frac{\omega^2 - (\alpha_2 q + \frac{\beta_2 q^2}{2})^2 \Delta\beta}{q^2 \beta^2} \right) = \\ & \exp \left[-\frac{1}{T} \left(\frac{\alpha_1^2 - \alpha_2^2}{2\beta_1} + \alpha q \frac{\Delta\beta}{\beta} \right) \right] \min \left(\frac{qT\beta^2}{\alpha\Delta\beta}, \Delta\alpha q - \beta q^2 \right). \quad (2.85) \end{aligned}$$

The two options in the last equation correspond to the cases when the upper limit in (2.85) can be set to infinity or not. We see that for $T \ll T^{**} = \frac{\alpha\Delta\alpha\Delta\beta}{\beta^2}$ and for $q \lesssim \frac{T\beta}{\alpha\Delta\beta} \ll q^*$ (which are the only relevant ones) the first option in the min-function is valid, while for larger T 's and $q < q^*$ it is the second one. This means that for $T \ll T^{**}$ I only have to check whether regions IV and V give comparable contribution to (2.80), while for $T^{**} \ll T \ll T^*$ one can set $\Delta\beta = 0$ and has to look at all regions surrounding III in order to prove that the contribution from III dominates.

From (2.83) one can see that summed up contributions to (2.82) from I, II, IV and V are of the order of

$$\exp \left[-\frac{1}{T} \left(\frac{\alpha_1^1 - \alpha_2^2}{2\beta_1} + \alpha q \frac{\Delta\beta}{\beta} \right) \right] \left(\frac{T\beta q}{\alpha} \right),$$

which is smaller than (2.85). (For $T \ll T^{**}$ it follows from $\Delta\beta \ll \beta$ and for $T^{**} \ll T \ll T^*$ it follows from $\Delta\alpha q = qT^*\beta/\alpha \gg qT\beta/\alpha$.³) In turn, for $q > q^*$ minimum of $A(\omega)$ is reached for $\omega = \alpha_1 q - \frac{\beta_1 q^2}{2}$ and the result of ω -integration is of the order of ($T \gg T^{**}$, so we set $\Delta\beta = 0$)

$$\exp \left(-\frac{\alpha q - \frac{\beta q^2}{2}}{T} \right) \left(\beta q^2 + \frac{T\beta q}{\alpha} \right),$$

³In fact, for q 's close enough to q^* the contribution for III tends to zero, but as the relevant value arises from the integration over q , we have to compare the integrated values. Doing so, I mention that the results of the q -integration over I,II, IV and V from 0 to q^* have an additional factor of $T/T^* \ll 1$.

(the first term in the parenthesis comes from VI and the second — from II and IV). Now it is easy to see that the contribution to (2.80) from $q > q^*$ also has an extra factor of $T/T^* \ll 1$ compared to the contribution from III (see also footnote).

Thus I have proved that for $T \ll T^*$ it is sufficient to integrate over III. Evaluating the ω -integral in (2.80) yields

$$\rho_D = \frac{64\pi e^2}{v_{F1}v_{F2}T} \operatorname{sgn}(\beta_1\beta_2) \exp\left[-\frac{1}{T}\left(\frac{\alpha_1^1 - \alpha_2^2}{2\beta_1}\right)\right] \times \int_0^{q^*} dq [K_0(qD)]^2 \exp\left(-\frac{\alpha q \Delta \beta}{\beta T}\right) \min\left(\frac{qT\beta^2}{\alpha \Delta \beta}, \Delta \alpha q - \beta q^2\right). \quad (2.86)$$

As the McDonald function is logarithmic for small arguments and falls off exponentially for large ones there are three scales for q : q^* , $T\beta/\Delta\beta\alpha$, and $1/D$. Depending on which of the three wave-vectors is smaller three results can be obtained:

$$\rho_D = \frac{64\pi e^2}{v_{F1}v_{F2}} \operatorname{sgn}(\beta_1\beta_2) \times \begin{cases} \exp\left[-\frac{1}{T}\left(\frac{\alpha_1^1 - \alpha_2^2}{2\beta_1}\right)\right] \left[\ln\left(D\frac{T\beta}{\Delta\beta\alpha}\right)\right]^2 \frac{T^2\beta^4}{\alpha^3\Delta\beta^3}, & T \ll T^{**}, T \ll \frac{\alpha\Delta\beta}{\beta D}; \\ \exp\left[-\frac{\alpha\Delta\alpha}{T\beta}\right] \left[\ln\left(D\frac{\Delta\alpha}{\beta}\right)\right]^2 \frac{\Delta\alpha^3}{6\beta^2T}, & T^{**} \ll T \ll T^*, q^* \ll \frac{1}{D}; \\ \exp\left[-\frac{\alpha\Delta\alpha}{T\beta}\right] \frac{1}{2D^2} \min\left(\frac{\beta^2}{\alpha\Delta\beta}, \frac{\Delta\alpha}{T}\right), & \frac{1}{D} \ll q^*, \frac{\alpha\Delta\beta}{\beta D} \ll T \ll T^*. \end{cases} \quad (2.87)$$

Now let us consider higher temperatures ($T \gg T^*$). For this temperature region it is possible to neglect the difference between α_1 and α_2 as well as the difference between β_1 and β_2 . So (2.82) reduces to

$$\int_0^\infty d\omega \frac{1}{\cosh^2\left[\frac{(\omega - \alpha q - \frac{\beta q^2}{2})(\omega + \alpha q - \frac{\beta q^2}{2})}{4\beta q^2 T}\right]} \frac{1}{\cosh^{-2}\left[\frac{(\omega - \alpha q + \frac{\beta q^2}{2})(\omega + \alpha q + \frac{\beta q^2}{2})}{4\beta q^2 T}\right]}. \quad (2.88)$$

I will show later that for $q \gg T/\alpha$ integral (2.88) falls off exponentially, so another temperature scale arises: the one at which $T/\alpha \sim 1/D$. For

smaller temperatures the cut-off in q -integration is T/α and for higher T 's it is $1/D$. If, as usually is the case in the experiment, D is of the order of the characteristic size of the potential then $1/D \ll \alpha/\beta$, so this temperature scale $T' = \alpha/D \ll \alpha^2/\beta$. For such temperatures we can rewrite (2.88) in the form: (after shifting the integration variable to $\tilde{\omega} = \omega - \alpha q - \frac{\beta q^2}{2}$)

$$\begin{aligned} \int_{-\infty}^{\infty} d\tilde{\omega} \cosh^{-2} \left[\frac{\tilde{\omega}\alpha}{2\beta q T} \right] \cosh^{-2} \left[\frac{(\tilde{\omega} + \beta q^2)\alpha}{2\beta q T} \right] \\ = \frac{2\beta q T}{\alpha} \int_{-\infty}^{\infty} \frac{dx}{\cosh^2 x \cosh^2 \left(x + \frac{q\alpha}{2T} \right)}. \end{aligned} \quad (2.89)$$

Indeed, it can easily be shown that for $T \lesssim T'$ relevant $\tilde{\omega}$'s in the integral are of the order of $\max(\beta q T/\alpha, \beta q^2) \ll \alpha q$, which allows to set $\omega + \alpha q - \frac{\beta q^2}{2} \approx 2\alpha q$ and extend the lower integration limit to $-\infty$.

The integral in (2.89) can be evaluated and yields

$$\frac{8\beta q T}{\alpha} \frac{\frac{q\alpha}{2T} \coth \frac{q\alpha}{2T} - 1}{\sinh^2 \frac{q\alpha}{2T}}, \quad (2.90)$$

which is, as expected, exponentially small for $q \gg T/\alpha$. Substituting it into (2.80) one obtains for ρ_D : (for $T \ll \alpha/D$)

$$\rho_D = \frac{64\pi\beta T^2 e^2}{\alpha^3 v_{F1} v_{F2}} \operatorname{sgn}(\beta_1 \beta_2) \ln^2 \left(D \frac{T}{\alpha} \right). \quad (2.91)$$

Ultimately for $T \gg \alpha/D$ the answer for the drag resistivity is

$$\rho_D = \frac{32\pi e^2 \beta}{3v_{F1} v_{F2} D^2 \alpha} \operatorname{sgn}(\beta_1 \beta_2). \quad (2.92)$$

The equations (2.87), (2.91) and (2.92) give the value of ρ_D for all possible combinations of parameters. It turns out that for smallest temperatures the behavior is activated, then for $T \sim \alpha\Delta\alpha/\beta$ there is a cross-over to T^2 -behavior, and finally for $T \sim \alpha/D$ quadratic dependence changes to constant. If $\alpha/D \lesssim \alpha\Delta\alpha/\beta$ the T^2 -regime is absent.

Now I have to check the validity of the approximations made. I started with neglecting the third-order term in (2.77). In order for it to be justified,

the second-order term must be larger than the third-order one. We will set $\epsilon_i(p) = -t_i \sin \frac{2\pi(p+p_{iF})l_H^2}{l}$. The second-order term is $\beta_i p^2/2$ and the third-order one is $-\alpha_i p^3 (2\pi l_H^2/l)^2/6$, with $\beta_i = t_i (2\pi l_H^2/l)^2 \sin \frac{2\pi p_{iF} l_H^2}{l}$ and $\alpha_i = -t_i (2\pi l_H^2/l) \cos \frac{2\pi p_{iF} l_H^2}{l}$. The ratio of the two terms is $6\pi p l_H^2/l \cot \frac{2\pi p_{iF} l_H^2}{l}$ and it should be small. This condition is likely to be violated in the vicinity of $p_{iF} = 0$, which corresponds to the inflection point of the potential, so we can replace $\cot x$ by $1/x$ and that leaves us with the inequality to be verified for relevant p 's:

$$3|p|/|p_{iF}| \ll 1.$$

From (2.79) we have

$$p_i = \frac{\omega}{\beta_i q} - \frac{\alpha_i}{\beta_i} \pm \frac{q}{2}. \quad (2.93)$$

If now one substitutes the typical values of ω/q and q it becomes evident that for $p_{iF} \lesssim \frac{\Delta\alpha}{\beta}$ the approximation (2.77) is wrong. Thus for this region of parameters a new approximation should be applied. This is done in the next part of the work.

The second approximation that was to be verified is the condition $p_{1,2}, q \ll d$ which allows to neglect the ω -dependence of the interaction matrix element. From (2.93) one sees that this condition is always fulfilled if $d \gg R_c$ which is assumed in all the above calculations.

Second method.

The approach elaborated in the previous section consisting of expanding $\epsilon(p)$ around the Fermi momentum fails in the interesting region of $p_F \approx 0$ that corresponds to a particle-hole symmetric situation. In particular, using that technique it is not possible to show that at the particle-hole symmetric point the drag is identically zero, which is a crucial feature. To account for this region of parameters I have developed another approach that is not as transparent as the first one, but more general. As we will see it gives the same results as the old one for most parameter regions. The exceptions to the above will be discussed separately.

Now, instead of expanding $\epsilon(p)$ around p_F and dealing with the variables α_i, β_i which are p_{F_i} -dependent, I expand around the inflection point of the potential ($\epsilon = 0, p = 0$) and carry out the calculations in more natural parameters i.e. those of the potential profile and the chemical potentials.

Let the dispersion relations (directly connected to the potential profiles) be

$$\epsilon_1(p) = t_1 \sin(p\gamma_1) \text{ and } \epsilon_2(p) = t_2 \sin(p\gamma_2)$$

for the drive and drag layer respectively. $\gamma_i \approx \frac{2\pi l_H^2}{L_i}$ characterizes the size L_i of the potential hill. In the 2D situation it corresponds to the correlation length of the potential. Even if it is the same in both layers, the local values of γ 's, characterizing the form of the potential at a given point may be different for the two layers, so we have to consider the general case. As I will show this leads to no qualitative changes in the results.

I expand the dispersions around the inflection point up to third order:

$$\epsilon_i = t_i \gamma_i p - \frac{t_i \gamma_i^3}{6} p^3. \quad (2.94)$$

Then, as in the previous section, I solve the energy conservation equation for a scattering process with given ω and q :

$$\begin{aligned} \epsilon_1(p_1^0 - \frac{q}{2}) - \epsilon_1(p_1^0 + \frac{q}{2}) + \omega &= 0, \\ \epsilon_2(p_2^0 - \frac{q}{2}) - \epsilon_2(p_2^0 + \frac{q}{2}) + \omega &= 0. \end{aligned}$$

I obtain

$$p_i^{02} = \frac{1}{\gamma_i^2} \left(2 \left(1 - \frac{\omega}{t_i \gamma_i q} \right) - \frac{(q\gamma_i)^2}{12} \right). \quad (2.95)$$

This implies that

$$\omega \leq t_i \gamma_i q \left(1 - \frac{(q\gamma_i)^2}{24} \right). \quad (2.96)$$

Suppose, $t_1 \gamma_1 > t_2 \gamma_2$ (in the opposite case no changes in the final result occur). I introduce a new variable δ instead of ω :

$$\omega = (1 - \delta) t_2 \gamma_2 q \left(1 - \frac{(q\gamma_2)^2}{24} \right). \quad (2.97)$$

Thus

$$\begin{aligned}
p_2^{02} &= \frac{2\delta}{\gamma_2^2} \left(1 - \frac{(q\gamma_2)^2}{24} \right); \\
p_1^{02} &= \frac{1}{\gamma_1^2} \left[\frac{t_1\gamma_1 \left(1 - \frac{(q\gamma_1)^2}{24} \right) - t_2\gamma_2 \left(1 - \frac{(q\gamma_2)^2}{24} \right)}{t_1\gamma_1} + \delta \frac{t_2\gamma_2}{t_1\gamma_1} \left(1 - \frac{(q\gamma_2)^2}{24} \right) \right].
\end{aligned} \tag{2.98}$$

We see that for every pair (q, ω) satisfying the condition (2.96) we have 4 different pairs of initial states that differ from each other by the signs of the p_i^0 's. So the expression (2.80) turns into

$$\begin{aligned}
\rho_D &= \frac{4\pi e^2}{v_{F1}v_{F2}T} \int dq d\omega K_0^2(qD) \\
&\times \left(\frac{1}{\cosh \frac{\epsilon_1(p_1^0 - \frac{q}{2}) - \mu_1}{2T} \cosh \frac{\epsilon_1(p_1^0 + \frac{q}{2}) - \mu_1}{2T}} - \frac{1}{\cosh \frac{\epsilon_1(p_1^0 - \frac{q}{2}) + \mu_1}{2T} \cosh \frac{\epsilon_1(p_1^0 + \frac{q}{2}) + \mu_1}{2T}} \right) \\
&\times \left(\frac{1}{\cosh \frac{\epsilon_2(p_2^0 - \frac{q}{2}) - \mu_2}{2T} \cosh \frac{\epsilon_2(p_2^0 + \frac{q}{2}) - \mu_2}{2T}} - \frac{1}{\cosh \frac{\epsilon_2(p_2^0 - \frac{q}{2}) + \mu_2}{2T} \cosh \frac{\epsilon_2(p_2^0 + \frac{q}{2}) + \mu_2}{2T}} \right).
\end{aligned} \tag{2.99}$$

After performing the multiplication of the two parenthesis in the integrand I get a sum of four expressions of the type of (2.80) (with obvious changes due to different expression for ϵ_i used), corresponding to the four possible initial states mentioned above. If $\mu_i \gg T$, than only one of the four terms survives and we return to the old expression (2.80). On the other hand, if either of the μ 's happens to be zero, the expression (2.99) yields zero which is the manifestation of the particle-hole symmetry. In the frame of the consideration in the previous method it is impossible to explicitly obtain this zero, while in the present one it comes out naturally. If μ_i are not zero, but still $\mu_i \ll T$ one can expand the expressions in the parenthesis in powers of μ_i/T and carry out the calculations in this region of parameters.

At this stage it is worth mentioning that the overall sign of ρ_D given by (2.99) is $\text{sgn}(\mu_1\mu_2)$, which means that in the situation, when one layer is

more than half-filled and the other is less than half-filled, the drag signal will be negative.

As in the previous section I restrict myself to the consideration of almost identical layers. In this case the calculations can be carried out analytically and I do not expect any qualitative changes if the parameters of the layers begin to differ significantly. So I consider $t_1\gamma_1 \approx t_2\gamma_2 \approx t\gamma$, $\gamma_1 \approx \gamma_2 \approx \gamma$ and $|\mu_1| \approx |\mu_2| \approx \mu$. The absolute values of the differences of the parameters in the two layers will be denoted respectively as $\Delta(t\gamma)$, $\Delta\gamma$ and $\Delta\mu$.

I start with the case $\mu \gg T$. As in the previous section I replace $\cosh(\frac{A}{2T})$ by $2 \exp(-\frac{|A|}{2T})$. This divides the (q, δ) plane into several regions, within each of which the arguments of the cosh's have constant signs. In principle, I proceed just as in the previous section: I set both μ 's positive and consider only the region of positive q 's, as the other cases are trivially obtained from this one due to symmetry properties of the integrand. As both μ 's are positive and $\gg T$, only the first terms in the parenthesis of (2.99) survive.

To determine the borders of the mentioned regions I solve the equations $\epsilon_i(p_i^0 \pm \frac{q}{2}) = \mu_i$. If, as I set before, $t_1\gamma_1 > t_2\gamma_2$, then these equations read (for the time being I keep some extensive terms):

$$\mu_2 = t_2\sqrt{2\delta} \left(1 - \frac{7(q\gamma_2)^2}{48}\right) \left(1 - \frac{\delta}{3}\right) \pm t_2\frac{q\gamma_2}{2} \left(1 - \frac{(q\gamma_2)^2}{24}\right) (1 - \delta), \quad (2.100)$$

$$\begin{aligned} \mu_1 = t_1 \sqrt{2 \left(\Delta + \delta \frac{t_2\gamma_2}{t_1\gamma_1 \left(1 - \frac{(q\gamma_2)^2}{24}\right)} \right) \left(1 - \frac{\Delta}{3} - \frac{\delta}{3} - \frac{(q\gamma_1)^2}{8}\right)} \\ \pm t_2\frac{q\gamma_2}{2} \left(1 - \frac{(q\gamma_2)^2}{24}\right) (1 - \delta), \quad (2.101) \end{aligned}$$

with

$$\Delta = \frac{t_1\gamma_1 \left(1 - \frac{(q\gamma_1)^2}{24}\right) - t_2\gamma_2 \left(1 - \frac{(q\gamma_2)^2}{24}\right)}{t_1\gamma_1}. \quad (2.102)$$

For $q^2 \ll 12 \frac{\Delta(t\gamma)}{t\gamma^2\Delta\gamma}$, $\Delta \approx \frac{\Delta(t\gamma)}{t\gamma}$, in the opposite limit $\Delta \approx -\frac{q^2}{12}\gamma\Delta\gamma$ ($\Delta\gamma = \gamma_1 - \gamma_2$).

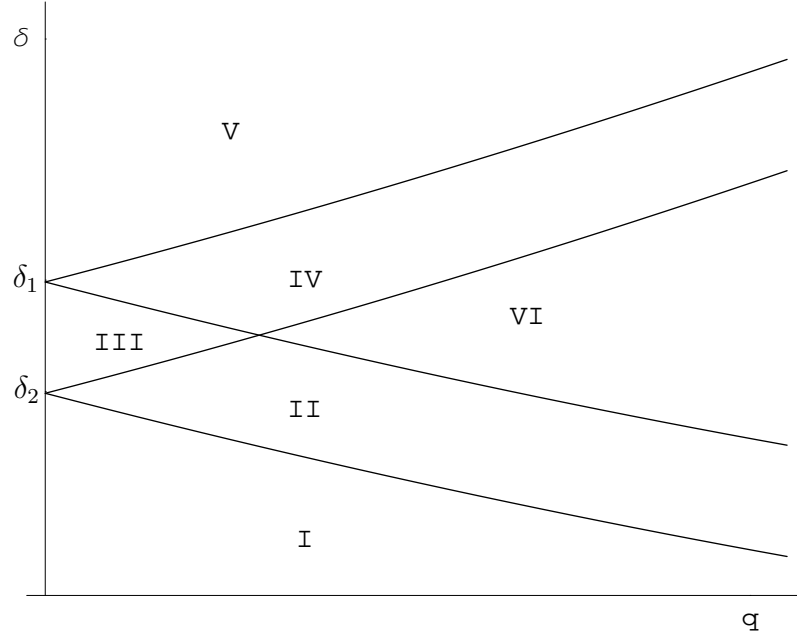


Figure 2.20: Regions of the (δ, q) -plane in which arguments of the cosh's in Eq. (2.99) keep their signs. $\delta_1 = \frac{1}{2} \left(\frac{\mu}{t}\right)^2$, $\delta_2 = \frac{1}{2} \left(\frac{\mu}{t}\right)^2 - \Delta$.

Solving the Eqs. (2.100), (2.101) (omitting this time the irrelevant small corrections, the consistency of this can be easily checked after solving the equations by direct comparison of the omitted terms with the kept ones), I get

$$\begin{aligned} \epsilon_2(p_2^0 \pm \frac{q}{2}) = \mu_2 \text{ for } \delta \approx \frac{1}{2} \left(\frac{\mu_2}{t_2} \mp \frac{q\gamma_2}{2} \right)^2, \\ \epsilon_1(p_1^0 \pm \frac{q}{2}) = \mu_1 \text{ for } \delta \approx \left[\frac{1}{2} \left(\frac{\mu_1}{t_1} \mp \frac{qt_2\gamma_2}{2t_1} \right) - \Delta \right] \frac{t_1\gamma_1}{t_2\gamma_2}. \end{aligned} \quad (2.103)$$

The notation of the regions (Fig. 2.20) corresponds to the one used in the previous section in the sense that the Fig. 2.20 is just a replotting of Fig. 2.19 in the coordinates (δ, q) instead of (ω, q) . The region where the approximation used there is applicable is $\left(\frac{\mu}{t}\right)^2 \gg \Delta$ or $\mu \gg \sqrt{\frac{t\Delta(t\gamma)}{\gamma}}$. If this condition is fulfilled, the quadratic term in the expansion of the dispersion around the Fermi point is much larger than the cubic one.

The end of region III (q^*) is given by $q^* = \frac{\Delta(t\gamma)}{\mu\gamma^2}$ (equivalent to $\frac{\Delta\alpha}{\beta}$ from the previous section). It can also be easily checked that for $\mu \gg \sqrt{\frac{t\Delta(t\gamma)}{\gamma}} \sqrt{\frac{\Delta\gamma}{\gamma}}$ the condition $q^2 \ll 12\frac{\Delta(t\gamma)}{t\gamma^2\Delta\gamma}$ holds within III and I can set $\Delta = \frac{\Delta(t\gamma)}{t\gamma}$ everywhere in III. We will see that, as in the previous section, it is the region III that gives the main contribution to the result. Unlike that case though, the maximum of the integrand is reached on the upper border of III, independent on which $\mu_i\gamma_i^2$ (analog of β_i in the previous section) is bigger. Indeed, in III the sum of absolute values of the arguments of cosh's is (in the first non-vanishing order in δ)

$$-\frac{1}{T} \left[t_2 \sqrt{2\delta} \left(1 - \frac{7(q\gamma_2)^2}{48} \right) - t_1 \sqrt{2 \left(\Delta + \delta \frac{t_2\gamma_2}{t_1\gamma_1} \right)} \left(1 - \frac{7(q\gamma_2)^2}{48} \right) - \mu_2 + \mu_1 \right]. \quad (2.104)$$

It is straightforward to show that apart from the pathological case $t\Delta\gamma \gg \Delta(t\gamma)$, the δ -derivative of this expression is negative and thus the maximum is reached on the upper border of III.

On the other hand, in IV the sum of the absolute values of the cosh's arguments becomes

$$-\frac{1}{T} \left[\mu_1 - t_1 \sqrt{2 \left(\Delta + \delta \frac{t_2\gamma_2}{t_1\gamma_1} \right)} \left(1 - \frac{7(q\gamma_2)^2}{48} \right) + t_2\gamma_2 q \left(1 - \frac{(q\gamma_2)^2}{24} \right) (1 - \delta) \right],$$

the δ -derivative of which positive and its absolute value is much greater than that of the δ -derivative in III. That proves the aforementioned statement, that the integral in the low temperature limit ($T \ll \frac{t\gamma\Delta(t\gamma)}{\mu\gamma^2}$) is determined by III.

To determine the exponential factor in the answer it is enough to substitute $\delta = \frac{1}{2} \left(\frac{\mu}{t} \right)^2$ in (2.104). It turns out that

$$\rho_D \propto \exp \left[-\frac{1}{T} \frac{t\Delta(t\gamma)}{\gamma\mu} \right]$$

in agreement with the results from the previous section. Hereby the difference between t_1 and t_2 in (2.104) turns out to be insignificant. To determine the pre-factor the δ - and q -integrals must be evaluated. It is done in a similar

manner as before. For the lowest temperatures the δ -integral is determined by the derivative of the argument of the exponent, and for higher ones — by the size of III. What becomes different is the definition of "low temperatures". Before it was determined by the value of $\Delta\beta$ (the analog of which now is $\Delta\mu$), but now, as can be seen from (2.104), the derivative of the argument of the exponent in the integrand does not depend on $\Delta\mu$.

I denote the expression in (2.104) as $A(\delta)$. To find the cross-over T one has to compare $A\left(\frac{1}{2}\left(\frac{\mu}{t} - \frac{q\gamma}{2}\right)^2\right) - A\left(\frac{1}{2}\left(\frac{\mu}{t} + \frac{q\gamma}{2}\right)^2 - \Delta\right)$ with unity. If it is much greater than unity, then the δ -integral converges within III and the lower limit can be extended to infinity; in the opposite case, within III the argument of the exponent can be considered constant and the integration becomes trivial.

The cross-over temperature is

$$T^* = \frac{t^2[\Delta(t\gamma)]^2}{\gamma^2\mu^3}. \quad (2.105)$$

For $T \ll T^*$ the lower limit of the δ -integral, as already mentioned, can be set to $-\infty$ after expanding the argument of the exponent in powers of $\left[\frac{1}{2}\left(\frac{\mu}{t} - \frac{q\gamma}{2}\right)^2 - \delta\right]$:

$$\int_{-\infty}^{\left(\frac{\mu}{t} - \frac{q\gamma}{2}\right)^2} e^A d\delta$$

with

$$A \approx -\frac{t\Delta}{T\left(\frac{\mu}{t} - \frac{q\gamma}{2}\right)} + \frac{t\Delta}{T\left(\frac{\mu}{t} - \frac{q\gamma}{2}\right)^3} \left[\left(\frac{1}{2}\frac{\mu}{t} - \frac{q\gamma}{2}\right)^2 - \delta \right].$$

Here, the second term comes from the expansion of the δ -dependent denominator. Other contributions are negligible. Keeping the q -dependence only in the exponent we get the result of the δ -integration:

$$\frac{T\left(\frac{\mu}{t}\right)^3}{t\Delta} \exp\left(-\frac{t\Delta}{T\left(\frac{\mu}{t} - \frac{q\gamma}{2}\right)}\right).$$

Expanding the exp's argument in q and evaluating the q -integral (keeping in mind that due to the variable change $\omega \rightarrow \delta$ one gets an additional factor

$t\gamma q$ in the integrand) I finally evaluate the q -integral in (2.99) to obtain the final result:

$$\rho_D = \frac{256\pi e^2 \gamma^2 T^2 \mu^7}{v_{F1} v_{F2} t^6 [\Delta(t\gamma)]^3} \operatorname{sgn}(\mu_1 \mu_2) \exp\left[-\frac{t\Delta(t\gamma)}{\gamma\mu T}\right] \ln^2\left(D \frac{T\mu^2}{t^2 \Delta(t\gamma)}\right). \quad (2.106)$$

For $T^* \ll T \ll \frac{t\Delta(t\gamma)}{\gamma\mu}$ I easily get the same answer as in the previous chapter:

$$\rho_D = \frac{32\pi e^2 [\Delta(t\gamma)]^3}{3v_{F1} v_{F2} T (\mu\gamma^2)^2} \operatorname{sgn}(\mu_1 \mu_2) \exp\left[-\frac{t\Delta(t\gamma)}{\gamma\mu T}\right] \ln^2\left(D \frac{\Delta(t\gamma)}{\gamma^2 \mu}\right). \quad (2.107)$$

For $T \gg \frac{t\Delta(t\gamma)}{\gamma\mu}$ the result (2.91) holds (of course changes in notation $\alpha \rightarrow t\gamma$ and $\beta \rightarrow \mu\gamma^2$ should be made).

There is no reason to search for any deep meaning in the fact that two different approximations give different results in the low temperature limit. It just means that the pre-factor in (2.106) is sensitive to the precise form of the potential and thus should not be taken literally. On the other hand, the exponential factor is universal. The mathematical reason for which the pre-factor differs in the two approximations (note that I am in the region where both approximations are self-consistent, i.e. all approximations made are justified by the final results, so it is not an indication that one approximation is "wrong" and the other one is "correct") is quite simple. In fact, as can be checked numerically, in a very broad region of parameters the values of ϵ_i given by the two approximations differ very insignificantly. But the values of p_i^0 which are determined from the energy conservation relations turn out to be quite sensitive to the approximations used, the reason for it is that the second order term in (2.77) is much smaller than the first order one in the considered range of parameters, and a slight change in it, not having any visible effect on the value of ϵ_i has a much larger effect on p_i^0 . Further, the value that is essential for the calculation is $\epsilon_2(p_2^0) - \epsilon_1(p_1^0)$. Its zero order term in δ happens not to depend on the approximation, while the first order term (which accounts for the pre-factor) turns out to depend strongly on the approximation used.

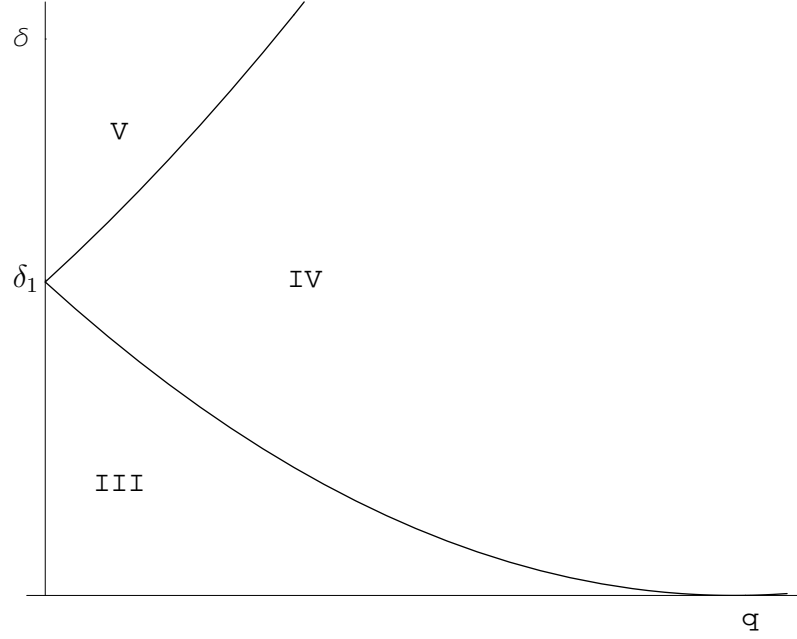


Figure 2.21: Regions of the (δ, q) -plane for $\mu \ll \sqrt{\frac{t\Delta(t\gamma)}{\gamma}}$; $\delta_1 = \frac{1}{2} \left(\frac{\mu}{t}\right)^2$.

Now I proceed to the case $T \ll \mu \ll \sqrt{\frac{t\Delta(t\gamma)}{\gamma}}$. In this parameter region the plot from Fig. 2.20 takes the form shown in Fig. 2.21 (I remind that δ is positive by definition). In this parameter region the approximation from the previous section is inapplicable, so there will be no comparison of the results from the two approaches. In this case the exponential factor comes from the cosh's with ϵ_1 in the argument. The value of the product of these two factors is approximately constant for relevant values of δ and is equal to

$$4 \exp \left(-\frac{1}{T} \sqrt{2 \frac{t\Delta(t\gamma)}{\gamma}} \right).$$

Indeed, for $\mu \ll \sqrt{\frac{t\Delta(t\gamma)}{\gamma}}$ and $\delta \sim \frac{1}{2} \left(\frac{\mu}{t}\right)^2$, $\Delta \gg \delta$ and $\epsilon_1 \approx t\sqrt{2(\Delta + \delta)} \approx t\sqrt{2\Delta}$. So I take the cosh factors with ϵ_1 out of the integral and consider only the other two factors which give the pre-exponential factor in the drag resistivity.

The contributions from III, IV, and V must be taken into account (see Fig. 2.21). Those from III and V are equivalent and give the same result.

The contribution from IV turns out to be of the same order of magnitude. Indeed, $A(\delta)$ in these three regions is given by (I leave only the relevant part, arising from the layer 2):

$$\begin{aligned} \text{III:} & \quad -\frac{1}{T} \left(\mu_2 - t\sqrt{2\delta} \right), \quad \delta \leq \frac{1}{2} \left(\frac{\mu_2}{t} - \frac{q\gamma}{2} \right)^2; \\ \text{IV:} & \quad -\frac{1}{T} \left(t\frac{q\gamma}{2} \right); \\ \text{V:} & \quad -\frac{1}{T} \left(-\mu_2 + t\sqrt{2\delta} \right), \quad \delta \geq \frac{1}{2} \left(\frac{\mu_2}{t} + \frac{q\gamma}{2} \right)^2. \end{aligned}$$

Expanding in δ around the borders of the regions III and V we get:

$$\begin{aligned} \text{III:} & \quad -\frac{1}{T} \left(\frac{tq\gamma}{2} - \frac{t^2}{\mu} \Delta\delta \right); \\ \text{V:} & \quad -\frac{1}{T} \left(\frac{tq\gamma}{2} + \frac{t^2}{\mu} \Delta\delta \right), \end{aligned}$$

where $\Delta\delta$ is the difference between δ and the border of the corresponding region. It is evident from the above that for $T \ll \mu$ the δ -integral converges in the bulk of the regions III and V and thus the above statement about the equivalence of this regions is correct. Within IV, A is independent on δ and the δ -integration is thus trivial and is determined by the size of the region IV. Collecting the above one gets:

$$\int d\delta e^A = \exp\left(-\frac{tq\gamma}{2T}\right) \left(\frac{2\mu T}{t^2} + \frac{q\mu\gamma}{t} \right), \quad (2.108)$$

from which it is easy to see that the contributions from III, IV, and V are of the same order as stated above. Finally the q -integral in (2.99) is taken to get the final result for ρ_D :

$$\rho_D = \frac{384\pi e^2 T^2 \mu}{v_{F1} v_{F2} t^3 \gamma} \operatorname{sgn}(\mu_1 \mu_2) \exp\left(-\frac{1}{T} \sqrt{2 \frac{t\Delta(t\gamma)}{\gamma}}\right) \ln^2\left(\frac{DT}{t\gamma}\right). \quad (2.109)$$

For $\mu \sim \sqrt{\frac{t\Delta(t\gamma)}{\gamma}}$ it is consistent with the case $\mu \gg \sqrt{\frac{t\Delta(t\gamma)}{\gamma}}$, $T \ll T^*$. One can also note that the condition $q^2 \ll 12 \frac{\Delta(t\gamma)}{t\gamma^2 \Delta\gamma}$ holds for $q \lesssim T/t\gamma$ for $T \ll \mu \ll \sqrt{\frac{t\Delta(t\gamma)}{\gamma}} \sqrt{\frac{\gamma}{\Delta\gamma}}$.

This rounds off the consideration of the case $\mu \gg T$. Now I turn to the other case, i.e. $\mu \ll T$. For this I return to the Eq. (2.99) and expand both parenthesis up the first order in $\frac{\mu}{T}$:

$$\begin{aligned} \rho_D = & \frac{4\pi e^2 \mu_1 \mu_2}{v_{F1} v_{F2} T^3} \int dq K_0^2(Dq) t \gamma q \\ & \times \int d\delta \frac{1}{\cosh \frac{\epsilon_1(p_1^0 - \frac{q}{2})}{2T}} \frac{1}{\cosh \frac{\epsilon_1(p_1^0 + \frac{q}{2})}{2T}} \frac{1}{\cosh \frac{\epsilon_2(p_2^0 - \frac{q}{2})}{2T}} \frac{1}{\cosh \frac{\epsilon_2(p_2^0 + \frac{q}{2})}{2T}} \\ & \times \left(\tanh \frac{\epsilon_1(p_1^0 - \frac{q}{2})}{2T} + \tanh \frac{\epsilon_1(p_1^0 + \frac{q}{2})}{2T} \right) \left(\tanh \frac{\epsilon_2(p_2^0 - \frac{q}{2})}{2T} + \tanh \frac{\epsilon_2(p_2^0 + \frac{q}{2})}{2T} \right). \end{aligned} \quad (2.110)$$

Two limiting cases must be considered: $T \ll \sqrt{\frac{t\Delta(t\gamma)}{\gamma}}$ and $T \gg \sqrt{\frac{t\Delta(t\gamma)}{\gamma}}$.

$$1) T \ll \sqrt{\frac{t\Delta(t\gamma)}{\gamma}}.$$

The cosh's stemming from the first layer, similarly to the case $T \ll \mu \ll \sqrt{\frac{t\Delta(t\gamma)}{\gamma}}$, account for the exponential factor $4 \exp\left(-\frac{1}{T} \sqrt{2\frac{t\Delta(t\gamma)}{\gamma}}\right)$. The parentheses with tanh's of ϵ_1 is equal to 2. So the δ -integral is reduced to

$$\begin{aligned} \int d\delta \frac{1}{\cosh \frac{t\sqrt{2\delta} + \frac{tq\gamma}{2}}{2T}} \frac{1}{\cosh \frac{t\sqrt{2\delta} - \frac{tq\gamma}{2}}{2T}} & \left(\tanh \frac{t\sqrt{2\delta} + \frac{tq\gamma}{2}}{2T} + \tanh \frac{t\sqrt{2\delta} - \frac{tq\gamma}{2}}{2T} \right) \\ & = \left(\frac{2T}{t} \right)^2 \frac{tq\gamma}{2T \sinh \frac{tq\gamma}{2T}}. \end{aligned} \quad (2.111)$$

The q -integral can now also be evaluated and yields the final result for the drag resistance:

$$\rho_D = \frac{1792\zeta(3)\pi e^2 \mu^2 T}{v_{F1} v_{F2} t^3 \gamma} \operatorname{sgn}(\mu_1 \mu_2) \exp\left(-\frac{1}{T} \sqrt{2\frac{t\Delta(t\gamma)}{\gamma}}\right) \ln^2\left(\frac{DT}{t\gamma}\right), \quad (2.112)$$

with $\zeta(3)$ being the Riemann zeta-function.

$$2) T \gg \sqrt{\frac{t\Delta(t\gamma)}{\gamma}}.$$

For such temperatures the Δ 's in the expressions for ϵ_1 can be neglected and the δ -integral turns to

$$\int d\delta \frac{1}{\cosh^2 \frac{t\sqrt{2\delta} + \frac{tq\gamma}{2}}{2T}} \frac{1}{\cosh^2 \frac{t\sqrt{2\delta} - \frac{tq\gamma}{2}}{2T}} \left(\tanh \frac{t\sqrt{2\delta} + \frac{tq\gamma}{2}}{2T} + \tanh \frac{t\sqrt{2\delta} - \frac{tq\gamma}{2}}{2T} \right)^2. \quad (2.113)$$

This integral can not be evaluated analytically, but it is easily shown that the answer for the drag differs from (2.112) only by the absence of the exponent and by a different numerical factor:

$$\rho_D = C \frac{e^2 \mu^2 T}{v_{F1} v_{F2} t^3 \gamma} \operatorname{sgn}(\mu_1 \mu_2) \ln^2 \left(\frac{DT}{t\gamma} \right), \quad (2.114)$$

with $C \approx 113$.

I now summarize all the above. In the schematic $T-\mu$ (Fig. 2.22) diagram one can see different regions of parameters in each of which ρ_D has different asymptotics:

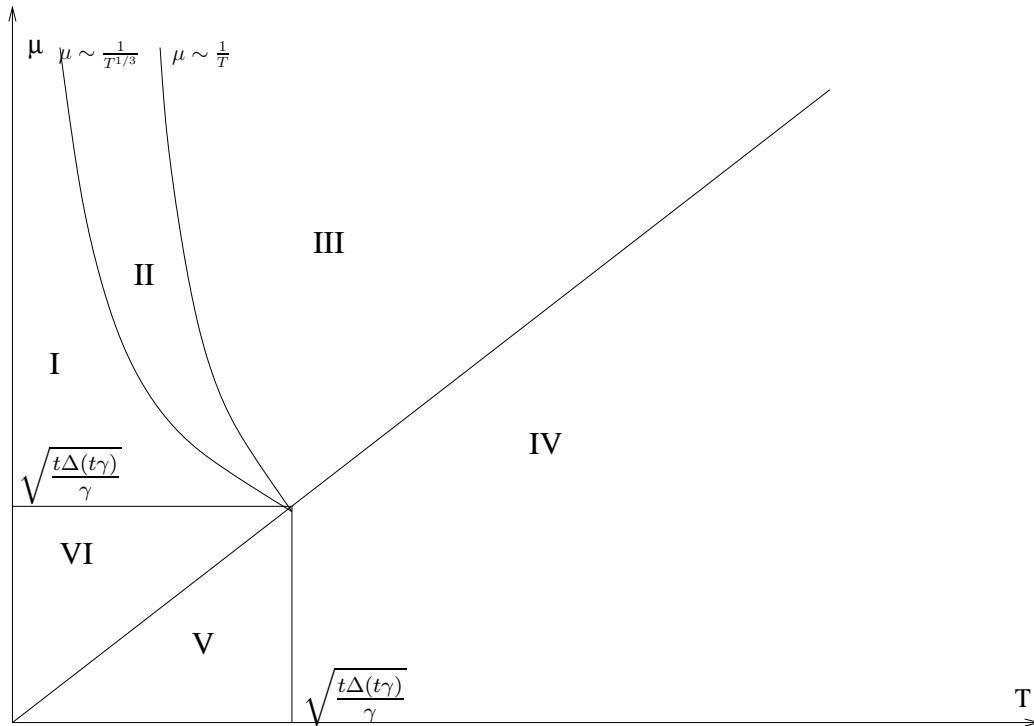


Figure 2.22: Regions of parameters T and μ for which ρ_D has different behavior.

$$\begin{aligned}
\text{I: } \rho_D &= \frac{256\pi e^2 \gamma^2 T^2 \mu^7}{v_{F1} v_{F2} t^6 [\Delta(t\gamma)]^3} \text{sgn}(\mu_1 \mu_2) \exp\left[-\frac{t\Delta(t\gamma)}{\gamma \mu T}\right] \ln^2\left(D \frac{T \mu^2}{t^2 \Delta(t\gamma)}\right); \\
\text{II: } \rho_D &= \frac{32\pi e^2 [\Delta(t\gamma)]^3}{3v_{F1} v_{F2} T (\mu \gamma^2)^2} \text{sgn}(\mu_1 \mu_2) \exp\left[-\frac{t\Delta(t\gamma)}{\gamma \mu T}\right] \ln^2\left(D \frac{\Delta(t\gamma)}{\gamma^2 \mu}\right); \\
\text{III: } \rho_D &= \frac{64\pi e^2 \mu T^2}{v_{F1} v_{F2} t^3 \gamma} \text{sgn}(\mu_1 \mu_2) \ln^2\left(\frac{DT}{t\gamma}\right); \\
\text{IV: } \rho_D &= C \frac{e^2 \mu^2 T}{v_{F1} v_{F2} t^3 \gamma} \text{sgn}(\mu_1 \mu_2) \ln^2\left(\frac{DT}{t\gamma}\right); \\
\text{V: } \rho_D &= \frac{448\zeta(3)\pi e^2 \mu^2 T}{v_{F1} v_{F2} t^3 \gamma} \text{sgn}(\mu_1 \mu_2) \exp\left(-\frac{1}{T} \sqrt{2 \frac{t\Delta(t\gamma)}{\gamma}}\right) \ln^2\left(\frac{DT}{t\gamma}\right); \\
\text{VI: } \rho_D &= \frac{384\pi e^2 T^2 \mu}{v_{F1} v_{F2} t^3 \gamma} \text{sgn}(\mu_1 \mu_2) \exp\left(-\frac{1}{T} \sqrt{2 \frac{t\Delta(t\gamma)}{\gamma}}\right) \ln^2\left(\frac{DT}{t\gamma}\right).
\end{aligned}$$

2.4.2 Drag between non-parallel links.

For parallel links, energy and momentum conservation restrict the allowed scattering processes very strongly. At low temperatures, this leads to an exponential suppression of the drag between non-equivalent parallel links. This has nothing to do with the exponential suppression of drag observed in the experiments, since the links are generally not parallel. For non-parallel links the sum of momenta on the two links is no longer conserved in the scattering process. In this section of the work I will compute the drag between non-parallel links.

Unlike the parallel links case, the interaction matrix element here can be evaluated analytically. Indeed, the integral

$$\int dx_1 dx_2 dy_1 dy_2 \frac{\psi_{n0}^*(x_1, y_1) \psi_{nq_1}(x_1, y_1) \psi_{n'0}^*(x_2, y_2) \psi_{n'q_2}(x_2, y_2)}{D(x_1, x_2, y_1, y_2)}$$

with

$$D(x_1, x_2, y_1, y_2) = \sqrt{d^2 + (y_1 - y_2 \cos \theta + x_2 \sin \theta)^2 + (x_1 - y_2 \sin \theta + x_2 \cos \theta)^2},$$

θ being the angle between the links, can be evaluated and yields:

$$V(q_1, q_2) = 2\pi e^2 \sqrt{2\pi} \frac{e^{-\frac{dQ}{|\sin\theta|}}}{Q} e^{-\frac{Q^2 l_H^2}{2 \sin^2 \theta}} L_n \left[\frac{Q^2 l_H^2}{2 \sin^2 \theta} \right] \\ \times L_{n'} \left[\frac{Q^2 l_H^2}{2 \sin^2 \theta} \right] \exp \left[i \frac{q_2^2 - q_1^2}{2} l_H^2 \cot \theta \right], \quad (2.115)$$

with $Q = \sqrt{q_1^2 + q_2^2 - 2q_1 q_2 \cos \theta}$. The last exponent in the matrix element is insignificant as it vanishes after taking the square of the absolute value of the matrix element. Above $x_{1,2}$ and $y_{1,2}$ respectively are the coordinates perpendicular to and along the links 1 and 2; the zero point for the $x_{1,2}$ -axes corresponds to the centers of the initial states and the zero-point of the $y_{1,2}$ -axes corresponds to the crossing of the projections of the center lines of the initial states along the z-axis (the direction of the magnetic field).

This expression should be inserted into (2.72). Proceeding as in the case of parallel links we can get the expression for the drag resistance. The main difference compared to the parallel links case is that instead of $\delta(q_1 - q_2)$ I get $\frac{\exp(-\frac{dQ}{|\sin\theta|})}{Q}$ which in principle allows any couple (q_1, q_2) of momentum transfers. This leads, as I will show, to nontrivial consequences, in particular to a T^2 behavior for the lowest temperatures for any $\theta \neq 0$. Before going on to the calculations, I will make some qualitative remarks. For any parameters of the layers it is possible to choose $q_{1,2}$ such that $t_1 q_1 \gamma_1 = t_2 q_2 \gamma_2$. From the calculations in the previous section it is quite clear that the ω - (or δ -) integral will have no exponential smallness for such $q_{1,2}$. On the other hand there might be an exponentially small factor stemming from the matrix element, as for $q_1 \neq q_2$, $dQ/|\sin\theta|$ can be much larger than unity. So, as now becomes clear, the qualitative analysis will consist in comparing the two exponents, one stemming from the matrix element, and the other is the one — known from the previous section — coming from the difference in Fermi velocities in the two layers.

Another point that should be mentioned is the sign of the drag signal, which can be determined without any additional calculations. Indeed, Eq. (2.75) will have $q_1 q_2$ in the integrand instead of q_y^2 . The sign of this

product has a vast effect on the value of the interaction matrix element: if $\cos \theta > 0$ then Q for $q_1 q_2 > 0$ is smaller than Q for $q_1 q_2 < 0$ provided the absolute values of q 's are the same. And vice versa. As Q enters the matrix element in the exponent, it is clear that for $\cos \theta > 0$ the q 's from the 1st and the 3rd quadrants dominate, and for $\cos \theta < 0$ it is the q 's from the 2nd and the 4th quadrants. For perpendicular links the drag is, of course, identically zero. The only other factor affecting the sign of the result is still the factor $\text{sgn}(\mu_1 \mu_2)$.

The above clearly shows that each pair of links from different layers of a real 2D sample gives contribution to the drag of the sign determined only by the relative sign of the local dispersions on the Fermi level. This, in turn, leads to the experimentally observed overall sign of the drag in a 2D sample.

Now to the quantitative analysis. Let us follow the calculations from the parallel links case and mention the differences. First in (2.72) I substitute (2.115) instead of (2.74). It leaves the factor $2\pi/L$ which was canceled for parallel links. L is the length of the link which corresponds to the correlation length of the 2D random potential. In (2.75) changes are evident: q_y in the arguments of ϵ_i are changed to q_i , the integration is done over $q_{1,2}$ instead of q_y and the factor $2\pi/L$ is still there.

I follow the line of calculations presented as "second" method. I will not keep trace of all numerical factors as some of the calculations below are only estimates and any numerical prefactor would not be reliable, rather I'll concentrate on the qualitative features. First I will look at the δ -integral and will determine its behavior as a function of $q_{1,2}$, then the $q_{1,2}$ -integrals will be estimated.

For estimating the δ -integral only some redefinitions should be made, in principle all the calculations are already done. The crucial point is the redefinition of Δ , which should now be defined as

$$\Delta = \frac{\Delta(t\gamma q)}{t\gamma q},$$

with $\Delta(t\gamma q) = |t_1\gamma_1q_1 - t_2\gamma_2q_2|$, rather than

$$\Delta = \frac{\Delta(t\gamma)}{t\gamma}$$

with $\Delta(t\gamma q) = |t_1\gamma_1q_1 - t_2\gamma_2q_2|$. This can be seen by rewriting the formulae (2.95)-(2.102) allowing for different q 's.

The obvious consequence is that the result of the δ -integration has the exponential part

$$\exp \left[-\frac{1}{T} \frac{t\Delta(t\gamma q)}{\gamma\mu q} \right], \quad (2.116)$$

and is *not* exponentially small for

$$\frac{t\Delta(t\gamma q)}{T\gamma\mu q} \sim 1. \quad (2.117)$$

I consider the case

$$\frac{t\Delta(t\gamma)}{T\gamma\mu} \gg 1, \quad (2.118)$$

as it is more interesting and allows to demonstrate interesting features of the crossed links. Conditions (2.117),(2.118) imply

$$\frac{\Delta q}{q} \approx -\frac{\Delta(t\gamma)}{t\gamma}, \quad (2.119)$$

and as can be seen from (2.117), $\Delta q/q$ must be close enough to these value:

$$\left| \frac{\Delta q}{q} + \frac{\Delta(t\gamma)}{t\gamma} \right| \lesssim \frac{\mu T}{t^2}. \quad (2.120)$$

The variation of $\Delta q/q$ is small compared with its absolute value if $T \ll \frac{t\Delta(t\gamma)}{\gamma\mu}$, which is the same condition that is necessary for the activated behavior of ρ_D for parallel links. The corresponding region is referred to in Fig. 2.23 as 1. The region 2 in this Fig. shows the values $q_{1,2}$ for which $dQ/|\sin\theta| \lesssim 1$.

The result of the δ -integration (for $\mu \gg T$) is obtained as the Eq. (2.90) with appropriate changes. As I'm not interested in numerical prefactors, I can write for it

$$\frac{\mu T}{t^2} e^{-qt\gamma/T}.$$

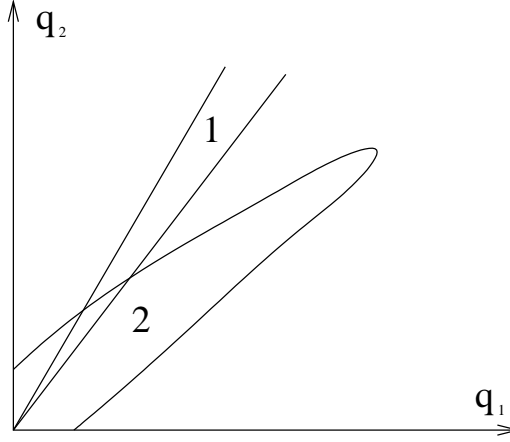


Figure 2.23: regions of the q_1q_2 -plane which give main contributions to the drag. Region 1 shows where the ω -integral is not exponentially small and region 2 shows where the interaction matrix element has a significant value. For details see the text.

Instead of $q_{1,2}$ I introduce $\Delta q = q_1 - q_2$ and $q = (q_1 + q_2)/2$. For the drag resistivity I can write:

$$\rho_D \sim \frac{e^2}{Lv_{F1}v_{F2}T} \int dq d\Delta q \frac{e^{-Qd/|\sin\theta|}}{Q^2} tq\gamma \frac{\mu T}{t^2} e^{-qt\gamma/T}, \quad (2.121)$$

with

$$Q^2 = \Delta q^2 \cos^2 \frac{\theta}{2} + 4q^2 \sin^2 \frac{\theta}{2}.$$

For $\theta \ll 1$ the last expression can be rewritten as

$$Q^2 = \Delta q^2 + q^2\theta^2. \quad (2.122)$$

The region of $(q, \Delta q)$ -plane that gives rise to the main contribution to the drag signal is given by (2.119,2.120). From here one can conclude that for $\theta \ll \left| \frac{\Delta(t\gamma)}{t\gamma} \right|$ it is the first term in (2.122) that dominates, while for larger θ 's it is the second term.

Looking at Fig. 2.23 one can notice that for sufficiently small temperatures the q -integral will converge inside the region 2 due to the exponent $\exp(-qt\gamma)/T$. This happens for

$$T \lesssim \frac{\theta (t\gamma)^2}{d \Delta(t\gamma)}.$$

For such temperatures and smallest θ 's, (2.121) can be rewritten as

$$\rho_D \sim \frac{e^2}{Lv_{F1}v_{F2}T} \int dq d\Delta q \frac{(t\gamma)^2}{q^2[\Delta(t\gamma)]^2} tq\gamma \frac{\mu T}{t^2} e^{-qt\gamma/T}. \quad (2.123)$$

(Δq has been substituted from (2.119)). The Δq -integral is determined by the width of region 1 in Fig. 2.23, which is given by (2.120). The q -integral afterwards is trivial. The result for the above-mentioned parameters is

$$\rho_D \sim \frac{e^2 \mu^2 T^2 \gamma^2}{Lv_{F1}v_{F2}t^2[\Delta(t\gamma)]^2}. \quad (2.124)$$

For $\mu \ll T$ there are no principle changes in the way the calculations are done. As for parallel links I expand the integrand in μ/T . The resulting δ -integral for q 's obeying (2.119,2.120) is the same as in Eq. (2.113). The result — as in the case of parallel links — differs from (2.124) only by changing one power of T to one power of μ :

$$\rho_D \sim \frac{e^2 \mu^3 T \gamma^2}{Lv_{F1}v_{F2}t^2[\Delta(t\gamma)]^2}. \quad (2.125)$$

For $T \gtrsim \frac{\theta}{d} \frac{(t\gamma)^2}{\Delta(t\gamma)}$, as can be seen from Fig. 2.23 the q -integral is cut off at $\frac{\theta}{d} \frac{t\gamma}{\Delta(t\gamma)} \ll \frac{1}{d}$. This leads to multiplying the above results by $\frac{\theta}{d} \frac{t\gamma}{\Delta(t\gamma)} \frac{t\gamma}{T} \ll \frac{1}{d} \frac{t\gamma}{T}$:

$$\rho_D \sim \frac{e^2 \mu^2 T \gamma^4}{Lv_{F1}v_{F2}[\Delta(t\gamma)]^3} \frac{\theta}{d}, \quad \text{for } \mu \gg T \quad (2.126)$$

and

$$\rho_D \sim \frac{e^2 \mu^3 \gamma^4}{Lv_{F1}v_{F2}[\Delta(t\gamma)]^3} \frac{\theta}{d}, \quad \text{for } \mu \ll T. \quad (2.127)$$

The above results are valid for lowest temperatures, when it is possible to neglect the contribution from the regions of the (q_1, q_2) -plane where the integrand is exponentially small. With growing temperature the contribution from these regions grows and for high enough T becomes bigger than the contribution from the region 1 of the Fig. 2.23. Now I will make quantitative estimates to substantiate these qualitative arguments. As stated above, I will not keep any numerical pre-factors. I also omit the factor $\text{sgn}(\mu_1\mu_2)$ as well as $\text{sgn}(\cos\theta)$ which was discussed above. In particular, I'll concentrate

on the case of very small θ which is interesting from the point of view of theoretical understanding of the drag between non-parallel links. The drag resistivity is given by

$$\begin{aligned} \rho_D &\sim \frac{e^2}{v_{F_1} v_{F_2} T L} \int \frac{dq dk d\delta}{Q^2} t q^2 \gamma \\ &\times \frac{e^{-Qd/|\sin\theta|}}{\cosh \frac{\epsilon_1(p_1^0 - \frac{q_1}{2}) - \mu_1}{2T} \cosh \frac{\epsilon_1(p_1^0 + \frac{q_1}{2}) - \mu_1}{2T} \cosh \frac{\epsilon_2(p_2^0 - \frac{q_2}{2}) - \mu_2}{2T} \cosh \frac{\epsilon_2(p_2^0 + \frac{q_2}{2}) - \mu_2}{2T}} \\ &= \frac{e^2}{v_{F_1} v_{F_2} T L} \int \frac{dq dk}{Q^2} t q^2 e^{-Qd/|\sin\theta|} \gamma B(q, k). \end{aligned} \quad (2.128)$$

Here $q = (q_1 + q_2)/2$, $k = (q_1 - q_2)/q$. Then $Q^2 \approx q^2(k^2 + \theta^2)$.

Using the intermediate results from the previous section we can write for the δ -integral which I denote $B(q, k)$:

$$B(q, k) = \begin{cases} 1) & e^{-\frac{t^2 \Delta}{T \mu}} \frac{T \mu^3}{t^4 \Delta} e^{-\frac{t^2 \Delta}{T \mu} \frac{q \gamma t}{\mu}}, & T \lesssim \frac{t^4}{\mu^3} \Delta^2; \\ 2) & e^{-\frac{t^2}{T \mu} \Delta} \left(\Delta - \frac{\mu q \gamma}{t} \right), & q < \frac{\Delta t}{\mu \gamma}, \frac{t^4}{\mu^3} \Delta^2 \lesssim T \lesssim \frac{t^2}{\mu} \Delta; \\ 3) & \frac{\mu T}{t^2} e^{-\frac{q t \gamma}{T}}, & \frac{t^2}{\mu} \Delta \lesssim T. \end{cases} \quad (2.129)$$

Here $\Delta = \left| \frac{\Delta(t\gamma)}{t\gamma} + \frac{\Delta q}{q} \right| \equiv |\Delta_0 + k|$.

Next the q -integration can be evaluated. It is done differently for the cases 1), 2), and 3) (see above). In fact, these cases correspond to different values of k (we concentrate on k 's between $-\Delta_0$ and 0 as it is clear that only these values can give significant contribution):

$$\begin{aligned} 1) & -\Delta_0 + \frac{\mu}{t^2} \sqrt{T \mu} \lesssim k; \\ 2) & -\Delta_0 + \frac{T \mu}{t^2} \lesssim k \lesssim -\Delta_0 + \frac{\mu}{t^2} \sqrt{T \mu}; \\ 3) & |\Delta_0 + k| \lesssim \frac{T \mu}{t^2}. \end{aligned} \quad (2.130)$$

The result is given by:

$$\rho_D \sim \frac{e^2}{L v_{F_1} v_{F_2} T} \int dk Y(k) \quad (2.131)$$

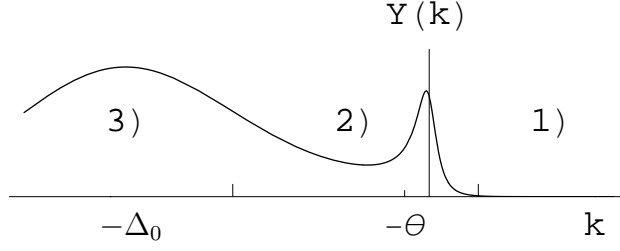


Figure 2.24: Typical plot of $Y(k)$. The definition of regions 1)-3) is given by (2.130); the depicted situation corresponds to the case considered in the text, when $k = 0$ belong to the region 2).

with

$$Y(k) = \begin{cases} 1) & e^{-\frac{t^2}{T\mu}|\Delta_0+k|} \frac{T\mu^3}{t^4|\Delta_0+k|} \frac{t\gamma}{k^2+\theta^2} \min\left(\frac{|\theta|}{d\sqrt{k^2+\theta^2}}, \frac{\mu^2 T}{\gamma t^3|\Delta_0+k|}\right); \\ 2) & e^{-\frac{t^2}{T\mu}|\Delta_0+k|} \frac{t\gamma}{k^2+\theta^2} |\Delta_0+k| \min\left(\frac{|\theta|}{d\sqrt{k^2+\theta^2}}, \frac{|\Delta_0+k|t}{\gamma\mu}\right); \\ 3) & \frac{\mu\gamma T}{t\Delta_0^2} \min\left(\frac{\theta}{\Delta_0 d}, \frac{T}{t\gamma}\right). \end{cases}$$

For lowest temperatures the region 3) dominates. I will now look at what happens for growing temperatures. For this I will look at the behavior of the function $Y(k)$ for different T and compare the integrated contribution to the drag signal from different regions. First of all I notice that in the case 3) it is the first option in the min's argument that must be realized, otherwise it is the region 3) that dominates, and this has been studied above. So I concentrate on the case when the q -integration in 3) is limited by the exponent from the interaction matrix element and not by the temperature. At some value of k the situation changes and the option in the min-function switches. A typical plot of $Y(k)$ can be seen on fig. 2.24⁴.

One has to distinguish two cases: $k = 0$ corresponds to 2) and to 1). These cases, as can be easily seen from (2.130) are determined by the same

⁴In fact the shown plot is rather specific. A slight change in the parameters of the plot immediately changes its character: one of the two peaks becomes dominating. This fact justifies the logarithmic accuracy calculations presented below.

restrictions for the temperature as those that limit the regions I and II from Fig. 2.22: if $T \lesssim \frac{t^4}{\mu^3} \Delta_0^2$ then $k = 0$ is in the region 1) and if $\frac{t^4}{\mu^3} \Delta_0^2 \lesssim T \lesssim \frac{t^2}{\mu} \Delta_0$ it is in the region 2). For simplicity I only consider the latter case, as it will be clear that the difference between them is purely calculative and considering the former case would not teach us anything new.

For $|k| \gtrsim |\theta|$, $k^2 + \theta^2$ in the expression for $Y(k)$ can be replaced by k^2 if I do not wish to calculate the numerical pre-factors. For k from 2) one can write:

$$Y(k) = e^{-\frac{t^2}{T\mu} |\Delta_0 + k|} \frac{t\gamma}{k^2} |\Delta_0 + k| \min \left(\frac{|\theta|}{d|k|}, \frac{|\Delta_0 + k|t}{\gamma\mu} \right). \quad (2.132)$$

For $k \sim \theta$ it crosses over to

$$Y(k) = e^{-\frac{t^2}{T\mu} \Delta_0} \frac{t\gamma}{\theta^2} \Delta_0 \min \left(\frac{1}{d}, \frac{\Delta_0 t}{\gamma\mu} \right). \quad (2.133)$$

The minimum of the first expression is reached for $|k| = \frac{3\mu T}{t^2} \ll \Delta_0$, for smaller absolute values of k , $Y(k)$ begins to grow and reaches its maximum at $k = 0$ and the width of this peak is $\sim \theta$. So I can estimate the contribution to ρ_D from all k 's outside of 3) as

$$\rho_D \sim \frac{e^2}{Lv_{F1}v_{F2}T} e^{-\frac{t^2}{T\mu} \Delta_0} \frac{t\gamma}{|\theta|} \Delta_0 \min \left(\frac{1}{d}, \frac{\Delta_0 t}{\gamma\mu} \right). \quad (2.134)$$

The contribution from the region 3) is given by the Eq. (2.126) which can be rewritten as

$$\rho_D \sim \frac{e^2}{Lv_{F1}v_{F2}T} \frac{\mu^2 T^2 \gamma |\theta|}{t^3 \Delta_0^3 d}.$$

Comparing the two contributions one can find with logarithmic accuracy that for

$$T \gtrsim \frac{t^2 \Delta_0}{\mu \ln \frac{\Delta_0}{|\theta|}} \quad (2.135)$$

the activated behavior stemming from the region where $|k| \lesssim |\theta|$ dominates, while in the broad region of smaller T 's one would observe a power law T -dependence. I do not consider in detail the whole variety of possible parameter relations as it would not lead to any qualitatively new results. The

main result: logarithmic dependence of the cross-over temperature on θ does not change.

Now, for some new insight, I look at the above from a different point of view: I fix T and consider ρ_D as a function of θ . Comparing (2.134) with (2.126) again I find that the first one dominates for

$$\theta \lesssim \Delta_0 \frac{t^2 \Delta_0}{\mu T} e^{-\frac{t^2 \Delta_0}{2\mu T}}.$$

For larger angles, but still $\theta \ll \Delta_0$ it is the power dependence contribution (2.126) that dominates. For even larger angles, $1 \gg \theta \gg \Delta_0$, $k \ll \theta$ everywhere in the relevant regions. That means that the expression (2.131) holds with the change of the first option in all min-functions in the expressions for $Y(k)$ to $1/d$, and, clearly $k^2 + \theta^2 \approx \theta^2$. Thus it becomes evident that $Y(k)$ reaches its maximum for $|\Delta_0 + k| = 0$ and the width of the peak is $\sim \frac{T\mu}{2}$. So, for $1 \gg \theta \gg \Delta_0$:

$$\rho_D \sim \frac{e^2}{Lv_{F1}v_{F2}T} \frac{\mu^2 T^2 \gamma}{t^3 \Delta_0^2} \min\left(\frac{1}{d}, \frac{T}{t\gamma}\right). \quad (2.136)$$

So, in agreement with (2.135), no exponential behavior is expected in any temperature range. In other words, already a relatively small non-parallelity is sufficient to kill any trace of the activated behavior, characteristic for the parallel links case. This means that this behavior, as was mentioned above, is just an artefact of the degenerate case of parallel links and it would have no effect after averaging over real two-dimensional samples, where θ 's take all possible values randomly.

Finally I touch the question of the limit $\theta \rightarrow 0$. Here the essential point is the size of the sample L . For parallel links of finite length, q_1 and q_2 can differ from one another by the value $\sim 1/L$; for nonparallel links this value is θ/d . Thus the cross-over value of θ is d/L . For such angles Eq. (2.115) is, as can be easily checked, no longer valid and for smaller angles it crosses over to Eq. (2.74). The last sentence should be understood in the sense that the expression (2.115) as a function of Δq tends to the δ -function with $\theta \rightarrow 0$ and the integrals over Δq of both expressions coincide for small θ 's.

As I have shown, for small θ 's (or for large enough T 's) the exponent in the expression for ρ_D is recovered. I failed to find a transparent way to see how the pre-factors of the expressions for the drag for parallel and non-parallel links cross-over to each other for $\theta \sim d/L$. More over I am quite convinced that to do this I need to obtain an analytic expression for the matrix element of the interaction for these angles which is definitely impossible. Still I'm sure that the arguments presented in this paragraph give enough insight to understand how the cross-over works.

2.4.3 Connection to two-dimensional drag.

In the previous parts of the work I have presented a detailed theory of the drag between two one-dimensional chiral spinless electron systems with an arbitrary angle between them. Spin can be easily included in the above picture. Since the interlayer interaction is spin independent, one simply has to sum over the two spin species (up and down) in both drive and drag layer, taking the (exchange enhanced) Zeeman spin splitting of the Landau levels into account. If the Fermi level of one layer lies between the centers of the highest occupied Landau levels for up and down spins, respectively, positive and negative contributions to the drag partially cancel each other. The cancelation is complete due to particle-hole symmetry in the case of odd integer filling, as observed in experiment.

As was mentioned in the beginning of the section 2.4, to get the result for the two-dimensional drag, knowing the results for the one-dimensional drag, one should in principle sum up the contributions from all crossing points between the links of the two random networks. The full accomplishing of this task presents a separate challenge and is not yet done. Still, many things can be seen already from simple arguments that have already to a large extent been mentioned above and that I recollect here.

Within our semiclassical picture anomalous drag, especially negative drag, is suppressed at temperatures above the Landau level width, because then electron- and hole-like states within the highest occupied level are almost equally populated. This agrees with the results from the Born approximation [18], and also with experiments.

It is plausible that localized states give small — if any — contribution to the drag. Indeed, such states represent electrons drifting around hills or valleys of the random potential and drag between two such states is formally zero as the contributions from the crossing points between them exactly cancel. The only way such localized states can affect the drag is if an electron scatters from such a state to a delocalized state, drifts along it away from its initial position and then scatters back to another localized state spatially separated from the first one. These processes are not forbidden as there is no energy conservation for a separate layer, so, unlike the one-layer transport problem, we can not restrict the role of these states to a reservoir for the delocalized ones. It is not clear whether the contribution of such processes to the drag is significant, still, it is clear that the delocalized states play a special role in the overall drag. Their contribution is largely determined by the Fermi filling factor at the percolation energy. If the Fermi level does not hit any extended states (for either spin species), the drag should vanish exponentially for $T \rightarrow 0$, since thermal activation or scattering of electrons into extended states is then suppressed by an energy gap. By contrast, for a Fermi level within the extended states band (for at least one spin species) the gap vanishes and the drag obeys generally quadratic low temperature behavior, as obtained for the drag between non-parallel links.

As to the sign of the drag, it is negative if one of the layers is more than half-filled and the other is less than half-filled, and positive in other cases. This follows from the results for the sign of the drag between two one-dimensional links that have been obtained above.

2.5 Conclusion

In summary, I have presented a semiclassical theory for electron drag between two parallel two-dimensional electron systems in a strong magnetic field, which provides a transparent picture of the most salient qualitative features of anomalous drag phenomena observed in recent experiments [2, 3, 13]. Lo-

calization plays a role in explaining activated low temperature behavior, but is not crucial for anomalous (especially negative) drag per se. In particular I have elaborated a detailed theory for the drag between two one-dimensional links (sections 2.4.1, 2.4.2). The temperature dependence of the drag has been derived for a whole variety of the parameters of the system as well as for parallel links and for non-parallel ones. I have also presented qualitative arguments to show to what consequences for the two-dimensional drag my results lead (section 2.4.3). A quantitative theory of drag which covers the whole range from low magnetic fields, where the Born approximation is valid, [21, 18] to high fields, where localization becomes important, remains an important challenge for work to be done in the future. A promising path here is a very general diagrammatic approach for long-range disorder systems which starts from the equation of the type (2.12). The averaging over disorder is done not for a single Green's function as usually ([16, 18]) but for the triangle function Γ as a whole and the Green's functions are taken in their exact form for a given random potential realization. This work is in progress now.

Chapter 3

Possible Jahn-Teller effect in Si-inverse layers

3.1 Introduction

In a symmetric configuration of atoms, the electronic state may be degenerate due to the high symmetry of the Hamiltonian. H. A. Jahn and E. Teller proved that such a symmetric configuration is unstable against a deformation lowering the overall symmetry of the Hamiltonian. The Jahn-Teller effect is well accounted for in molecules and crystals [31, 32]. The kinetic energy of electrons in the 2D electron gas (2DEG) under the conditions of quantum Hall effect is quenched. Electron states become macroscopically degenerate forming Landau levels. Interaction may remove some of this degeneracy. Nevertheless, one finds the global valley degeneracy at integer fillings¹. In this chapter we raise the question whether a lattice deformation — Jahn-Teller effect — lifts this valley degeneracy.

The theory of the 2DEG at integer ν uses [33, 34] the Hartree-Fock approximation in the limit of the small parameter: $E_c/\hbar\omega_c$, where $E_c = e^2/l_H$ is the energy of the Coulomb interaction and ω_c is the frequency of the cyclotron resonance. At $\nu = 1$ the theory predicts a ferromagnetic ground

¹If we neglect the Zeeman splitting this degeneracy turns to a spin-valley one.

state with degenerate uniform spin orientation. The elementary excitations are electron-hole pairs or neutral excitons, which correspond to gapless and noninteracting [35] spin-waves for vanishing momentum and vanishing effective g -factor. In the limit of large exciton momentum the electron and the hole become independent charged excitations. A special topological spin texture in a 2D ferromagnet called "skyrmion" [36] has unit charge and half of the quasiparticle energy [37]. In this chapter such textures are considered in the presence of a Jahn-Teller effect.

In bulk Si there is a six-fold valley degeneracy of low energy electron states in the conduction band. It is reduced to two-fold degeneracy for the (100) orientation of the 2D-plane due to the transverse quantization of electron motion in a quantum well [38]. Even for the (111) orientation of the 2D-plane with six equivalent valleys only two valleys connected by the time reversal symmetry are actually occupied in a strong magnetic field [39]. This effect is governed by the anisotropy of the effective mass of electrons and corresponds to a spontaneous breaking of valley symmetry. Here we study the effects related to this valley degeneracy and show that such a bivalley system is similar to the bilayer systems. The bilayer setup has been extensively studied theoretically for $\nu = 1$ [40, 41] and $\nu = 2$. [42, 43] The layer degeneracy of electron states can be described by a four component spinor in combined spin-layer space. In former works [44, 45] the total 2DEG Hamiltonian was subdivided into a symmetric part and a small anisotropic part which reduces the symmetry. The symmetric part is invariant under a SU(4) group of electron spinor rotations in the combined spin and layer Fock space. This SU(4) group has the apparent SU(2) \otimes SU(2) subgroup of separate rotations in spin and valley spaces.

The electron annihilation operator can be expanded using one electron orbital functions:

$$\psi_\alpha(\vec{\rho}) = \sum_{\tau} \psi_{\alpha\tau}(\vec{r})\chi(z)e^{i\tau Qz/2}, \quad (3.1)$$

where α is the spin index, z is the coordinate perpendicular to the 2D plane and \vec{r} is the in-plane coordinate vector. The index $\tau = \pm 1$ numerates the two valleys. Valley wave functions of electrons in a Si inverse layer:

$\chi(z) \exp(\pm iQz/2)$, are normalized and almost orthogonal for smooth, real $\chi(z)$ with the negligible overlap $\int \chi^2(z) \exp(iQz) dz$ [38]. Q is the shortest distance between the valley minima in reciprocal space, equals approximately to $2/a_{Si}$, with a_{Si} being the lattice constant. $\psi_{\alpha\tau}(\vec{r})$ is the electron wave function of in-plane motion in valley τ with spin α and constitutes a four component spinor. Electrons in the system will strongly interact with phonons with momentum $\pm Q$, giving rise to scattering from one valley to another. The Jahn-Teller effect (JTE) in Si-inverse layers corresponds to a displacement of silicon atoms in z -direction. The new equilibrium is determined from the balance of electron-phonon and elastic energies. A strong magnetic field is essential for JTE. Indeed, in its absence a coherent JT state would lead to an appearance of one Fermi-sphere instead of two smaller ones for two different valley states. This would lead to an increase of the electrons' kinetic energy that makes the JTE energetically unprofitable. In the following sections we discuss the possible JTE in detail.

This chapter is structured as follows. In section 3.2 we introduce the Hamiltonian of the system and subdivide it into SU(4)-symmetric and -asymmetric parts. Section 3.3 is devoted to a discussion of the SU(4)-symmetric case. In the sections 3.4, 3.5 the anisotropic terms in the Hamiltonian are included and the ground state of the system for different parameters is found. In section 3.6 the effect of the anisotropic terms on the energy of the skyrmion is considered. And finally a brief review of the results of this chapter is presented in the conclusion.

3.2 Hamiltonian of electron gas on Si interface

The Hamiltonian of the Si inverse layer describes the electron system interacting with phonons:

$$\hat{H} = \hat{H}_e + \hat{H}_{e-ph} + \hat{H}_{ph}. \quad (3.2)$$

For a narrow quantum well, the Hamiltonian of the 2DEG in a magnetic field can be expressed in terms of a spinor $\psi_{\alpha\tau}(\vec{r})$ and reads (we use the system of

units where: $\hbar = 1$, $e = c$, $B = 1$ and the magnetic length $l_H = \sqrt{c\hbar/eB} = 1$)

$$\begin{aligned} \hat{H}_e = & \int \psi_{\alpha\tau}^\dagger(\vec{r}) \left(\frac{1}{2m} \left[-i\vec{\nabla} + \vec{A} \right]^2 + g\mu_B \vec{B} \vec{\sigma} \right)_{\alpha\beta} \psi_{\tau\beta}(\vec{r}) d^2\vec{r} \\ & + \frac{e^2}{2\kappa} \int \frac{\psi_{\alpha\tau_1}^\dagger(\vec{r}_1) \psi_{\beta\tau_2}^\dagger(\vec{r}_2) \psi_{\beta\tau_2}(\vec{r}_2) \psi_{\alpha\tau_1}(\vec{r}_1)}{|\vec{r}_1 - \vec{r}_2|} d^2\vec{r}_1 d^2\vec{r}_2, \end{aligned} \quad (3.3)$$

where g is the conduction band gyromagnetic ratio, κ is the dielectric constant of Si, μ_B is Bohr magneton and \vec{B} is the uniform magnetic field in z -direction. Here and in the following summation over repeated greek indices is assumed. We neglect small terms with different valley indices in the electron density operator and we use the Debye model for phonons with large momenta $\pm Q$

$$\hat{H}_{ph}[u_z] = \frac{\rho_{Si}}{2} \int \left[(\partial_t u_z)^2 + c^2 (\vec{\nabla} u_z)^2 \right] d^3\vec{\rho}, \quad (3.4)$$

where $u_z(\vec{\rho})$ is the lattice displacement in z -direction. We consider only the valley-mixing electron-phonon interaction:

$$\begin{aligned} \hat{H}_{e-ph} = & \Theta \int \psi_{\alpha\tau_1}^\dagger(\vec{r}) \tau_{\tau_1\tau_2}^\pm \psi_{\alpha\tau_2}(\vec{r}) \times \\ & \left(\int \chi^2(z) e^{\pm iQz} \nabla_z u_z(\vec{\rho}) dz \right) d^2\vec{r}, \end{aligned} \quad (3.5)$$

with Θ and ρ_{Si} being the deformation potential and the density of Si respectively. Here and in the following c is the speed of sound. τ^μ and σ^μ , with $\mu = x, y$ and z , are the Pauli matrices in valley and spin spaces and $\tau^\pm = (\tau^x \pm i\tau^y)/2$. $\vec{A}(\vec{r}) = (0, Bx)$ is the vector-potential in Landau gauge.

In a magnetic field we expand the electron operator over Landau orbital states $\phi_{n,p}(\vec{r})$ in the Landau gauge:

$$\hat{\psi}_{\alpha\tau}(\vec{r}) = \sum_{n,p} \phi_{n,p}(\vec{r}) \hat{c}_{np,\alpha\tau}, \quad (3.6)$$

where $c_{np,\alpha\tau}^\dagger$ and $c_{np,\alpha\tau}$ are electron creation and annihilation operators in the τ valley with spin α , n enumerates Landau levels and the continuous parameter p specifies states within one Landau level.

We assume that the electrons are confined to the lowest Landau level $n = 0$ in the ground state. The electronic part of the Hamiltonian contains the Coulomb and the kinetic energy in the lowest Landau level:

$$H^{sym} = \frac{1}{2m} \sum_p c_{p\alpha\tau}^\dagger c_{p\alpha\tau} + \frac{1}{2} \int \frac{d^2\vec{q}}{(2\pi)^2} V(\vec{q}) N(\vec{q}) N(-\vec{q}), \quad (3.7)$$

where

$$V(\vec{q}) = 2\pi e^2 / \kappa q \quad (3.8)$$

is the 2D Fourier transform of the Coulomb interaction. Notice that in our system of units $1/m$ is the cyclotron frequency. The electron density operator is:

$$N(\vec{q}) = \sum_p c_{p\alpha\tau}^\dagger c_{p-q_y \alpha\tau} e^{-iq_x(p-q_y/2)-q^2/4}. \quad (3.9)$$

Unitary transformations of electron operators

$$c_{p\alpha\tau_1} = U_{\alpha\tau_1, \beta\tau_2} c_{p\beta\tau_2} \quad (3.10)$$

in the combined spin and valley space leave the Hamiltonian (3.7) invariant if U is a matrix from the $SU(4)$ Lie group. For the Landau level filling factors $\nu = 1, 2, 3$ ($\nu = 4$ corresponds to a fully filled zeroth Landau level) we assume that the ground state is uniform with electrons of spin α_i and valley τ_i filling every orbital of the lowest Landau level:

$$\Psi(\alpha_1\tau_1 \dots \alpha_\nu\tau_\nu) = \prod_{i=1}^{\nu} \prod_p c_{p\alpha_i\tau_i}^\dagger |vac\rangle. \quad (3.11)$$

One can check that any such wave-function (3.11) represents an eigenfunction of H^{sym} Eq. (3.7). The state (3.11) is degenerate and a set of related eigenstates can be generated by applying uniform rotations U .

The remaining terms in the Hamiltonian (3.2) arise from a valley splitting term due to a singularity of the well potential on the Si/SiO₂ interface [38], Zeeman term, electron-phonon interaction and the phonon energy:

$$\begin{aligned} H^{an} &= -t \sum_p c_{p\alpha\tau_1}^\dagger \tau_{\tau_1\tau_2}^x c_{p\alpha\tau_2} \\ &- |g|\mu_B H \sum_p c_{p\alpha\tau}^\dagger \sigma_{\alpha\beta}^z c_{p\beta\tau} + H_{e-ph} + H_{ph}, \end{aligned} \quad (3.12)$$

where t is the phenomenological valley-splitting constant. This part breaks the SU(4) symmetry and lifts the degeneracy of the eigenstates of SU(4)-symmetric Hamiltonian (3.2). The splitting of energy levels is determined by small matrix elements of the anisotropic Hamiltonian (3.12) projected onto a linear space of the symmetric Hamiltonian (3.7) level degeneracy. There is no renormalization of the anisotropic Hamiltonian parameters (3.12) due to electron-electron interaction in the symmetric part Eq. (3.7). Thus the Hartree-Fock approach is valid up to $O(H^{an}/\omega_H)$ terms for $\nu = 1, 2, 3$.

The total Hamiltonian $H^{sym} + H^{an}$, Eqs. (3.7,3.12), can be treated as in the theory of magnetism and can be expressed in terms of an order parameter matrix $\hat{Q}(\vec{r})$. According to the Goldstone theorem the symmetric part Eq. (3.7) can be expanded in powers of spatial derivatives of the order parameter: $\vec{\nabla}\hat{Q}(\vec{r})$, whereas the anisotropic part Eq. (3.12) depends on the local value of the order parameter in the leading order.

3.3 SU(4) Symmetric Case

Non-homogeneous states can be generated from the ground state (3.11) by slow rotations, with the effective action being dependent on the rotation matrix $U(t, \vec{r})$:

$$S[U] = -i \text{Tr} \log \int \mathcal{D}\psi \mathcal{D}\psi^\dagger \exp \left(i \int \mathcal{L} dt \right), \quad (3.13)$$

where the spin-valley symmetric Lagrangian of the 2DEG is

$$\begin{aligned} \mathcal{L} = & \int \psi_\alpha^\dagger \left[i \frac{\partial}{\partial t} - \frac{1}{2m} \left(-i\vec{\nabla} + \vec{A}_0 + \vec{\Omega} \right)^2 \right]_{\alpha\beta} \psi_\beta d^2\vec{r} \\ & - \int \psi_\alpha^\dagger \Omega_{\alpha\beta}^t \psi_\beta d^2\vec{r} + \frac{1}{2} \sum_{\vec{q}} V(\vec{q}) N(\vec{q}) N(-\vec{q}), \end{aligned} \quad (3.14)$$

where $\Omega^t = -i U^\dagger \partial_t U$ and $\vec{\Omega} = -i U^\dagger \vec{\nabla} U$. We treat the nonhomogeneous matrix U as a classical field and therefore the effective action (3.13) describes a macroscopic motion of the corresponding spin-texture. The essential points

here are the slow variation of $U(\vec{r})$ on the microscopic scale given by the magnetic length and the use of the gradient expansion assuming a locally ferromagnetic ground state. The effective action (3.13) for multivalley systems was found in the work of Arovas et al. [46] We derive it here following the method of Ref. [47].

The Hamiltonian corresponding to (3.14) with $\vec{\Omega} = 0$ has a uniform ground state (3.11). We consider three filling factors: $\nu = 1$ with $\Psi(\uparrow +1)$, $\nu = 2$ with $\Psi(\uparrow +1, \downarrow -1)$ and $\nu = 3$ reducing to the case $\nu = 1$ under the electron-hole transformation. The reference state is alternatively given by an electron occupation diagonal matrix: $N_{\alpha\tau_1, \beta\tau_2} = (1, 0, 0, 0)$ in the case $\nu = 1$, and $N_{\alpha\tau_1, \beta\tau_2} = (1, 1, 0, 0)$ in the case $\nu = 2$. The Green function for electron propagation in the lowest Landau level evaluated over the ground state reads

$$G_{\alpha\tau_1, \beta\tau_2}^0(\epsilon, p) = \frac{N_{\alpha\tau_1, \beta\tau_2}}{\epsilon + E_0 + \mu - i0} + \frac{(\hat{1} - N)_{\alpha\tau_1, \beta\tau_2}}{\epsilon + \mu + i0}, \quad (3.15)$$

where $\mu = -E_0/2$ is the chemical potential and exchange constants in the limit of vanishing thickness of the electron layer are

$$E_0 = 2E_1 = \sqrt{\frac{\pi}{2}} \frac{e^2}{\kappa l_H}. \quad (3.16)$$

The effective action is $S[\Omega] = S_0[\Omega] + S_2[\Omega]$, where $S_0[\Omega] = i \text{Tr} \log(G/G_0)$, whereas $S_2[\Omega]$ is represented by the two diagrams on Fig. 3.1. The first order perturbation correction to the action Eq. (3.13) depends on the Green function of electron propagation in the first excited Landau level [47]:

$$G_{\alpha\tau_1, \beta\tau_2}^1(\epsilon) = \frac{N_{\alpha\tau_1, \beta\tau_2}}{\epsilon - \omega_c + E_1 + \mu + i0} + \frac{(\hat{1} - N)_{\alpha\tau_1, \beta\tau_2}}{\epsilon - \omega_c + \mu + i0}. \quad (3.17)$$

The two terms of the Hamiltonian depending on the gradient matrix field are:

$$H_1 = \frac{1}{2m} \int \psi_{\alpha\tau_1}^\dagger \left(\Omega^+ \hat{\Pi}_- + \hat{\Pi}_+ \Omega^- \right)_{\alpha\beta\tau_1\tau_2} \psi_{\beta\tau_2} d^2\vec{r}, \quad (3.18)$$

$$H_2 = \frac{1}{2m} \int \psi_{\alpha\tau_1}^\dagger \left(\vec{\Omega}^2 - \epsilon_{\mu\nu} \partial_\mu \Omega_\nu \right)_{\alpha\beta\tau_1\tau_2} \psi_{\beta\tau_2} d^2\vec{r}, \quad (3.19)$$

where $\Omega_\pm = \Omega_y \mp i\Omega_x$, and the differential operators $\hat{\Pi}_\pm$ shift an electron to the adjacent Landau levels: $\hat{\Pi}_- \phi_{np}(\vec{r}) = \sqrt{2n} \phi_{n-1p}(\vec{r})$, $\hat{\Pi}_+ \phi_{n-1p}(\vec{r}) =$

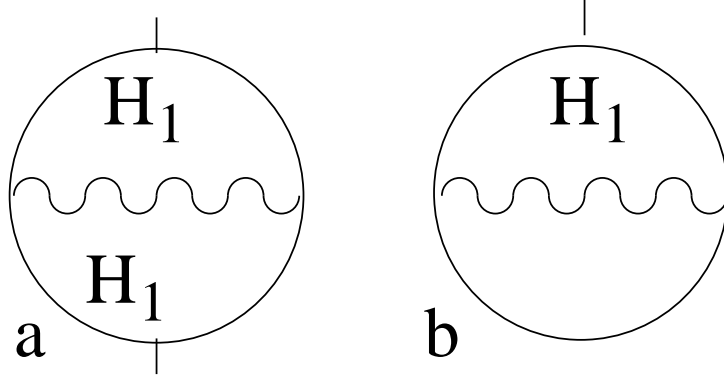


Figure 3.1: Second order (a) and the anomalous first order (b) diagrams. Solid and wavy lines represent the electron Green functions and the Coulomb interaction respectively.

$\sqrt{2n}\phi_{np}(\vec{r})$, though only the $n = 0$ and $n = 1$ Landau level states are relevant for this problem. An expansion of the 2DEG action up to the second order of Hamiltonian (3.18) gives:

$$S_0[\Omega] = i\text{Tr}(H_1 G_0) + \frac{i}{2}\text{Tr}(H_1 G_0 H_1 G_0) + i\text{Tr}(H_2 G_0). \quad (3.20)$$

The Hartree-Fock diagram in Fig. 3.1a has been calculated in Ref. [47] whereas the anomalous diagram in fig. 3.1b is calculated in Appendix A. The resulting effective Lagrangian is

$$\begin{aligned} \mathcal{L}_{eff}[\Omega] = & \int \left(\text{Tr}(\Omega_t(t, \vec{r}) \hat{N}) + \frac{E_0 + E_1}{2} \epsilon_{\mu\nu} \nabla_\mu \Omega_\nu^z - \right. \\ & \left. - \frac{E_1}{2} \text{Tr} [N \Omega_+(t, \vec{r}) (\hat{1} - N) \Omega_-(t, \vec{r})] \right) \frac{d^2 \vec{r}}{2\pi}, \end{aligned} \quad (3.21)$$

where $\Omega_\mu^z = -i \text{Tr}(N U^\dagger \partial_\mu U)$. The matrices N and $\hat{1} - N$ are projecting operators onto the physical rotations that form a subset of the SU(4) Lie group. The matrix field Ω_μ can be expanded in the basis of fifteen generators of the SU(4) group: $\{\Gamma^l\}$, with $l = 1..15$. They form two complementary sets: the first *even* set includes those generators that do commute with N , whereas the second *odd* set includes the remaining generators. Generators of the *even* set constitute an algebra themselves. This algebra has a normal

Abelian subalgebra formed by a single traceless generator: $N - \nu/4$. A Lie group generated by the *even* set is a stabilizer sub-group \mathcal{S} of the $SU(4)$ group. The *odd* set contains an even number of generators: eight in the case of $\nu = 2$ and six in the case $\nu = 1, 3$.

The Hamiltonian is invariant under time reversal symmetry. The time reversal operation transforms the rotation matrix as $U \rightarrow U^*$, the gradient field as $\vec{\Omega} \rightarrow -\vec{\Omega}^T$ and also inverts the magnetic field B^z . Accordingly, we rewrite the energy in the Lagrangian (3.21) in a time reversal symmetric form:

$$E_{eff}[\Omega] = \int \frac{d^2\vec{r}}{2\pi} \left[\frac{E_1}{2} \text{Tr} (N\Omega_\mu(\hat{1} - N)\Omega_\mu) - \frac{E_0}{2} \text{sgn}(B^z)\epsilon_{\mu\nu}\nabla_\mu\Omega_\nu \right], \quad (3.22)$$

where the identity $\epsilon_{\mu\nu}\text{Tr}(\Omega_\mu\Omega_\nu N) = i\epsilon_{\mu\nu}\nabla_\mu\Omega_\nu^z$ is used. It follows immediately that $E_{eff} \geq 0$. The first term is the gradient energy whereas the second term is proportional to the topological index of the spin texture:

$$\mathcal{Q} = \int \epsilon_{\mu\nu}\nabla_\mu\Omega_\nu^z \frac{d^2\vec{r}}{2\pi} = Z, \quad (3.23)$$

where Z is an integer. The states with $Z \neq 0$ are called skyrmions after T. H. R. Skyrme who has first considered such textures. The case $\mathcal{Q} = \pm 1$ corresponds to the simplest spin skyrmions in the first valley which can be rotated by a $SU(4)$ matrix to become a general bivalley skyrmion. The spin stiffness in E_{eff} Eq. (3.22) coincides identically with that of the one-valley case [47]. This means that the bivalley skyrmion energy is the same as that found for one valley. The charge in the bivalley skyrmion core is distributed over the two valleys with long divergent tails: $n_{\pm 1}(\vec{r}) \sim \pm 1/(R^2 + r^2)$, if one neglects anisotropy. But the total charge of the two valleys follows a convergent distribution identical to the charge density in the one valley case [37]:

$$n(\vec{r}) = \frac{\epsilon_{\mu\nu}\nabla_\mu\Omega_\nu^z(\vec{r})}{2\pi} = \frac{R^2}{\pi(R^2 + r^2)^2}, \quad (3.24)$$

where R is the radius of the skyrmion core.

The expectation value of any operator A in the ground state $\langle A \rangle = \text{Tr}(A\hat{Q})$ can be expressed in terms of the order parameter matrix

$$\hat{Q}(\vec{r}) = U(\vec{r})NU^+(\vec{r}). \quad (3.25)$$

Obviously rotations from the small sub-group \mathcal{S} leave the order parameter invariant. Thus, rotations in Eq. (3.25) can be restricted to a physical space of the bivalley 2DEG which is the complex Grassmannian manifold $G_{4\nu}^C = U(4)/U(\nu) \otimes U(4 - \nu)$. We rewrite Eq. (3.22) in terms of \hat{Q} :

$$E_{eff}[\hat{Q}] = \frac{E_1}{4} \int \text{Tr} \left(\vec{\nabla} \hat{Q} \vec{\nabla} \hat{Q} \right) \frac{d^2 \vec{r}}{2\pi} - \frac{E_0}{2} \mathcal{Q}. \quad (3.26)$$

In this representation the topological index \mathcal{Q} is an index of a map from the 2D plane onto the coset space of the order parameter. The rule (3.23) is a consequence of the homotopy group

$$\pi_2(G_{4\nu}^C) = \mathbb{Z}, \quad (3.27)$$

proven in Appendix B.

Varying the effective Lagrangian consisting of the first kinetic term Eq. (3.21) (rewritten as the Wess-Zumino term [46]) and the energy Eq. (3.26), we find the matrix Landau-Lifshitz equation

$$\left[\hat{Q} \partial_t \hat{Q} \right]_- = \frac{E_1}{2} \vec{\nabla}^2 \hat{Q}. \quad (3.28)$$

It describes three ($\nu = 1$) and four ($\nu = 2$) degenerate "spin-valley"-waves with dispersion $\omega(\vec{q}) = E_1 q^2/2$.

3.4 Jahn-Teller effect

The Jahn-Teller effect is the deformation of a lattice which lowers the energy $H_{e-ph} + H_{ph}$. Phonons interact with the local electron density. We illustrate the main points of our approach for $\nu = 1$, keeping the spin of electrons fixed and up. The electron annihilation operator (3.1) is expanded in the basis of two mutually orthogonal valley wave functions $\tau = \pm 1$. The density

operator $\hat{n}(\vec{\rho}) = \hat{\psi}^\dagger(\vec{\rho})\hat{\psi}(\vec{\rho})$ has the diagonal element uniform over the 2D plane: $\chi^2(z)\langle\hat{\psi}_\tau^\dagger(\vec{r})\hat{\psi}_\tau(\vec{r})\rangle = \nu\chi^2(z)/2\pi l_H^2$, where the average is taken over the ground state (3.11), and the term oscillating in z direction: $\delta\hat{n}(\vec{\rho}) = \chi^2(z)(\hat{\psi}_{+1}^\dagger(\vec{r})\hat{\psi}_{-1}(\vec{r})e^{iQz} + h.c.)$. We use the electronic order parameter (3.25) to express the average oscillating density as

$$\delta n(\vec{\rho}) = \frac{\chi^2(z)}{2\pi l_H^2} \left(\text{Tr}(\hat{Q}\tau^+)e^{iQz} + \text{Tr}(\hat{Q}\tau^-)e^{-iQz} \right). \quad (3.29)$$

The omitted diagonal density term couples electrons to phonons with in-plane momentum $\vec{q}_\perp = 0$ and can be neglected in the thermodynamic limit. The oscillatory part of the average electron density allows for lowering of the energy by a static lattice deformation which oscillates with wave vector Q inside the quantum well:

$$\nabla_z u_{st}^z(\vec{\rho}) = \frac{\Theta}{\rho_{Si}c^2} \delta n(\vec{\rho}). \quad (3.30)$$

This deformation is a phonon "condensate" or Jahn-Teller effect. The corresponding energy gain is found from the minimization of $H_{e-ph} + H_{ph}$ as

$$E_{st} = -\mathcal{N}G\text{Tr}(\hat{Q}\tau^+)\text{Tr}(\hat{Q}\tau^-). \quad (3.31)$$

where $\mathcal{N} = A/2\pi l_H^2$ is the number of states within Landau level for a sample with area A and $G = \Theta^2 \int \chi^4(z)dz / 2\pi l_H^2 \rho_{Si}c^2$ is the strength of the electron-phonon interaction. The integral in the last definition is the inverse width of the 2D layer in z -direction.

This static deformation causes a new equilibrium position of the lattice. Assuming that the static deformation is small, we neglect the change of the phonon spectrum due to anharmonic effects. However we do take into account the dynamical phonons which produce a polaronic effect in second order of the electron-phonon interaction. Expanding the phonon field around the new equilibrium: $u^z(\vec{\rho}) = u_{st}^z(\vec{\rho}) + \delta u^z(\vec{\rho})$, we obtain

$$\begin{aligned} \hat{H}_{e-ph} = & \Theta \int \psi_{\alpha\tau_1}^\dagger(\vec{r})\tau_{\tau_1\tau_2}^\pm\psi_{\alpha\tau_2}(\vec{r}) \times \\ & \left(\int \chi^2(z)e^{\pm iQz}\nabla_z\delta u_z(\vec{\rho}) dz \right) d^2\vec{r}, \end{aligned} \quad (3.32)$$

where the lattice deformation

$$\delta u_z(\vec{\rho}) = \sum_{\vec{q}} \sqrt{\frac{\hbar}{2V\rho_{Si}\omega(q)}} \left(b_{\vec{q}} e^{i\vec{q}\vec{\rho}} + b_{\vec{q}}^\dagger e^{-i\vec{q}\vec{\rho}} \right),$$

can be expanded in phonon creation and annihilation operators $b_{\vec{q}}^\dagger$ and $b_{\vec{q}}$. In order to find the ground state energy we sum up diagrams for the thermodynamic potential expanded in powers of the (assumed to be) weak electron-phonon and Coulomb interactions using the Matsubara method [48]. We express the energy in terms of the order parameter matrix \hat{Q} .

The electron Green function can be expressed in terms of \hat{Q} as

$$G^0(\varepsilon_n, p) = \frac{\hat{Q}}{i\varepsilon_n + E_0/2} + \frac{\hat{1} - \hat{Q}}{i\varepsilon_n - E_0/2}. \quad (3.33)$$

We include the coordinate dependent electron wave-functions in the interaction vertices. The phonon Green function is [48]

$$D(\omega_n, q) = -\frac{\omega^2(q)}{\omega_n^2 + \omega(q)^2}. \quad (3.34)$$

For small momentum transfers the Coulomb interaction is much larger than the phonon propagator. In the opposite case of large transferred momentum with $\pm Q$ z -component we neglect the Coulomb interaction. Therefore in the Coulomb vertex the valley index is conserved as well as the spin index. Due to the identity $\hat{Q}(1 - \hat{Q}) = 0$, all one loop diagrams with only Coulomb lines vanish.

The expression for the electron-phonon vertex in Landau gauge reads

$$g(pp', \vec{q}) = \frac{\Theta}{\sqrt{\rho_{Si}c^2}} \delta_{p, q_y + p'} e^{-q_\perp^2/4 - q_x(p+p')/2} \chi^2(q_z - Q),$$

where \vec{q} is the phonon momentum and the envelope function $\chi^2(q_z) = \int \chi^2(z) e^{iq_z z} dz$ has a characteristic width l^{-1} in momentum space. The polaron contribution to the energy assuming weak Coulomb interaction: $E_0/\omega(Q) \rightarrow 0$, is

$$E_{e-ph}^0 = \sum_{\varepsilon_n \omega_n pp'} \text{Tr} (G^0(\varepsilon_n, p) \tau^+ G^0(\varepsilon_n + \omega_n, p') \tau^-) \sum_{\vec{q}} g^2(pp', \vec{q}) D(\omega_n, q) = \mathcal{N}G \left(\text{Tr}(\hat{Q}\tau^+\hat{Q}\tau^-) - \frac{\nu}{2} \right). \quad (3.35)$$

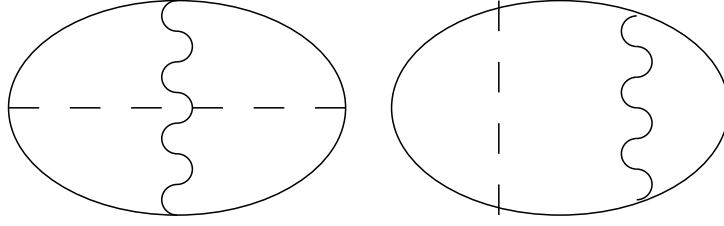


Figure 3.2: The two diagrams that give easy-plane anisotropy in the case $\nu = 1$. Solid, dashed and wavy lines are the electron, the phonon propagators and the Coulomb interaction respectively.

Summing it up with Eq. (3.31) we get the total electron-phonon energy in second order of the electron-phonon interaction. Here we neglect small terms of the order $(Ql)^{-4}$ due to the discontinuity of the derivative of the wave function $\chi(z)$ at the interface [40]. For $\nu = 1$ the total energy given by the sum of Eqs. (3.31,3.35) is isotropic in spin-valley space. Thus, if we neglect the Coulomb interaction corrections to the electron-phonon interaction we find that the degeneracy in isospin direction is not lifted. Physically, the polaron energy is a single electron energy and there is no anisotropy operator for a single electron because of the Pauli matrix identity $\tau_i^2 = 1$.

The Coulomb interaction creates the easy-plane anisotropy in the case $\nu = 1$. The essential diagrams are shown in Fig.(3.2), where the wavy line represents 2D Coulomb potential $V(q)$ whereas the solid and the dashed lines represent the electron, Eq. (3.33), and the phonon, Eq. (3.34), propagators. Direct calculation neglecting the dependence of $\omega(Q)$ on the in-plane momentum q_{\perp} shows that the sum of the two diagrams in Fig. 3.2 is

$$E_{e-ph}^{\delta} = -\mathcal{N}G\delta\text{Tr}\left(\hat{Q}\tau^+\hat{Q}\tau^-\right), \quad (3.36)$$

where $\delta = E_{ex}/\omega(Q)$ is the ratio between the Coulomb exchange energy

$$E_{ex} = \frac{e^2}{\pi\kappa} \int \frac{d^2q_{\perp} dq_z}{q_{\perp}^2 + q_z^2} |\chi^2(q_z)|^2 e^{-q_{\perp}^2 l_H^2/2} \left(1 - e^{-q_{\perp}^2 l_H^2/2}\right), \quad (3.37)$$

to the energy of the valley-mixing phonon. Obviously, $\delta > 0$ ($E_{ex} > 0$), and the anisotropy is of the the easy-plane type. The above result is valid if $E_0 \ll \omega(Q)$.

The sum of the static, polaronic and the Coulomb correction energies, Eqs. (3.31,3.35,3.36), gives the total anisotropic energy:

$$E_{ep} = G \int \left[-\text{Tr}(\hat{Q}\tau^+)\text{Tr}(\hat{Q}\tau^-) + (1-\delta)\text{Tr}(\hat{Q}\tau^+\hat{Q}\tau^-) \right] \frac{d^2\vec{r}}{2\pi}. \quad (3.38)$$

Thus the JTE is energetically favorable and corresponds to the easy-plane valley anisotropy.

The easy-plane anisotropy changes the dispersion of collective excitations. Let us consider this effect in the limit of vanishing valley symmetry breaking t and Zeeman h anisotropies. We add the easy-plane term (3.38) to the Landau-Lifshitz equation (3.28):

$$\left[\hat{Q} \partial_t \hat{Q} \right]_- = \frac{E_1}{2} \vec{\nabla}^2 \hat{Q} + G\delta \left(\tau^+ \text{Tr}(\hat{Q}\tau^-) + \tau^- \text{Tr}(\hat{Q}\tau^+) \right). \quad (3.39)$$

This equation can be linearized in the vicinity of $Q = N$. It describes two "spin"-modes (the same as for the symmetric case) and one acoustic mode with dispersion $\omega = \sqrt{G\delta E_1}q$ in analogy to the bilayer case [40].

3.5 Phase diagram

The anisotropic bivalley energy in the uniform state is the diagonal matrix element of the anisotropic Hamiltonian (3.2) expressed in terms of the order parameter \hat{Q} :

$$E_{an}/\mathcal{N} = -t \text{Tr}(\hat{Q}\tau^x) - h \text{Tr}(\hat{Q}\sigma^x) + G \left[(1-\delta)\text{Tr}(\hat{Q}\tau^+\hat{Q}\tau^-) - \text{Tr}(\hat{Q}\tau^+)\text{Tr}(\hat{Q}\tau^-) \right], \quad (3.40)$$

where $h = |g_e|\mu_B H$. The order parameter \hat{Q} can be parameterized by six ($\nu = 1, 3$) or eight ($\nu = 2$) angles. The diagonal matrix elements are real despite the fact that in external magnetic field there is no time reversal symmetry. Therefore the ground state can be chosen real, produced from the reference state by SO(4) sub-group rotations. This sub-group has 6

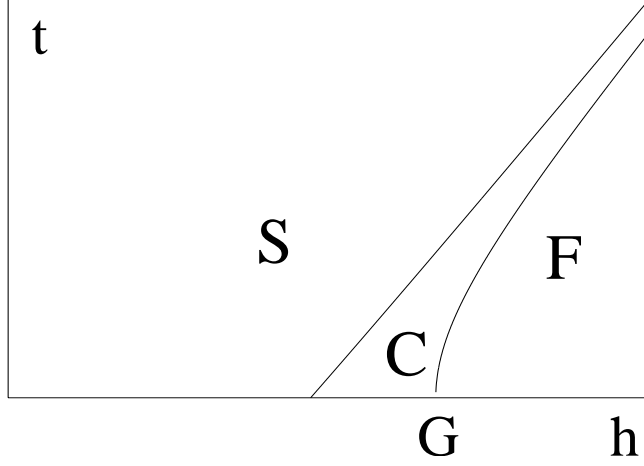


Figure 3.3: Phase diagram in the case $\nu = 2$ and $\delta = 0$. F, S and C are ferromagnetic, spin-singlet and canted antiferromagnetic phases, respectively.

parameters with two of them falling into the denominator sub-group (for $\nu = 2$). One of the remaining four angles corresponds to global rotation of all spins and is fixed by the magnetic field direction z . Thus, the ground state is obtained from the reference state by just three rotations (for $\nu = 2$).

First we consider the case $\nu = 1$. The ground state is $U\Psi(\uparrow +1)$, where $U = P(\vartheta)R(\theta)$. The matrix R rotates the \uparrow -spin component in valley space by an angle θ , and then the matrix P rotates the valley components of the resulting state in spin space by an angle ϑ . Substituting $\hat{Q}(\vartheta, \theta)$ Eq. (3.25) into Eq. (3.40) we obtain the energy per electron:

$$E_{an}^1 = -h \sin \vartheta - t \sin \theta + G\delta \cos^2 \theta. \quad (3.41)$$

The minimum of this energy is reached at $\vartheta = \pi/2$ and $\theta = \pi/2$ corresponding to the ferromagnet phase in spin and valley spaces. The case $\nu = 3$ is identical to $\nu = 1$ due to electron-hole symmetry.

In the case $\nu = 2$ the ground state is $U\Psi(\uparrow +1, \downarrow -1)$ where $U = P(\vartheta)R(\theta_{\uparrow}, \theta_{\downarrow})$. The matrix R rotates the \uparrow, \downarrow -spin components by angles $\theta_{\uparrow, \downarrow}$ in valley space and then the matrix P rotates the ± 1 -valley components by angles $\pm \vartheta$ in spin space. We find $\theta_{\uparrow} = \theta_{\downarrow}$. Substituting the corresponding

$\hat{Q}(\vartheta, \theta)$ into Eq. (3.40) we get:

$$E_{an}^2 = -2t \cos \vartheta \sin \theta - 2h \sin \vartheta \cos \theta + G(1 - \delta) \left(\frac{1}{2} \cos^2 \theta - \cos^2 \vartheta \right) - G\delta \cos^2 \vartheta \sin^2 \theta. \quad (3.42)$$

The last term represents the easy-plane anisotropy and the antiferromagnetic exchange interaction between spins in two valleys. The phase diagram in the case $\delta = 0$ is shown in Fig. 3.3. Here *F* is the spin ferromagnetic and the valley singlet phase ($\vartheta = \pi/2, \theta = 0$), *S* is the spin singlet and the valley ferromagnetic phase ($\vartheta = 0, \theta = \pi/2$), *C* is the canted antiferromagnetic phase in spin and valley spaces.

At $\delta = 0$, we find two lines of continuous phase transitions between *F* and *C* phases: $(h - G)(h - G/2) = t^2$, and between *S* and *C* phases: $(t + G)(t + G/2) = h^2$. Small positive δ transforms the *S-C* phase transition into a discontinuous first order one. The *C* phase ends at some critical $h_c(\delta)$, and the direct *S-F* first order transition occurs at $h > h_c(\delta)$ on the line: $t = h - G(3 - \delta)/4$. For $\delta > 0.33$ the *C* phase disappears. A detailed examining of Eq. (3.42) is given in the Appendix C.

At typical magnetic fields $B \sim 5 - 10\text{T}$ the Zeeman energy in Si is a few times larger than the valley splitting $t \sim 2\text{K}$ [49]. To our knowledge, the deformation potential at large phonon momentum is unknown. Therefore we could only assume the value electron-phonon energy, speculatively: $G \sim 0.2 - 2\text{K}$. Probably, to observe phases of Fig. 3.3 in Si one would need to lower the effective electron *g*-factor artificially.

3.6 Anisotropic energy of skyrmion

Many experiments found activation gaps for diagonal conductivity in QHE systems. For symmetry broken "ferromagnetic" systems theory predicts the conductivity to be mediated by charged topological textures — skyrmions, with activation energies being determined by a large exchange constant E_1 from Eq. (3.26). Contrary to this, experiments find much lower gaps [50].

One possible explanation is that some intrinsic inhomogeneity, like defects or a long range slow variation of the electrostatic potential, makes skyrmions of opposite topological charges to be already present in the system and therefore experiments reveal either a depinning activation energy or a skyrmion mobility activation energy. In both cases the gap is determined by the small anisotropic part of the skyrmion energy. In this section we compute this anisotropic energy for a bivalley skyrmion.

Belavin and Polyakov (BP) found the skyrmion solution in the case of a S^2 order parameter [36]. Their solution is readily generalized for a general Grassmannian order parameter. The non-homogeneous order parameter that represents one skyrmion in the symmetric case with $|\mathcal{Q}| = 1$ is given by

$$\hat{Q}_{BP}(z, \bar{z}) = \hat{N} + \frac{1}{R^2 + |z|^2} \begin{pmatrix} -R^2|v_f\rangle\langle v_f| & zR|v_f\rangle\langle v_e| \\ \bar{z}R|v_e\rangle\langle v_f| & R^2|v_e\rangle\langle v_e| \end{pmatrix} \quad (3.43)$$

where $z = x + iy$, R is the radius of the skyrmion core and $|v_f\rangle$ and $|v_e\rangle$ are two vectors of dimension ν and $4 - \nu$. We choose $|v_{f,e}\rangle = (1, 0, \dots, 0)$ in (3.43). The skyrmion order parameter has to be rotated by a homogeneous matrix U calculated in the previous section in such a way that the order parameter far away from the skyrmion center minimizes the anisotropy energy. In addition to this rotation, we have to allow the global rotations W from the denominator sub-group \mathcal{S} that transform the skyrmion order parameter (3.43): $\hat{Q}(\vec{r}) = UW\hat{Q}_{BP}(z, \bar{z})W^+U^+$. For the case $\nu = 2$ the block diagonal matrix $W = (W_f, W_e)$ can be parameterized by seven angles:

$$W_{e,f} = \begin{pmatrix} \cos \frac{\beta_{e,f}}{2} e^{i(\gamma_{e,f} + \alpha_{e,f})} & \sin \frac{\beta_{e,f}}{2} e^{i(\gamma_{e,f} - \alpha_{e,f})} \\ -\sin \frac{\beta_{e,f}}{2} e^{i(-\gamma_{e,f} + \alpha_{e,f})} & \cos \frac{\beta_{e,f}}{2} e^{i(-\gamma_{e,f} - \alpha_{e,f})} \end{pmatrix}. \quad (3.44)$$

The additional seventh parameter angle of the denominator sub-group rotates the coordinates: $z \rightarrow e^{i\gamma} z$. We find explicitly that the skyrmion anisotropic energy does not depend on the angles γ_e , γ_f and γ_7 whereas $\alpha_e = 0$ and $\alpha_f = \pi$ correspond to the energy minimum. Thus the order parameter inside the core of the skyrmion depends on the two angles β_e and β_f . Beside these

angles the BP solution depends on arbitrary conformal parameters that do not change the energy of the skyrmion. We consider here the simplest case of topological index $|\mathcal{Q}| = 1$ Eq. (3.43), where only one such conformal parameter R is essential. Calculating the energy of the skyrmion we encounter different spatial integrals with one integral being logarithmically large:

$$K(R) = \left(\frac{R}{l_H}\right)^2 \log\left(\frac{l_H}{R} \sqrt{\frac{E_1}{\mathcal{E}_{min}^{sk}}}\right), \quad (3.45)$$

and we neglect all the others. In this way we find the Zeeman energy of the skyrmion to be $E_Z^{sk} = K(R)\mathcal{Z}$, where

$$\mathcal{Z} = 2h(2 \sin \vartheta \cos \theta - \cos \vartheta (\sin \beta_f + \sin \beta_e) \sin \theta) \quad (3.46)$$

The bare valley splitting energy of the skyrmion is given by: $E_t^{sk} = K(R)\mathcal{T}$, where

$$\mathcal{T} = 2t(2 \cos \vartheta \sin \theta - \sin \vartheta (\sin \beta_f + \sin \beta_e) \cos \theta) \quad (3.47)$$

Finally, the Jahn-Teller energy of the skyrmion is given by: $G_{sk} = K(R)\mathcal{G}$, where

$$\begin{aligned} \mathcal{G} = G \left[-\frac{1}{2} + 3 \cos^2 \vartheta + \frac{1}{2} \cos^2 \theta \cos(\beta_e + \beta_f) - \right. \\ \left. -\frac{3}{2} \cos^2 \theta - \left(\frac{1}{2} - 2 \cos^2 \vartheta\right) \cos(\beta_e - \beta_f) \right]. \end{aligned} \quad (3.48)$$

The total energy of a skyrmion also includes the energy of direct Coulomb repulsion of an additional charge distribution $n(\vec{r})$ (3.24):

$$E_C^{sk} = \int \frac{e^2 n(\vec{r}) n(\vec{r}')}{2\kappa |\vec{r} - \vec{r}'|} d^2\vec{r} d^2\vec{r}' = \frac{3\pi^2}{64} \frac{e^2}{\kappa R} = \mathcal{E}_C \frac{l_H}{R}. \quad (3.49)$$

The minimum of the total anisotropic skyrmion energy, the sum of Eqs. (3.46)-(3.48): $\mathcal{E}^{sk} = \mathcal{Z} + \mathcal{T} + \mathcal{G}$, with respect to β_e and β_f was found numerically and is denoted as: \mathcal{E}_{min}^{sk} . Next, we find a minimum of the total skyrmion energy including Eq. (3.49): $E^{sk} = K(R)\mathcal{E}_{min}^{sk} + \mathcal{E}_C/R$, with respect to the skyrmion radius R :

$$\Delta = \frac{E_1|\mathcal{Q}| - E_0\mathcal{Q}}{2} + \frac{3}{2} \left(\mathcal{E}_{min}^{sk} \mathcal{E}_C^2 \log \frac{E_1}{\mathcal{E}_{min}^{sk}} \right)^{1/3}. \quad (3.50)$$

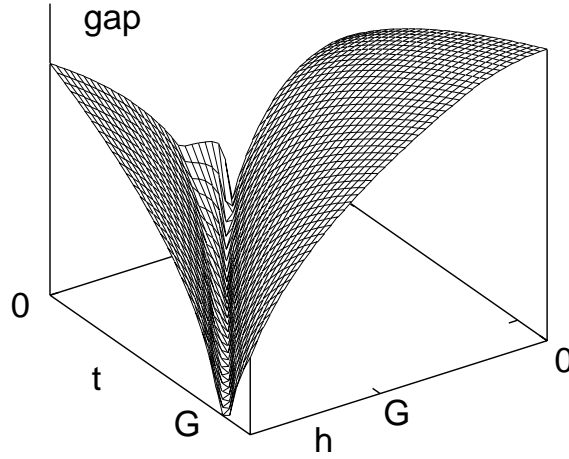


Figure 3.4: Anisotropic part of skyrmion energy gap at $\nu = 2$ and $\delta = 0$

This equation is valid in the limit $\mathcal{E}_{min}^{sk} \ll E_1$. The resulting anisotropic part of the skyrmion gap is shown in the Fig. 3.4. Note that the prominent minimum of the skyrmion anisotropy energy gap coincides with the phase transition line C-F from the phase diagram Fig. 3.3.

This skyrmion anisotropic energy is similar to the bilayer case [45] with t being the hopping constant between the two layers. In an experiment on a GaAs bilayer [51], a profound reduction of the thermal activation gap has been found in some interval on the $\nu = 2$ line.

In the case $\nu = 1$ we parameterize general rotations from the denominator sub-group by four angles:

$$|v_e\rangle = \left(\cos \frac{\beta}{2}, \sin \frac{\beta}{2} \cos \alpha e^{i\lambda_1}, \sin \frac{\beta}{2} \sin \alpha e^{i\lambda_2} \right) \quad (3.51)$$

The skyrmion energy does not depend on the angles $\lambda_{1,2}$ whereas $\alpha = \pi/2$ corresponds to the energy minimum. We find the Zeeman energy $\mathcal{Z} = h(1 - \cos \beta)$, the valley splitting energy $\mathcal{T} = 2t \cos^2(\beta/2)$ and the easy-plane Jahn-Teller energy $\mathcal{G} = G\delta(1 + \cos \beta)$. The minimum of the sum of these

energies with respect to β and α : $\mathcal{E}_{min}^{sk} = 2 \min(t + G\delta, h)$, determines the charge activation gap Δ in Eq. (3.50). The case $\nu = 3$ is identical to the case $\nu = 1$.

3.7 Conclusion

We have shown that the valley degeneracy for a Si(100) MOSFET can lead to a Jahn-Teller effect in a strong magnetic field with a longitudinal lattice deformation within the width of a quantum well. This deformation has an atomic periodicity corresponding to the momentum difference between the two valley minima in the direction perpendicular to the plain. The integer fillings $\nu = 1, 3$ and $\nu = 2$ are treated in different ways. For $\nu = 1, 3$ the Jahn-Teller effect alone can not remove the valley degeneracy and the Coulomb interaction is crucial. The level splitting here is small if the Coulomb energy is small compared to the Debye energy. For the $\nu = 2$ case the Jahn-Teller effect removes the valley degeneracy via an easy-plane anisotropy similar to that found in the 2D bilayer system in strong magnetic fields. The phase diagram as a function of different physical parameters was established and the anisotropic energy of a topological skyrmion-like texture was calculated.

3.8 Appendix A

Here we calculate the second diagram in Fig. 3.1 which was overlooked in Ref. [47]. It represents the change of Hartree-Fock exchange energy in the presence of a spin texture. The spatial part of the electron Green function in Landau gauge is:

$$G_{0s}(z, z') = \frac{(z - z')^s}{\sqrt{2^s s!}} e^{-|z-z'|^2/4 + i(x+x')(y-y')/2}, \quad (3.52)$$

where $z = x + iy$, s is the Landau level and $G_{s0} = G_{0s}^*$. The bottom part of Fig. 3.1b features the G_{00} Green function whereas the upper part has the G_{10}

and G_{00} Green functions. Evaluating the two frequency integrals we find:

$$\delta E = \frac{1}{\sqrt{2}} \int \frac{d^2 z}{2\pi} \frac{d^2 z'}{2\pi} \frac{d^2 \xi}{2\pi} G_{00}(z, z') V(z - z') \\ (G_{00}(z' \xi) \Omega_+(\xi) G_{01}(\xi z) + G_{10}(z' \xi) \Omega_-(\xi) G_{00}(\xi z)), \quad (3.53)$$

Expanding $\Omega(\xi)$ around the center point of the diagram, $z_0 = (z + z')/2$: $\Omega_{\pm}(\xi) = \Omega_{\pm}(z_0) \pm (\xi - z_0) \epsilon_{\mu\nu} \nabla_{\mu} \Omega_{\nu}^z(z_0)$, we evaluate the energy δE in Eq. (3.53) as ($z_0 = \vec{r}$):

$$\int d^2 z \left(1 - \frac{|z|^2}{4}\right) V(|z|) e^{-|z|^2/2} \int \epsilon_{\mu\nu} \nabla_{\mu} \Omega_{\nu}^z(\vec{r}) \frac{d^2 \vec{r}}{2\pi}. \quad (3.54)$$

The front integral is evaluated for the Coulomb interaction and equals: $(E_1 + E_0)/2$.

3.9 Appendix B

Eq. (3.27) is proved using a principal bundle of the complex Stiefel manifold $V_{nk}^C = SU(n)/SU(n-k)$ — that is defined as a manifold of k orthogonal complex vectors in n dimensional complex linear space — over the Grassmannian manifold G_{nk}^C with a layer $U(k)$. The exact map sequence for this bundle is

$$\dots \pi_2(V_{nk}^C) \rightarrow \pi_2(G_{nk}^C) \rightarrow \pi_1(U(k)) \rightarrow \pi_1(V_{nk}^C) \dots \quad (3.55)$$

The Stiefel manifold has the property $\pi_j(V_{nk}^C) = 0$ for $j < 2(n-k)$ [52], proven using the principal bundle $SU(n)$ over V_{nk}^C with a layer $SU(n-k)$. Eq. (3.55) means that $\pi_2(G_{nk}^C) = \pi_1(U(k))$. The Lie group $U(k)$ is a product of $SU(k)$ and $U(1)$ groups with the fundamental homotopy group: $\pi_1(U(k)) = \pi_1(SU(k)) + \pi_1(U(1)) = \mathbb{Z}$ [52].

3.10 Appendix C

In this Appendix we derive the results for the ground state phase diagram for the case $\nu = 2$ and also present some other formal results which are too

specific for the main part of the work. We start with the expression (3.42) for the energy of a homogeneous state as a function of the angles θ and ϑ . First we derive the expressions for the lines of the phase transitions between F, C, and S phases for $\delta = 0$. To do this we compute the second derivative matrix for the energy and check the positiveness of its minors. In this appendix all energies are measured in units of G .

For the F phase the corresponding condition reads:

$$\begin{vmatrix} 2h - 2 + 2\delta & 2t \\ 2t & 2h - 1 + \delta \end{vmatrix} > 0 \quad (3.56)$$

or

$$(h - (1 - \delta)/2)(h - (1 - \delta)) > t^2. \quad (3.57)$$

Generally this expression gives only the region where the F phase is stable (metastable), but for the 2nd order F-C transition, we get the phase transition line for $\delta = 0$:

$$(h - 1)(h - 1/2) = t^2.$$

In the same way we get the condition for the (meta)stability of the S phase:

$$(t + 1)(t + (1 + \delta)/2) > h^2, \quad (3.58)$$

which for $\delta = 0$ gives the phase transition line

$$(t + 1)(t + 1/2) = h^2.$$

Both the phase transition lines tend to $h = t + 3/4$ for large t and h .

The line of the direct first order transition between the F and S phases for large t and h and $\delta > 0$ is obtained by direct comparison of the energies of the two phases: the energy of the F phase

$$E_F = -2h + \frac{1}{2}(1 - \delta)$$

and the energy of the S phase

$$E_S = -2t - 1.$$

We get

$$t = h - \frac{3 - \delta}{4}. \quad (3.59)$$

In order to find the phase transition lines for arbitrary δ we need to find the values for θ and ϑ in the C phase. This is quite a difficult problem and here we give an analytical solution for it in some limiting cases. First we find the C phase for $\delta = 0$. To do it a variable change is convenient: instead of θ and ϑ we use $\alpha = \vartheta - \theta$ and $\beta = \vartheta + \theta$. In these variables we get consequently:

$$E_{an}^2 = -t(\sin \beta - \sin \alpha) - h(\sin \beta + \sin \alpha) + \frac{1}{4}(3 \sin \alpha \sin \beta - \cos \alpha \cos \beta); \quad (3.60)$$

$$\frac{\partial E_{an}^2}{\partial \alpha} = -(h - t) \cos \alpha + \frac{1}{4}(3 \sin \beta \cos \alpha + \sin \alpha \cos \beta), \quad (3.61)$$

$$\frac{\partial E_{an}^2}{\partial \beta} = -(t + h) \cos \beta + \frac{1}{4}(\sin \beta \cos \alpha + 3 \sin \alpha \cos \beta). \quad (3.62)$$

The conditions $\partial E_{an}^2 / \partial \alpha = 0$, $\partial E_{an}^2 / \partial \beta = 0$ yield:

$$\begin{aligned} \sin \alpha &= \frac{3(h + t) - A(h - t)}{2}, \\ \sin \beta &= \frac{3(h - t) - A^{-1}(h + t)}{2} \end{aligned} \quad (3.63)$$

with

$$A = \frac{\cos \alpha}{\cos \beta} = \pm \left[\frac{2(h + t)^2 - 1}{2(h - t)^2 - 1} \right]^{1/2}.$$

Notice that, as can be seen from Eq. (3.42), θ and ϑ for the ground state must be in the first quadrant that means that $\cos \alpha \geq 0$. Calculating the second derivative matrix and checking the stability of the found states we can show that $\cos \beta < 0$ corresponds to a maximum of the energy rather than a minimum.

Finally, substituting (3.63) into (3.60), we find the energy of the C phase:

$$E_C = \frac{\sqrt{(2(h - t)^2 - 1)(2(h + t)^2 - 1)} - 6(h^2 - t^2) - 1}{4}.$$

Comparing it to E_F and E_S at the F-C and S-C transition lines calculated above, we see that at the transition lines the energies are equal, which proves that the transition is indeed of the second order.

Now we examine the case of vanishing t and arbitrary δ . The conditions $\partial E_{an}^2/\partial\theta = 0$ and $\partial E_{an}^2/\partial\vartheta = 0$ for $t = 0$ read as follows:

$$\begin{aligned} 2h \sin \vartheta \sin \theta - \frac{1}{2} \sin 2\theta - \frac{\delta}{2} \cos 2\vartheta \sin 2\theta &= 0, \\ -2h \cos \vartheta \cos \theta + \sin 2\vartheta - \delta \sin 2\vartheta \cos^2 \theta &= 0. \end{aligned} \quad (3.64)$$

Apart from the trivial solutions corresponding to the F and S phases we find the C phase given by

$$\theta = 0, \quad \sin \vartheta = \frac{h}{1 - \delta}. \quad (3.65)$$

Other solutions are either non-stable or lose in energy to other states. This C phase is stable for

$$(1 - \delta) \sqrt{\frac{1 + \delta}{2}} < h < (1 - \delta).$$

(The S phase is stable for $h < \sqrt{(1 + \delta)/2}$ and the F phase for $h > 1 - \delta$.) Comparing the energies of the S and C phases we find the point of the S-C transition:

$$h_{S-C} = \sqrt{\frac{1 - \delta^2}{2}};$$

this is a first order phase transition with regions of metastability for both phases on either side of it. The C-F transition occurs at $h_{C-F} = 1 - \delta$, this transition is of 2nd order.

To find δ at which the C phase disappears we need to set $h_{C-F} = h_{S-C}$, this gives $\delta = 0.33$ as mentioned in the main part of the work.

Finally, to find the ending point $h_c(\delta)$ of the C phase we can find the intersection of the two known phase transition lines: (3.57) and (3.59). We get:

$$h_c(\delta) = \frac{1 + 10\delta - 7\delta^2}{16\delta}. \quad (3.66)$$

Chapter 4

Summary

In this thesis I have presented the results on two subjects: the Coulomb drag and Jahn-Teller effect in two-dimensional electron systems in a strong magnetic field.

A semiclassical theory for electron magneto-drag between two parallel two-dimensional electron systems, which provides a transparent picture of the most salient qualitative features of anomalous drag phenomena observed in recent experiments, is presented. Localization plays a role in explaining activated low temperature behavior, but is not crucial for anomalous (especially negative) drag per se. In particular a detailed theory for the drag between two one-dimensional links has been elaborated. The temperature dependence of the drag has been derived for a whole variety of the parameters of the system for parallel links as well as for non-parallel ones. Also, qualitative arguments showing to what consequences for the two-dimensional drag my results lead are presented.

The Jahn-Teller effect in bivalley Si(100) MOSFET under conditions of quantum Hall effect at integer filling factors $\nu = 1, 2, 3$ has been studied. This system is described by an approximate SU(4) symmetry. At $\nu = 2$ static and dynamic lattice deformations give rise to an easy-plane anisotropy and antiferromagnetic exchange and lift the valley degeneracy. At $\nu = 1, 3$ the Coulomb interaction is essential to produce weak easy-plane anisotropy. At

$\nu = 2$ three phases: ferromagnetic, canted antiferromagnetic and spin-singlet, have been found. The anisotropy energy of a charged skyrmion excitation in every phase has been calculated.

Bibliography

- [1] K. v. Klitzing, G. Dorda, M. Pepper. New Method for High-Accuracy Determination of the Fine-Structure Constant Based on Quantized Hall Resistance. *Phys. Rev. Lett.* **45**, 494 (1980).
- [2] X. G. Feng, S. Zelakiewicz, H. Noh, T. J. Ragucci, and T. J. Gramila. Negative Electron Drag and Holelike Behavior in the Integer Quantum Hall Regime. *Phys. Rev. Lett.* **81**, 3219 (1998).
- [3] J. G. S. Lok, S. Kraus, M. Pohl, W. Dietsche, K. von Klitzing, W. Wegscheider, and M. Bichler. Spin effects in the magnetodrag between double quantum wells. *Phys. Rev. B* **63**, 041305 (2001).
- [4] T. J. Gramila, J. P. Eisenstein, A. H. MacDonald, L. N. Pfeiffer and K. W. West. Mutual friction between parallel two-dimensional electron systems. *Phys. Rev. Lett.* **66**, 1216 (1991).
- [5] M. B. Pogrebinskiĭ. Mutual drag of carriers in a semiconductor-insulator-semiconductor system. *Fiz. Tekh. Poluprovodn.* **11**, 637 (1977) [*Sov. Phys. Semicond.* **11**, 372 (1977)].
- [6] P. J. Price. Hot-electron effects in heterolayers. *Physica* **117/118** B+C, 750 (1983).
- [7] A. G. Rojo. Electron-drag effects in coupled electron systems. *J. Phys.: Condens. Matter* **11**, R31 (1999).

- [8] U. Sivan, P. M. Solomon, and H. Shtrikman. Coupled electron-hole transport. *Phys. Rev. Lett.* **68**, 1196 (1992).
- [9] J. P. Eisenstein, G. S. Boebinger, L. N. Pfeiffer, K. W. West, and Song He. New fractional quantum Hall state in double-layer two-dimensional electron systems. *Phys. Rev. Lett.* **68**, 1383 (1992).
- [10] N. P. R. Hill, J. T. Nicholls, E. H. Linfield, M. Pepper, D. A. Ritchie, A. R. Hamilton and G. A. C. Jones. Frictional drag between parallel two-dimensional electron gases in a perpendicular magnetic field. *J. Phys.: Condens. Matter* **8**, L557 (1996).
- [11] H. Rubel, A. Fischer, W. Dietsche, K. von Klitzing, and K. Eberl. Observation of Screening in the Magneto-Coulomb Drag between Coupled Two-Dimensional Electron Systems. *Phys. Rev. Lett.* **78**, 1763 (1997).
- [12] M. P. Lilly, J. P. Eisenstein, L. N. Pfeiffer, and K. W. West. Coulomb Drag in the Extreme Quantum Limit. *Phys. Rev. Lett.* **80**, 1714 (1998).
- [13] K. Muraki, J. G. S. Lok, S. Kraus, W. Dietsche, K. von Klitzing, D. Schuh, M. Bichler, and W. Wegscheider. Coulomb Drag as a Probe of the Nature of Compressible States in a Magnetic Field. *Phys. Rev. Lett.* **92**, 246801 (2004).
- [14] A.-P. Jauho and H. Smith. Coulomb drag between parallel two-dimensional electron systems. *Phys. Rev. B* **47**, 4420 (1993).
- [15] L. Zheng and A. H. MacDonald. Coulomb drag between disordered two-dimensional electron-gas layers. *Phys. Rev. B* **48**, 8203 (1993).
- [16] A. Kamenev and Y. Oreg Coulomb drag in normal metals and superconductors: Diagrammatic approach. *Phys. Rev. B* **52**, 7516 (1995).
- [17] K. Flensberg and B. Y.-K. Hu. Coulomb Drag as a Probe of Coupled Plasmon Modes in Parallel Quantum Wells. *Phys. Rev. Lett.* **73**, 3572 (1994).

- [18] I. V. Gornyi, A. D. Mirlin, and F. von Oppen. Coulomb drag in high Landau levels. *Phys. Rev. B* **70**, 245302 (2004).
- [19] F. von Oppen, S. H. Simon, and A. Stern. Oscillating Sign of Drag in High Landau Levels. *Phys. Rev. Lett.* **87**, 106803 (2001).
- [20] T. Ando and Y. Uemura. Theory of Quantum Transport in a Two-Dimensional Electron System under Magnetic Fields. I. Characteristics of Level Broadening and Transport under Strong Fields. *J. Phys. Soc. Jpn.* **36**, 959 (1974).
- [21] M. E. Raikh and T. V. Shahbazyan. High Landau levels in a smooth random potential for two-dimensional electrons. *Phys. Rev. B* **47**, 1522 (1993).
- [22] M. M. Fogler, A. Yu. Dobin, V. I. Perel, and B. I. Shklovskii. Suppression of chaotic dynamics and localization of two-dimensional electrons by a weak magnetic field. *Phys. Rev. B* **56**, 6823 (1997).
- [23] M. Tsukuda. On the Tail States of the Landau Subbands in MOS Structures under Strong Magnetic Field. *J. Phys. Soc. Jpn.* **41**, 1466 (1976).
- [24] S. V. Iordanskii. On the conductivity of two dimensional electrons in a strong magnetic field. *Solid State Commun.* **43**, 1 (1982).
- [25] R. F. Kararinov and S. Luryi. Quantum percolation and quantization of Hall resistance in two-dimensional electron gas. *Phys. Rev. B* **25**, 7626 (1982).
- [26] S. A. Trugman. Localization, percolation, and the quantum Hall effect. *Phys. Rev. B* **27**, 7539 (1983).
- [27] B. Shapiro. Dissipative transport in transition regions between quantum Hall plateaus. *Phys. Rev. B* **33**, 8447 (1986).
- [28] D. B. Chklovskii, B. I. Shklovskii, and L. I. Glazman. Electrostatics of edge channels. *Phys. Rev. B* **46**, 4026 (1992).

- [29] N. R. Cooper and J. T. Chalker. Coulomb interactions and the integer quantum Hall effect: Screening and transport. *Phys. Rev. B* **48**, 4530 (1993).
- [30] J. T. Chalker and P. D. Coddington. Percolation, quantum tunneling and the integer Hall effect. *J. Phys. C* **21**, 2665 (1988).
- [31] L. D. Landau and E. M. Lifshitz. *Course of theoretical physics, Vol. 3 Quantum Mechanics*, (Nauka, Moscow 1989).
- [32] A. Abragam and B. Bleaney. *Electron Paramagnetic Resonance of Transition Ions*, (Clarendon, Oxford 1970).
- [33] Yu. A. Bychkov, S. V. Iordanskii and G. M. Eliashberg. Two-dimensional electrons in a strong magnetic field. *Pis'ma Zh. Eksp. Teor. Fiz.* **33**, 152 (1981) [*JETP Lett.* **33** 143 (1981)].
- [34] C. Kallin and B. I. Halperin. Excitations from a filled Landau level in the two-dimensional electron gas. *Phys. Rev. B* **30**, 5655 (1984).
- [35] I. V. Lerner and Yu. E. Lozovik. The influence of correlation effects on phase transitions in quasi-two-dimensional semimetals in a strong magnetic field. *Zh. Eksp. Teor. Fiz.* **82**, 1188 (1982) [*Sov. Phys. JETP* **55**, 691 (1982)].
- [36] A. A. Belavin and A. M. Polyakov. Metastable states of two-dimensional isotropic ferromagnets. *Pis'ma Zh. Eksp. Teor. Fiz.* **22**, 503 (1975) [*JETP Lett.* **22** 245 (1975)].
- [37] S. L. Sondhi, A. Karlhede, S. A. Kivelson and E. H. Rezayi. Skyrmions and the crossover from the integer to fractional quantum Hall effect at small Zeeman energies. *Phys. Rev. B* **47**, 16419 (1993).
- [38] T. Ando, A. B. Fowler and F. Stern. Electronic properties of two-dimensional systems. *Rev. Mod. Phys.* **54**, 437-672 (1982).

- [39] Yu. A. Bychkov and S. V. Iordanskii. Many-valley two-dimensional electron systems in a strong magnetic field. *Zh. Eksp. Teor. Fiz.* **93**, 1049 (1987) [*Sov. Phys. JETP* **93**, 701 (1987)].
- [40] M. Rasolt, B. I. Halperin, and D. Vanderbilt. Dissipation due to a "valley" wave channel in the quantum Hall effect of a multivalley semiconductor. *Phys. Rev. Lett.* **57**, 126-129 (1986).
- [41] K. Moon, H. Mori, K. Yang, S. M. Girvin, A. H. MacDonald, L. Zheng, D. Yoshioka, and S. Zhang. Spontaneous interlayer coherence in double-layer quantum Hall systems: Charged vortices and Kosterlitz-Thouless phase transitions. *Phys. Rev B* **51**, 5138 (1995).
- [42] S. Das Sarma, S. Sachdev and L. Zheng. Double-Layer Quantum Hall Antiferromagnetism at Filling Fraction $\nu = 2/m$ where m is an Odd Integer. *Phys. Rev. Lett.* **79**, 917 (1997).
- [43] S. Das Sarma, S. Sachdev, and L. Zheng. Canted antiferromagnetic and spin-singlet quantum Hall states in double-layer systems. *Phys. Rev. B* **58**, 4672 (1998).
- [44] A. H. MacDonald, R. Rajaraman and T. Jungwirth. Broken-symmetry ground states in $\nu = 2$ bilayer quantum Hall systems. *Phys. Rev. B* **60**, 8817 (1999).
- [45] S. V. Iordanskii and A. Kashuba. Phase Diagram and Skyrmion Energy for Bilayer Heterostructures at Integer Filling Factors. *Pis'ma Zh. Eksp. Teor. Fiz.* **71**, 496 (2000) [*JETP Lett.* **71**, 345 (2000)].
- [46] D. P. Arovas, A. Karlhede and D. Lilliehook. $SU(N)$ quantum Hall skyrmions. *Phys. Rev. B* **59**, 13147-13150 (1999).
- [47] S. V. Iordanskii, S. G. Plyasunov and V. I. Falko. Skyrmions in electron gas with nonlocal exchange in a strong magnetic field. *Zh. Eksp. Teor. Fiz.* **115**, 716 (1999) [*JETP* **88**, 392 (1999)].

- [48] A. A. Abrikosov, L. P. Gorkov and I. E. Dzyaloshinski. *Methods of Quantum Field Theory in Statistical Physics*, (Dover, New York, 1975).
- [49] V. M. Pudalov, A. Punnoose, G. Brunthaler, A. Prinz, G. Bauer. Valley Splitting in Si-Inversion Layers at Low Magnetic Fields. *cond-mat/0104347*.
- [50] S. P. Shukla, M. Shayegan, S. R. Parihar, S. A. Lyon, N. R. Cooper, and A. A. Kiselev. Large skyrmions in an $\text{Al}_{0.13}\text{Ga}_{0.87}\text{As}$ quantum well. *Phys. Rev. B* **61**, 4469-4472 (2000).
- [51] V. S. Khrapai, E. V. Deviatov, A. A. Shashkin, V. T. Dolgoplov, F. Hastreiter, A. Wixforth, K. L. Campman, and A. C. Gossard. Canted Antiferromagnetic Phase in a Double Quantum Well in a Tilted Quantizing Magnetic Field. *Phys. Rev. Lett.* **84**, 725 (2000).
- [52] B. Dubrovin, S. P. Novikov and A. Fomenko, *Modern Geometry*, (Moscow, Nauka 1986).

Acknowledgments.

First I would like to thank Prof. Dr. Walter Metzner for inviting me to do my PhD at the Max-Planck Institut für Festkörperforschung, for the interesting topic proposed, and for many helpful discussions during the work.

I thank Prof. Dr. Sergey Iordanskii, the supervisor during my diploma work and during the first year of my PhD in Institute for Theoretical Physics, Chernogolovka for his constant support and advice as well in the time of our collaboration as also after I went to Stuttgart.

I thank Prof. Dr. Alejandro Muramatsu for accepting to be the co-reporter of my thesis.

My special thanks goes to Prof. Dr. Leonid Glazman, University of Minnesota. I always enjoyed the stimulating discussions with him which greatly influenced this thesis.

I would like to thank Dr. A. Kashuba, Institute for Theoretical Physics, for the collaboration during the work on the second part of the thesis.

I thank my father, Dr. Efim Brener for his constant interest in my work and for the idea of the arguments presented in the end of section 2.3.2.

I have the pleasure of thanking all members of the Theorie II department of

the Max-Planck Institut für Festkörperforschung for the pleasant atmosphere and all the interesting conversations.

Same goes for the members of the ITP and ISSP in Chernogolovka. In particular I would like to thank Pavel Ostrovskiy, Mikhail Feigel'man, and Vladislav Timofeev.

My regards go to Ingrid Knapp for all her organizational support.

I thank Prof. Dr. V. Falko for offering me the opportunities to participate in very interesting workshops in Dresden and Windsor which gave boosts to my work.

Finally I would like to thank all the people who were near me during all these years, in particular my wife Katia, my mother, my brother, and my two children, for the various support and help.

Publications.

The content of this thesis is partly published in the following journals:

- S. Brener, S. V. Iordanskii, and A. Kashuba. Possible Jahn-Teller effect in Si inverse layers. *Phys. Rev. B* **67**, 125309 (2003).
- S. Brener, W. Metzner. Semiclassical theory of electron drag in strong magnetic fields. *Pis'ma Zh. Eksp. Teor. Fiz.* **81**, 618 (2005) [*JETP Lett.* **81**, 498 (2005)].

Lebenslauf

Name	Sergej Brener
Geboren am	16. Oktober 1978
Geburtsort	Tschernogolowka, Moskauer Gebiet, Russland
Seit Juli 2002	Wissenschaftlicher Mitarbeiter bei Prof. Dr. W. Metzner, Max-Planck-Institut für Festkörperforschung in Stuttgart
Juli 2001 – Juli 2002	Wissenschaftlicher Mitarbeiter bei Prof. Dr. S. Iordanskii, Institut für Theoretische Physik in Tschernogolowka
Sep. 1995 – Juni 2001	Studium der Physik an der Moskauer Physikalisch-Technische Hochschule
1985 – 1995	Schule, Tschernogolowka Abschluss Juni 1995